António Vieira
Resat Oyguc

Geomorphology

Current Perspectives

Chapter 1

Geodiversity as a Tool for the Nature Conservation

Luis M. Nieto

Abstract

Geodiversity and biodiversity are the two fundamental components of Nature that must be analyzed simultaneously for good management of the natural environment. Geodiversity, including geomorphodiversity, has values that make it possible to define the geosystem services on the basis of which it is possible to establish protocols for the sustainable development of the territory analyzed. Both the values of geodiversity and the geosystem services they provide are key elements for the definition of Natural Protected Areas (NPAs). Furthermore, it is also necessary to consider the assessment of the geodiversity and geomorphodiversity of the territory under consideration, so that a zoning can be established in terms of the geodiversity index (geodiversity/geomorphodiversity gradient) that favors the establishment of specific geoconservation protocols according to the value of these indices. In addition, NPAs should be considered as elements belonging to a network in which the different natural systems of the territory in which the network is defined are represented. In the case of geodiversity or geomorphodiversity, the network must be supported by the definition of geological contexts, representative of the major geological units that are observable in the territory.

Keywords: geodiversity, biodiversity, geomorphodiversity, geodiversity assessment, natural protected areas, sustainable development

1. Introduction

Geodiversity is a term first used as analogous to biodiversity, but their development in the scientific and administrative sectors has been very different. A formal definition of biodiversity was presented in Río de Janeiro Earth Summit in 1992 and was quickly incorporated in the national and international guidelines for nature conservation, whereas geodiversity was not formally defined. Although a proposal was made to this respect [1], its international impact was limited. Geodiversity did not acquire an international scientific dimension until the publication of Gray's book in 2004 [2], where the conceptual bases of geodiversity are developed. Later, the concept was analyzed and a preliminary methodology for the assessment of geodiversity [3] was presented, to be applied in the management of Natural Protected Areas (NPAs). The book edited by Reynard et al. in 2009 [4] was another important milestone in the analysis of geological features and their interest on nature conservation. In this book, the concept of geomorphosites is unified, a comprehensive analysis of the state of the art was made, and the foundations are laid for the rigorous analysis of geomorphological features of the territory with goals as diverse as their conservation, simply because they are natural elements with some value, or as a support for biodiversity that may be conditioned by them. Panizza, in 2009 [5], proposed a definition of geomorphodiversity. This author considers that it is the specific assessment of geomorphological features of an area, considering the scale of the studied area. Recently, Worboys et al. [6] edited a comprehensive book about the management of natural protected areas where the geodiversity, geological heritage, and geomorphosites have been considered.

Consolidation of the term geodiversity came in the wake of another key concept, the sustainable development (World Commission of Environment and Development, or Brundtland Commission [7]). Strongly anchored in this concept is the notion of the nature conservation (goal 13: climate action; goal 14: life below water; goal 15: life on land; www.un.org/sustainabledevelopment). Geology and Geomorphology adopted a perspective centered on the relationship between the man and environment, accenting not just the use, but the sustainable use, of natural resources, while avoiding or preventing hazards for the population and minimizing the degradation of nature [3, 5, 8–10]. Thus, Environmental Geology arose to safeguard nature and the conceptual framework embracing geodiversity, and its methodology began to evolve. The need to consider geodiversity when defining or managing NPAs has since gained importance, especially from the International Union for Conservation of Nature (IUCN) Congress of 2008 and 2012, where the 4.040 and 5.048 resolutions respectively highlight that the geodiversity as part of the nature and geoheritage belongs to natural heritage (https://portals.iucn.org/library/node).

Traditionally, in the Anglo-Saxon literature (any of the papers cited so far can be reviewed), Geology and Geomorphology, although Earth Sciences, have been considered independent, which has been transferred to the field of geoconservation, with geodiversity and geological heritage being considered separately from geomorphodiversity and geomorphological heritage. This has led to the distinction between geosites and geomorphosites. Panizza [5] makes a detailed analysis of this problem. Besides, definitions of geodiversity that integrates in its totality all those topics related to the conservation of geomorphological features of the terrain [1–3] have been proposed. The geodiversity has been defined as the number and the variety of structures (sedimentary, tectonic, geomorphological, hydrogeological, and petrological) and geological materials (minerals, rocks, fossils, and soils) that made up the lithosphere in a given region, upon which organic activity is settled, including anthropic activity. This concept was complemented adding to study of the geological elements of a specific zone, there is a need to appraise the relationship existing among them, so that geological processes are seen as a further trait of the geodiversity of the zone under study [3–6].

In this way, geodiversity is perceived as an intrinsic property of a territory that allows one to establish its geological interest [1, 2, 5, 11]. Geodiversity materializes in certain tangible geological elements: outcrops, landforms, their groupings… A detailed analysis of numerous studies on geodiversity valuation [8–10] shows that geomorphodiversity and geomorphosites play an important role in the final value of geodiversity. The geodiversity elements should not merely be studied in independent fashion, but rather in view of their interrelations. The geodiversity of two or more regions can thus be compared by assessment of this property in each one. The fact that geodiversity can be analyzed at very different scales, from global (continents and oceans) to elemental (atoms and ions), is something it shares with biodiversity, which can likewise be studied at macroscales (global ecosystems), the scale of genetic diversity, or the scale of biotechnology and microbiology [11–17].

The goal of this paper is to analyze the role of geodiversity, and the geomorphodiversity as part of it, as components of the natural environment, in delimiting Natural Protected Areas (NPAs) and the development management protocols for these natural areas, always from the standpoint of sustainable development. To achieve this goal, it is necessary to know what values geodiversity has, how it contributes to human well-being from the consideration of the geosystem services, and what relationship it has with biodiversity. An important tool to develop these actions is the assessment of geodiversity/geomorphodiversity of the territory where the NPA is located and enclosed it.

2. Geodiversity values

Geodiversity values reflect the physical basis upon which ecosystems and anthropic activity settle. The geodiversity entails seven values [2, 14]: (a) intrinsic, (b) cultural, (c) esthetic, (d) economic, (e) functional, (f) scientific, and (g) educational.

An intrinsic value is understood as the value given to a geological element by virtue of its existence, and geodiversity is upheld as a nonrenewable resource. Ethical and philosophical dimensions of the relations between society and nature condition belief that things have value because they are useful to man. Certain authors [18] have equated intrinsic and scientific values. However, the two values should be seen as distinct, since intrinsic value is directly and exclusively related to the existence of the geodiversity itself, while scientific value should be associated with certain qualities that at least provide knowledge. Intrinsic value should be understood as a value that is the support on which others can be developed.

Cultural value is attributed by society to some qualities of the abiotic part of the environment owing to its social significance or its role in the community. Variants of cultural value are folkloric value (geomythology), archeological/historical value, spiritual value, and a sense of dependence on "Mother Earth." Closely related with cultural value is the educational value. Knowledge of the composition and origin of an area's geodiversity can be shared with the local population and visitors, promoting social development as well as the communication of geological hypotheses and theories. These ideas were basics by the firstly development of the Granada Geopark (South Spain; **Figure 1A** and **B**). So, the diversity of clays outcropped in this territory and the forestry they conditioned were explained to population of the territory as the source of the ceramics and economic activities as the manufacture of grass tools (www.geoparquedegranada.com). On the other hand, the badlands landscape of this territory is the main goals of the natural tourism of the region (**Figure 1C**). This is because the development of this landscape is the immediate expression of the desertification of the region, which has been commonly associated with an impact of climate change, although it is indeed the result of a change in the base level of a paleo-fluvial system [19].

The esthetic value is closely related to the geomorphodiversity. It evokes a visual or sensual appreciation obtained through incentives from the physical setting. It is related to a contemplation of landscapes (geomorphosites) or the development of recreational activities in the physical environment (i.e., geotourism, **Figure 1C**). The esthetic value often has implications for economic value, given that many geological materials are essential for the socioeconomic development of a region, a country, or a continent, when geodiversity or geomorphodiversity is used from a sustainable standpoint as a touristic or cultural resource. For example, the badlands landscape of the Guadix-Baza basin (Betic Cordillera, South Spain; **Figure 1A**) is the main attractive of

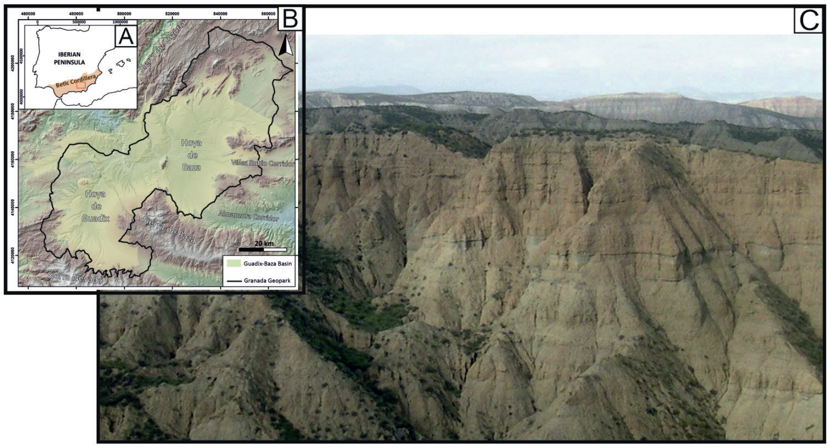

Figure 1.
A: Location of the Granada Geopark in the Iberian Peninsula. B: The Guadix-Baza Basin and the border of the Granada Geopark. C: The badlands landscape of the Granada Geopark is the main attraction to the geotourism, as well as the main regulating factor for the vegetation of the zone. The figures A and B have been made by Dr. Iván Medina.

the nature tourism of the region where the Granada Geopark is delimited (**Figure 1B** and **C**). Other examples where the esthetic value of geomorphodiversity and geomorphosites is highlighted include those related to volcanic areas, karst regions, or areas particularly sensitive to natural hazards [4].

Notwithstanding, the economic value of geodiversity is also linked to the classification of geological materials as resources: fossil fuels, mineral resources, industrial, metallic or precious minerals, or building materials. Related to this topic, in the south of Alicante province (Southeast Spain), the diversity of limestones and dolostones has favored the proliferation of economic activities associated to the ornamental rocks used in the building industry. The economic value of an abiotic environment should also include fossils, soils, and landscapes, as these geological features may lend economic wealth to the place where they are found, either as a means of sustaining agricultural activity or as natural resources to be exploited in the realm of tourism. In this sense, the diversity of ammonoids sites was an important feature considered to define as global geopark the Sierras Subbéticas Natural Park (Betic Cordillera, Córdoba province, South Spain [20]).

Soils, sediments, rocks, landforms, minerals… all play a functional role in the environmental system, which gives them a functional value [2]. Two subdivisions of functional values can be established, depending on whether the elements are perceived as utilitarian values to human society, or as essential substrates to support physical and ecological systems of the Earth. Geodiversity in situ, in its broadest meaning, is useful, regardless of its consideration from an economic standpoint. It is the substrate upon which organic activity settles, providing a means of supporting biodiversity's development.

3. Geodiversity and sustainable development. Geosystem services

Sustainable development has been defined as development that meets the needs of the present without compromising the ability of future generations to meet their own needs (https://www.un.org/sustainabledevelopment/development-agenda/; [7]). For sustainable development to be achieved, it is crucial to harmonize three core elements: economic growth, social inclusion, and environmental protection. These elements are interconnected and are basics for the well-being of individuals and societies.

When dealing with environmental protection, both biotic and abiotic resources must be considered, but in different fashion, according to their nature [11, 12, 21, 22]. The definition of ecosystem according to the Convention on Biological Diversity reads a dynamic complex of plants, animals, and microorganisms and their non-living environment, which interact as a functional unit. This definition assumes that the ecosystem includes abiotic elements, the elements of the geodiversity, as well as social elements (**Figure 2**). The World Forum on Natural Capital specifies the world's stocks of natural assets, which include geology, soil, water, and all living things (https://naturalcapitalforum.com/about/), considering geological elements as essential components of the natural environment (Essential Geodiversity Variables, EGV; [10]). The Forum furthermore states that these elements are to be treated differently depending on whether they are renewable or nonrenewable [17]. The latter, which include mineral and energy resources of a geological nature (minerals, industrial rocks, coal, oil, natural gas, etc.) undergo extraction processes that entail environmental impact, particularly visible because it often leads to a deterioration of the wider landscape (biotic and abiotic component), leading to a degradation of the geomorphodiversity [9, 23]. In order to keep this impact minimal, extraction processes that are less and less aggressive with the environment are being designed, and extraction itself is being minimized, with recycling promoted as a sustainability tool [11].

The exploitation of natural resources, integrated into the concept of natural capital, represents benefits for man. These benefits have recently been called ecosystem services [11, 14, 24–26]. However, there are authors [27, 28] who consider that the benefits provided by abiotic elements should not be considered within ecosystem services [11, 29]. This is the reason why some authors have distinguished between ecosystem services, directly linked to biotic natural elements, and geosystem services, provided by abiotic natural elements [14, 17, 29–32].

Geosystem services are directly dependent on the values of geodiversity (intrinsic/scientific, educational, economic, cultural, esthetic, functional). The geosystem services can be defined as the benefits and functions provided to society by the elements that make up geodiversity. Like ecosystem services, geosystems can provide four main types of services [11, 12, 26, 29]: regulating services, supporting services,

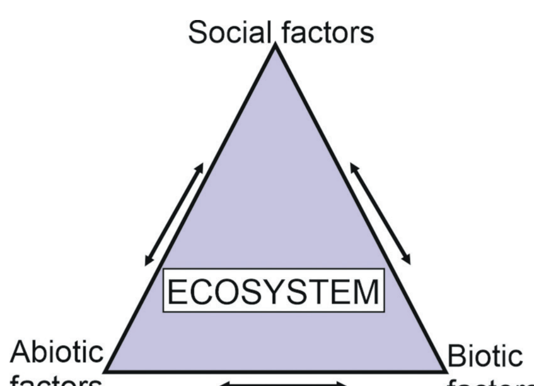

Figure 2.
The three main components of an ecosystem according to the definition of the Convention on Biological Diversity.

provisioning services, and cultural services, which coincide with those proposed by the Millennium Ecosystem Assessment [24]. Besides, Gray [17] has recently proposed a fifth geosystem service, called knowledge, which is related to the fact that Geology provides evidence about the evolution of the planet, both from an inorganic perspective and considering the evolution of life. Regulating services include the natural processes that regulate the environment (oceanic and atmospheric processes, the rock cycle, biogeochemical cycles, flood processes, or the regulation of water quality). These services could be considered at local and regional scales, because should rapport information about the geodiversity of the studied territory and favoring to understand its influence in the human activity.

Supporting services are those processes that serve as a foundation for natural environments, including soil processes, habitat dynamics, land and water as supports for human activity, or the service provided by rocks and sediments for burial and storage. In design and management of the NPAs, the supporting services related to the geodiversity of the territory can firstly understand as the substratum on the living activities is developed. Related to the human activities, the kinds of soils are determinant of the farming activities developed, for example. This is in line with the fact that the consideration of EGVs, especially geomorhodiversity and land uses, entails important heterogeneities in the development of supporting services [9, 10].

Provisioning services are available when natural materials are used by society (water for human consumption, minerals as a source of nutrients or energy (coal, oil, natural gas, tides, winds); ornamental and industrial rocks, fossils, nature conservation, the design of an NPA network …). In the context of the NPA, the provisioning services can be considered according to the use of some rocks in the traditional building activities of the area considered or other local infrastructures.

Finally, cultural services are derived from non-tangible elements of nature that provide spiritual benefits to man (environmental quality, design of natural protected areas, geotourism and leisure, or artistic inspiration, for example). The design of geoturism ways has their support in the cultural services of the geodiversity [8, 9, 33].

Despite this differentiation between ecosystem and geosystem services, several authors [10, 22, 31, 32] propose that both should be considered from a holistic point of view, since both provide well-being to man. However, geosystem services are largely based on the use of nonrenewable natural elements. Their degradation is normally irreversible and cannot be regenerated on the human timescale. However, the analysis of a region's geodiversity and its integration with biodiversity contributes to a higher valuation of geosystem services, especially in natural protected areas, as it provides a better understanding of the natural processes, facilitating the achievement of sustainable development of the NPA under consideration.

4. Relationship between geodiversity and biodiversity

The holistic conservation of nature is an important issue. The coining of terms such as "biophysical management" or "geoecological management" [14, 26] attests to this importance. As used in the definition of IUCN-protected areas, the term "natural" refers to both biodiversity and geodiversity. Following some authors [34, 35], there is a predominance of issues related to biodiversity compared with those of geodiversity, which this organization does not expressly contemplate until its 2008 Congress in Barcelona [21, 22]. Resolution 4040 was approved, urging to design, organize, and oversee activities related with geodiversity and the geological heritage.

To approach the problem of integrated management of the conservation of nature with due precision, the interrelations existing between biodiversity and geodiversity highlighted by several authors [17, 22, 36–38]. They stated that there could be no biodiversity without geodiversity. According to this idea, definitions of geodiversity considered the shared origins, and an interdependency between the two was established. Analysis of these interrelations must consider three levels, global, regional, and local [14, 35].

At the global scale, recognizing the interdependence of biological and geological systems leads inevitably to the hypothesis of Gaia, formulated by Lovelock [39, 40]. He claimed that an interaction among the organic and inorganic components of the Earth existed. The organic elements, along with the air, the oceans, and the terrestrial surface, made up a complex system that may be considered as a cybernetic organism, able to self-adjust through feedback in order to maintain an optimal physical and chemical environment for life on the planet. This integration of biological and geological systems found substantial support with the development of Earth System Science [41–43], investigating the relationships among lithosphere, biosphere, atmosphere, and hydrosphere, in a temporal framework matched to the geological timescale.

Geodiversity, then, incorporates many environmental processes and patterns that manage the biodiversity. They include climate, topography, geology, and hydrology, which altogether provide sources of energy, water, space, and nutrients. In turn, the biological dynamic takes part in processes such as the acceleration or delay of erosion, the stability of hillslopes, fluvial dynamic, and surface water and underwater flow. Knowledge of the action rates of external geological processes, which shape the relief, allows us to know the potential stability of the habitats and the species found in them. A change in these rates would lead to changes in the development of soils, hydrogeological and hydrological conditions, and in short, imbalances in ecosystems [14–16].

At the regional scale, conservation of biodiversity can be best understood through the conservation of geodiversity. It has been postulated that geological factors exert a primary influence on biodiversity patterns [44]. Factors such as the number of rock types, latitude, or the elevation and quantity of carbonate rocks can be used to predict the diversity of species with a high degree of certainty (correlation coefficient $R^2 = 0.94$, according to this research, [44]). These authors conclude that biodiversity is best protected when the geological settings are protected. At this scale, analysis of the relationships between biodiversity and geodiversity cannot overlook three main ideas [3]. The first one is that the spatial-temporal scales of geological and biological processes are different. The second is that the biological processes are interrelated and evolve simultaneously, as do geological processes, but with different rhythms and different timescales. Finally, the third idea is that geological features are related by chronostratigraphic parameters that account for events of short duration as well as events lasting millions of years.

At the local scale, one important step to achieve an integration of biodiversity and geodiversity is to establish relationships among the specific elements to one and other. Three forms of such relations can be distinguished [3]: (a) relations of exclusivity, (b) relations of dependence, and (c) no relation. Relations of exclusivity occur when certain living beings develop in areas with specific geological characteristics. Dependence would prevail when organisms need some (even just one) particular geological feature to develop. For example, vultures need great vertical cliffs to nest, although it does not matter if they are limestone, granite, or conglomerate cliffs. Finally, there is no relation when the living beings of a zone and its geological features have no apparent relationship. In fact, the relationships a and b above as biodiversity-geodiversity interactions should be referred to as dependency relationships between biodiversity and gemorphodiversity, given that organisms can condition their life activity to the development of different landforms that may favor them [22, 44–46].

From the perspective of management and conservation of biodiversity and geodiversity, there is a clear relationship, because both depend on administrative services in charge of the environment. Effective management and conservation of biodiversity call for managing the preservation of the heterogeneity of soils and sediments that ensure its preservation. The degradation of biodiversity in flood plains, for instance, reflects that the methods used to manage the river or changes in land use in the geomorphological fluvial system have led to a separation of the fluvial dynamics and the riverside areas, with the subsequent reduction of natural vegetation diversity [45, 47].

The conservation of nature in areas of high biodiversity should be undertaken from both bioconservation and geoconservation perspectives [2, 14, 35–37]. To this goal, geodiversity and geomorphodiversity must be integrated in the planning of Natural Protected Areas, bearing in mind that they are parts of the ecosystems and that the Earth System approach should entail an integration of biotic and abiotic factors in plans for management and conservation [8–10, 37].

5. Assessment of geodiversity/geomorphodiversity and natural protected areas

The assessment of geodiversity is a subject that has been approached from different perspectives, qualitative or quantitative [11]. The qualitative methods consist of a description of the elements of geodiversity in one area and an explanation of its values based on expert knowledge of the zone. The second group, quantitative methods, attempts to express the spatial variability of the geological elements from an analysis of the diversity, frequency, and distribution of these elements in the studied area (**Table 1**; [3, 46, 48–52]).

Some authors support the assessment on numerical determination of the variety of geosites [53]. It is assumed that a large database of geosites within a given territory means high geodiversity. Other authors look at the geological and geomorphological properties (number of physical elements, roughness coefficient, and surface of the geological/geomorphological unit) of units in a region to define a geodiversity index per geomorphological unit [46, 54]. Other numerical assessments are founded in the use of morphometric, morphoclimatic, and geological classifications to calculate geodiversity indices on the Iberian Peninsula [49]. The use of parameters such as the variety, frequency, and distribution of geological features in a territory has also been proposed as a way of assessing the geodiversity of the territory under study [3].

The assessment of geodiversity based in the variety, frequency, and distribution of geological features considers that the geodiversity is a continuous property of the territory, defining the geodiversity gradient as a measure of the continuous variation of the geodiversity index [3]. Related to the geodiversity gradient, the concept of geodiversity hot-spot has been redefined as geographic areas that harbor very high levels of geodiversity being threatened by human activities [55]. In addition, closely related to the geodiversity hot-spot concept, the antagonistic term geodiversity cold-spot is proposed. Between both areas that have been classified as such, a gradual and continuous change in geodiversity index values could be detected. As geodiversity hot-spots

Method	Parameters/Index			Comments
Serrano and Ruiz-Flaño [46]	Geodiversity index (Gd)	$Gd = Eg\frac{R}{lnS}$	R: roughness coefficient of the geomorphological unit Eg: number of abiotic elements S: Surface of the geomorphic unit	They use the geomorphological units as reference to attribute the geodiversity values because these units include structure, lithology, soils, climates or vegetation.
Carcavilla et al. [3]	Intrinsic geodiversity (Gi)	$Gi = \frac{C}{S}$	C: geodiversity kinds. S: Surface of the studied area.	The geodiversity is a territory feature. This can change into them as progressive manner. To valuing this, it must be designed isoline maps; each of isolines will link points with the same numerical value of intrinsic geodiversity.
	Kind frequency (Fc)	$Fc = \frac{r_c}{S}$	r_c enclosure number of a geodiversity kind. S: Surface of the studied area.	
	Fragmentation degree (Gf)	$Gf = \frac{r}{S}$	r: number of enclosures in a territory. S: Surface of the studied area.	
Pereira et al. [48]	The geodiversity index is the sum of partial indices of some geological features of the studied area. They are calculated from the corresponding maps with a grid of regular size and superimposed in a GIS.	Geological index: it results from the consideration of geological units (lithologies) that they are present in each square of the grid.		The geodiversity index for each square grid is the sum of partial indices. From this value, that is considered in the center of each square, it does an interpolation between the closest centers to the goal to draw isolines that link points with the same geodiversity index value.
		Geomorphological index: it is the sum of two sub-index, the topography and the hydrography features. The first one gives the main geomorphology features of the studied area. The second one is calculated from the influence of the hydrographic features in the geomorphology.		
		Paleontological index: number of fossiliferous formations that outcropped in each one of the squares of the grid.		
		Pedological index: soils count that outcrop in the pedological maps of the studied area. It is considered the number of soils nature in each square of the grid.		
		Mineral index: into this index, could be included several kinds of minerals (extractable or not), oil, coal, gas, radioactive minerals, minerals water, springs.		

Table 1.
Synthesis of the main methods for assessing geodiversity.

are particularly threatened areas, it is also possible to calculate a threat index, which, together with the geodiversity index, leads to the definition of the sensitivity index and the sensitivity map, which represents areas in urgent need of geoconservation measures [55]. These hot-spots tend to be surrounded by zones where the application of geoconservation measures is not a great concern (cold-spots).

In consonance with the notion of geodiversity gradient, several authors [48] develop a methodology to calculate the index of geodiversity of a territory from the design of a geographic information system (GIS) made up of different layers. This method has been improved by several groups of researchers [50, 51, 56–58], who have added several parameters to characterize the geodiversity of a territory, compiling geological and geomorphological data on the studied area (**Table 1** and **Figure 3**). The geodiversity index shall be the result of the sum of several partial indices (**Figure 3**): (a) lithological index, (b) geomorphological index, (c) paleontological index, (d) pedological index, (e) mineral occurrence index, (f) water resources index, and (g) geosites index. The indices "a" to "e" were proposed by Pereira et al. [48]. Araujo and Pereira [58] added the water resources index and Fernández et al. [51] included the geosites index. An important topic of this methodology is that different maps of partial indices of geodiversity are obtained, including the geomorphological index, which allows us to know the geomorphodiversity of the territory analyzed.

However, the methodology developed by these authors leads to the design of maps of partial geodiversity indices associated with a space determined by a grid of a specific size (**Figure 3**). Certain partial indices, such as the lithological, geomorphological or pedological indices, as well as the geodiversity index, should not be considered as indices of discrete geological properties of the territory, but as the previous step to define maps of continuous properties, so that between indices of adjacent grids it is possible to establish gradients, such as the geodiversity gradient map designed by some authors [48, 51, 52, 58]. According to this idea, from the geomorphological index map (**Figure 4A**), it is possible to obtain a geomorphodiversity gradient map (**Figure 4B**) by applying Kriging techniques between adjacent grid squares in the defined grid. The geomorphodiversity gradient map allows us to know the variability

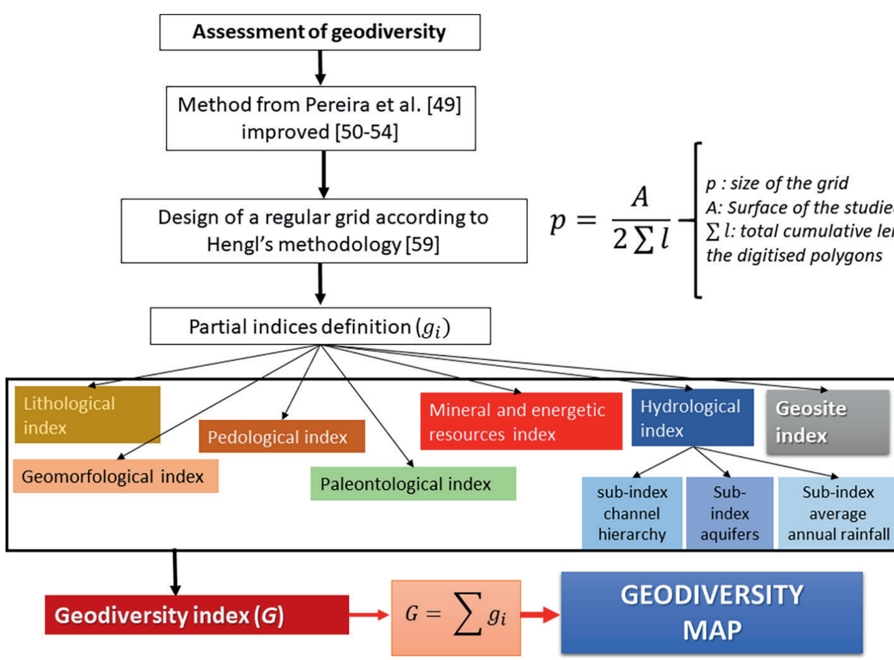

Figure 3.
Flow chart summarizing the geodiversity assessment procedure (see the text) [48, 50, 51, 56–59].

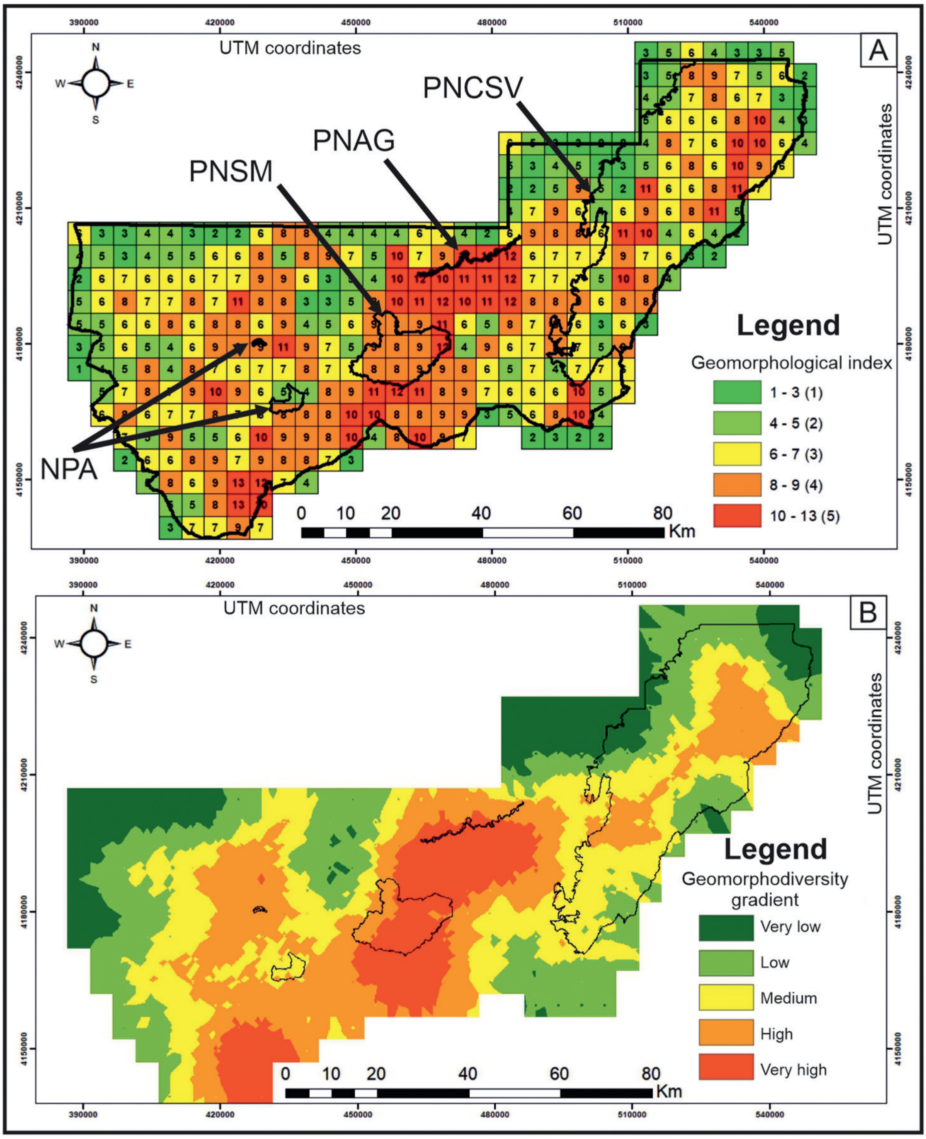

Figure 4.
A: Geomorphological index map of the south and east of the Jaén province determined from the methodology described by Fernandez et al. [51]. The grid has 5×5 km (25 km²). B: Geomorphodiversity gradient map developed to applying kriging on the geomorphological index map. In both maps, PNCSV: boundaries of the Natural Park of Sierra de Cazorla, Segura y Las Villas; PNAG: Alto Guadalquivir Natural Place; PNSM: Natural Park of Sierra Mágina; NPA: other natural protected areas. Both maps are part of an in-progress research project.

of the geomorphological qualities of the territory analyzed, considering that it is a continuous property.

Methods categorized as quantitative are based on a conception of geodiversity index as a measure of the intensity of a certain geological feature or a set of geological elements that characterize the natural setting [60]. This definition of geodiversity indices is useful for reduce the amount of territorial data to be studied, while enhancing the comparability of data belonging to the different areas investigated. On the other hand, the consideration of the lithological, geomorphological, pedological, and water resources indices involves the introduction of the essential variables of geodiversity (EGV, [22]), which have been used, together with other geoenvironmental maps for the assessment of geodiversity and to establish an adequate use of the territory, so that maps on the effects of anthropic activity on the natural heritage are also included in this assessment [10].

Whatever the method applied, the point of departure should be consideration of geodiversity as a key element behind ecosystem dynamics (understood from an integral standpoint, **Figure 2**) for the management of a territory and the use of land and for the development of anthropic activities in a sustainable way. The basic system of representation for an assessment of geodiversity or geomorphodiversity should be the map [60]. This kind of presentation is in line with the conception of both as continuous properties of the territory, in which discrete elements can be delimited and valued independently, but as part of a continuum. A common misconception associated with considering discrete elements of geodiversity (geosites/geomorphosites) as parameters for valuing geodiversity/geomorphodiversity, which is a continuous property, has led to confusion between geodiversity and geological heritage [48].

6. Geodiversity/geomorphodiversity and natural protected areas (NPA)

Several authors argue that to ensure effective management of Natural Protected Areas (NPAs), it is essential to consider the values and the relevance of their geodiversity and the geological heritage as elements of nature [8, 14, 17, 38, 61–63]. This basic notion must materialize and be developed by means of international norms and national laws [64, 65]. Furthermore, it is necessary to establish close links between the inhabitants around the NPA, the geological and biological features of the NPA, and the manager of NPA so that the values of nature, as geodiversity as biodiversity, and the geo- and eco-system services they provide, are clearly inserted in the popular traditions. In UNESCO's definition of Geopark, this is expressed as a basic condition [13, 16, 66].

In the international context, recognition of the importance of geodiversity in general and geomorphodiversity in particular, as well as the geological heritage in a broad sense, calls for their consideration as basic elements of nature, according to the International Union for Conservation of Nature, IUCN [62]. In successive congress, the IUCN has incorporated resolutions about the interest of geoconservation and the need to manage it, within plans for the development of NPAs (Resolution 4040, IUCN 2008; Resolution 5048, IUCN 2012; Resolution 6083, IUCN 2016). It is moreover essential that the principles of geoconservation (**Table 2**) be implemented in the daily practice of NPA management [67, 68].

At this point, it is wise to take a closer look at current Spanish laws of nature conservation. In agreement with article 17 of the Law of Natural Heritage and Biodiversity (Law 42/2007, December, 13, BOE number 299, December, 14, 2007), the goals of Natural Resources Planning (in Spanish, PORN) include the identification and georeference of significant spaces and elements of the natural heritage of a territory. Geodiversity hot-spots [55, 69] are areas on the Earth's surface having a high geodiversity index, but also a high sensitivity index, where geodiversity provides support to biodiversity. In order to conserve geodiversity, it is moreover necessary to consider areas with a low index of geodiversity with the presence of geosites and/or geomorphosites with some heritage value. In both situations, a correct assessment of

1	The values of geodiversity and geological heritage must be recognized
2	Effective geoconservation requires a systematic approximation of all aspects of geosite identification and its management
3	Natural systems management must be a work developed in the nature
4	Natural systems and processes must be managed in a comprehensive way
5	It must be recognized that natural changes are inevitable
6	The effects of global climate change must be considered and acted upon
7	The sensitivity of natural systems must be recognized and managed in accordance with the limits of their ability to change
8	Management of the conservation of active systems must be based on knowledge of abiotic processes
9	Sensitive geosites should manage the number of visitors and promote the education and interpretation of the natural heritage as a whole
10	The interaction and interdependence of geodiversity and biodiversity must be considered in the management of the integral conservation of nature

Table 2.
The ten key points of geoconservation [67].

geodiversity is necessary. Any one of the methods mentioned in the **Table 1** may be used, though the most objective methodology is that of Pereira et al. [48] (**Figure 3** and **Table 1**), improved by subsequent authors. Thus, Araujo and Pereira [58] developed a geodiversity map of the Brazilian state of Ceará with two hot spots, one in the northwest part of the state, and another in the south, where the Global Geopark of Araripe is located. For this same territory, Bétard and Peulvast [55] show a map of the sensitivity index in which the hot-spots—also defined considering biodiversity—do not exactly coincide with those of the previous authors [58]. Nonetheless, the Araripe Geopark hot-spot is nearly coincident in the two research studies.

Mapping helps to zone and regulate land uses that would be formulated in the PORN of the NPA, and in its Plan of Use and Management (PRUG in Spanish). These documents, besides identifying the geological values, should register the risk of degradation of the NPA. In addition, they should check the state of conservation of the geodiversity, so that more adequate management and zoning can be proposed. By distinguishing areas of different geodiversity index values and geosystem services, those with a greater value come to occupy the central zone of the NPA (core zone), surrounded by zones of lesser geodiversity index values, denoted as buffer zones. The maps in **Figure 4** show the boundaries of several NPAs, including the Cazorla, Segura y Las Villas Natural Park (PNCSV), the Alto Guadalquivir Natural Place (PNAG), and the Sierra Mágina Natural Park (PNSM). In these maps it can be seen that the areas covered by these NPAs contain in their central part areas of high geomorphodiversity (PNCSV) or very high geomorphodiversity (PNSM, PNAG), which would be considered as core zones of each of these natural areas. The map of geodiversity gradients can then be confronted with biodiversity maps, affording greater precision and resolution when the limits, zoning, and uses of a territory or NPA are established [51]. Such core zones may contain geosites, to be favored by means of the protection protocols defined for the zone. If a geosite/geomorphosite is located in areas with a low geodiversity index but within a NPA, then the PORN and PRUG could set forth specific actions for the geoconservation of these geosites in view of their nonrenewable nature and according to the key principles shown in **Table 2**.

A common practice for the administrations in charge of NPAs is grouping them in networks of protected natural areas that have common objectives for conservation and management. The network could be defined as a set of natural systems most representative of the territory to which they belong or a synthesis of the best natural heritage. This concept has been developed by the administration in charge of management of the natural environment in Spain. The law governing the National Park Network (Law 5/2007, April 4, of the National Parks Network, BOE n° 81, April 4, 2007) covers the outstanding natural heritage of Spain, whether of a biological or a strictly geological character. The geological ones are defined in frameworks within the Global Geosites Project [70].

The concept of network is advantageous for the management of NPAs as they can ensure an adequate framework for the conservation of natural systems, help the integration of sustainable development models in the area of socioeconomic influence of NPAs, and contribute to raising awareness of the importance of nature conservation in society. The analysis of geodiversity and geomorphodiversity is highly useful in achieving these goals. The continuum of geodiversity or geomorphodiversity allows us to understand the distribution of biodiversity in the NPA in terms of the relationships that can be established between both [67]. On the other hand, the recognition of geodiversity/geomorphodiversity gradients provides information on the natural processes occurring in the territory of the NPA. If areas of high sensitivity are detected (geodiversity hot-spot), specific conservation measures will have to be established for them.

Where anomalies in natural geological processes are detected, specific monitoring measures should be put in place to reveal what is causing the disturbance. Specific conservation protocols will then be established. These situations are particularly easy to observe when analyzing geomorphodiversity [67], as changes in geomorphodiversity often lead to negative impacts on ecosystems and thus changes in biodiversity. It should be considered that the degradation of geomorphodiversity can lead to the development of new geomorphosites associated with new topographic, climatic, hydrological, and pedological conditions, which translate into new environmental conditions that favor the proliferation of biodiversity.

7. Conclusions

Geodiversity, understood in a broad sense, also considering geomorphodiversity, is an element of Nature that is closely related to the biotic components of ecosystems, so that no management of the natural environment can be conceived without considering the interrelations between biodiversity and geodiversity. To this goal, it must be borne in mind that the values of geodiversity (intrinsic, cultural, esthetic, economic, functional, scientific, and educational) provide criteria that support the characterization of the territory. They also help to define the geosystem services that geodiversity entails, so that, from the interaction between geosystem and ecosystem services, it is possible to analyze and design activities that enhance the socioeconomic development of the territory within a framework of sustainability. In order to make a good definition of the NPA, it is also necessary to have an assessment of geodiversity and geomorphodiversity, which provides information on the distribution of the abiotic environment that is considered in the delimitation and definition of the NPA. From this assessment, geodiversity and geomorphodiversity gradient maps are obtained that show geodiversity hot-spot and geodiversity cold-spot, areas of higher geodiversity, with special sensitivity, and areas of lower geodiversity and, therefore, with less restrictive geoconservation needs, respectively. This variability in geodiversity and, in particular, on geomorphodiversity is usually associated with biodiversity, so that areas with high geodiversity or geomorphodiversity are associated with higher biodiversity. Between geodiversity hot-spots and geodiversity cold-spots, there is a gradual transition, which materializes the continuous value of the geodiversity and geomorphodiversity of any territory, which can be an indicator of progressive biodiversity variability.

Of particular interest is the consideration of NPA networks, systems that consider that NPAs are not isolated territorial units, but are closely interrelated on the basis of their natural values (bio- and geo-diversity). The NPAs integrated in the network must be representative of the natural systems of the territory in which the network is defined. From a geodiversity perspective, the network must be based on the consideration of geological contexts (frameworks) that are representative of the main geological units observable in the territory (region, country, ...) in which the network is defined. This variability in geodiversity associated with the differences between geological units (frameworks) leads to biological diversity and the need to establish specific conservation measures (geological and biological), which must be included in the management plans of the NPAs.

Acknowledgements

This research has been funded by the Research Group RNM-200 (Andalusian Regional Government). The Natural Heritage Lab (CEACTEMA) and the research projects 06.17.02.80.AE, funded by Instituto de Estudios Giennenses, and 1380715 FEDER-UJA also have contributed.

References

[1] Nieto LM. Geodiversidad: Propuesta de una definición integradora. Boletín Geológico y Minero. 2001;**112**:3-12

[2] Gray M. Geodiversity: Valuing and Conserving Abiotic Nature. Chichester: Wiley; 2004. p. 434

[3] Carcavilla L, López-Martínez J, Durán JJ. Patrimonio geológico y geodiversidad: Investigación, conservación, gestión y relación con los espacios naturales protegidos. Madrid: IGME; 2007. p. 360

[4] Reynard E, Coratza P, Regolini-Bissing G. Scientific research on geomorphosites over the last eight years: Improvements and aims of the book. In: Reynard E, Coratza P, Regolini-Bissig G, editors. Geomorphosites. München: Verlag Dr Friedrich Pfeil; 2009. pp. 5-8

[5] Panizza M. The Geomorphodiversity of the Dolomites (Italy): A key of Geoheritage Assessment. Geoheritage. 2009;**1**:33-42. DOI: 10.1007/s12371-009-0003-z

[6] Worboys GL, Lockwood M, Kothari A, Feary S, Pulsford I, editors. Gobernanza y gestion de áreas protegidas. Canberra: ANU Press; 2019. p. 1013. DOI: 10.22459/GGAP.2019

[7] Brundtland Commission. Our Common Future [Internet]. 1987. Available from: http://www.un-documents.net. [Accessed: 2022-February]

[8] PelliteroR,González-AmuchasteguiMJ, Ruiz-Flaño P, Serrano E. Geodiversity and geomorphosite assessment applied to a natural protected area: The Ebro and Rudron Gorges Natural Park (Spain). Geoheritage. 2011;**3**:163-174. DOI: 10.1007/s12371-010-0022-9

[9] Cameron E. Outside geomorphosites. Geoheritage. 2022;**14**:13. DOI: 10.1007/s12371-022-00652-5

[10] Pereira-Balaguer L, Motta-Garcia da G M, Leite-Ribeiro de L MA. Combined assessment of geodiversity as a tool to territorial management: Application to Southeastern Coast of State of São Paulo, Brazil. Geoheritage. 2022;14:60. DOI: 10.1007/s12371-022-00696-7

[11] Brilha J, Gray M, Pereira DI, Pereira P. Geodiversity: An integrative review as a contribution to the sustainable management of the whole of nature. Environmental Science and Policy. 2018;**86**:19-28. DOI: 10.1016/j.envsci.2018.05.001

[12] Alahuhta J, Ala-Hulkko T, Tukiainen H, Purola L, Akujärvi A, Lampinen R, et al. The role of geodiversity in providing ecosystem services at broad scales. Ecological Indicators. 2018;**91**:47-56. DOI: 10.1016/j.ecolind.2018.03.068

[13] Gordon JU, Bailey JJ, Larwood JG. Conserving nature's stage provides a foundation for safeguarding both geodiversity and biodiversity in protected and conserved areas. Parks Stewardship Forum. 2022;**38**(1):46-55. DOI: 10.5070/P538156118

[14] Gray M. Geodiversity: Valuing and conserving abiotic nature. 2nd ed. Chichester: Wiley-Blackwell; 2013. p. 512

[15] Gray M. Geodiversity: The backbone of geoheritage and geoconservation. In: Reynard E, Brilha J, editors. Geoheritage. Assessment, Protection and Management. Amsterdam: Elsevier; 2018. pp. 13-25. DOI: 10.1016/B978-0-12-809531-7.00001-0

[16] Gray M. Geodiversity, geoheritage and geoconservation for society. International Journal of Geoheritage and Parks. 2019;7:226-236. DOI: 10.1016/j.ijgeop.2019.11.001

[17] Gray M. Geodiversity: A significant, multi-faceted and evolving, geoscientific paradigm rather than a redundant term. Proceedings of the Geologists' Association. 2021;**132**:605-619. DOI: 10.1016/j.pgeoIa.2021.09.001

[18] Brilha J. Inventory and quantitative assessment of geosites and geodiversity sites: A review. Geoheritage. 2016;**8**:119-134. DOI: 10.1007/s12371-014-0139-3

[19] Calvache ML, Viseras C. Long-term control mechanisms of stream-piracy processes in southeast Spain. Earth Surface Processes and Landforms. 1997;**22**:93-105. DOI: 10.1002/(SICI)109-9837

[20] Carruana-Herrera D, Martínez-Murillo JF. Valoración de la geodiversidad del Parque Natural y Geoparque de las Sierras Subbéticas (Córdoba, sur de España). Cuaternario y Geomorfología. 2020;**34**(1-2):5. DOI: 10.17735/cyg.v34i1-2.75529

[21] Gill JC. Geology and the sustainable development goals. Episodes. 2017;**40**(1):70-76. DOI: 10.18814/epiiugs/2017/v40i1/017010

[22] Schrodt F, Bailey JJ, Kissling WD, Rijsdijk KF, Seijmonsbergen AC, van Ree D, et al. To advance sustainable stewardship, we must document not only biodiversity but geodiversity. Proceedings of the National Academy of Sciences. 2019;**116**(33):16155-16158. DOI: 10.1073/pnas.1911799116

[23] Prikryl R. Geomorphosites and quarries. In: Reynard E, Coratza P, Regolini-Bissig G, editors. Geomorphosites. München: Verlag Dr Friedrich Pfeil; 2009. pp. 225-233

[24] Millenium Ecosystem Assessment. Ecosystems and Human well-being: A framework for assessment [Internet]. 2005. Available from: https://wedocs.unep.org/20.500.11822/8768. [Accessed: 2022-June-2]

[25] Gray M. Other nature: Geodiversity and geosystem services. Environmental Conservation. 2011;**38**:271-274. DOI: 10.1017/S0376892911000117

[26] Gray M, Gordon JE, Brown EJ. Geodiversity and the ecosystem approach: The contribution of geoscience in delivering integrated environmental management. Proceedings of the Geologists' Association. 2013;**124**:659-673. DOI: 10.1016/j.pgeola.2013.01.003

[27] Diaz S, Demissew S, Carabias J, Joly C, Lonsdale M, Ash N, et al. The IPBES conceptual framework – Connecting nature and people. Current Opinion in Environmental Sustainability. 2015;**14**:1-16

[28] Haines-Young R, Potschin M. Common International Classification of Ecosystem Services (CIDES) V5.1: Guidance on the Application of the Revised Structure [Internet]. 2018. Available from: http://www.cices.eu. [Accessed: 2020-February-15]

[29] Van Ree CCDF, Beukering PJH. Geosystem services: A concept in support of sustainable development of the subsurface. Ecosystem Services. 2016;**20**:30-36. DOI: 10.1016/j.ecoser.2016.06.004

[30] Gordon JE, Barron HF. Scotland's geodiversity: Development of the basis for a National framework. Scottish Natural Heritage Commissioned Report. 2011. p. 417

[31] Gordon JF, Barron HF. Valuing geodiversity and geoconservation: Developing in more strategic ecosystem approach. Scottish Geographical Journal. 2012;**128**:278-297. DOI: 10.1080/14702541.2012.725861

[32] Gordon JE, Barron HF, Hanson JD, Thomas MF. Engaging with geodiversity – Why it matters. Proceedings of the Geologists' Association. 2012;**123**:1-6. DOI: 10.1016/j.pgeola.2011.08.002

[33] Panizza M, Piacente S. Cultural geomorphology and geodiversity. In: Reynard E, Coratza P, Regolini-Bissig G, editors. Geomorphosites. München: Verlag Dr Friedrich Pfeil; 2009. pp. 35-48

[34] Dingwall PR. Legislation and international agreements: The integration of the geological heritage in nature conservation policies. In: Barettino D, Wimbledon WAP, Gallego E, editors. Geological Heritage: Its Conservation and Management. Madrid: ITGE; 2000. pp. 15-28

[35] Matthews TJ. Integrating geoconservation and biodiversity conservation: Theoretical foundations and conservation recommendations in a European Context. Geoheritage. 2014;**6**:57-70. DOI: 10.1007/s12371-013-0092-6

[36] Pemberton M. Conserving geodiversity, the importance of valuing our geological heritage. National Conference, Geological Society of Australia Inc [Internet]. 2001. Available from: https://dpipwe.tas.gov.au/Documents/geocon_abstract.pdf. [Accessed: 2019-December-14]

[37] Peña L, Monge-Ganuzas M, Onaindia M, Fernández de Manuel B, Mendia M. A holistic approach including biological and geological criteria for integrative management in protected areas. Environmental Management. 2017;**59**:325-337. DOI: 10.1007/s00267-016-0781-4

[38] Crofts R, Tormey D, Gordon JE. Introducing new guidelines on geoheritage conservation in protected and conserved areas. Geoheritage. 2021;**13**:33. DOI: 10.1007/s1237-021-00552-0

[39] Gaia LJ. Una nueva visión de la vida sobre la Tierra. Barcelona: Orbis; 1979. p. 126

[40] Lovelock J. The ages of Gaia. 2nd ed. Oxford: Oxford University Press; 1995. p. 255

[41] Lohmann G, Grosfeld K, Wolf-Gladrow D, Unnitham V, Notholt J, Wegner A. Earth System Science: Bridging the Gaps Between Disciplines. Berlín: Springer Briefs in Earth Sciences; 2013. p. 134. DOI: 10.1007/978-3-642-32235-8

[42] Kump LR, Kasting JF, Crane RG. The Earth System. 3rd ed. Harlow: Pearson; 2014. p. 432

[43] Stanley SM. Earth System History. 4th ed. New York: Freeman and Company; 2015. p. 624

[44] Anderson MG, Ferree CE. Conserving the stage: Climate change and the geophysical underpinnings of species diversity. PLoS One. 2010;**5**:e11554. DOI: 10.1371/journal.pone.0011554

[45] Richards K, Brasington J, Hughes F. Geomorphic dynamics of floodplains: Ecological implications and a potential modelling strategy. Freshwater Biology. 2002;**47**:559-579. DOI: doi.org/10.1046/j.1365-2427.2002.00920.x

[46] Serrano E, Ruiz-Flaño P. Geodiversidad: Concepto, evaluación y

aplicación territorial. El caso de Tiermes Caracena (Soria). Boletín de la AGE. 2007;**45**:79-98

[47] Lane SN, Tayefi V, Reid SC, Yu D, Hardy RJ. Interactions between sediment delivery channel change, climate change and flood risk in a temperate upland environment. Earth Surface Process Landforms. 2007;**32**:429-446. DOI: 10.1002/esp.1404

[48] Pereira DI, Pereira P, Brilha J, Santos L. Geodiversity assessment of Paraná State (Brazil): An innovative approach. Environmental Management. 2013;**52**:541-552. DOI: 10.1007/s00267-013-0100-2

[49] Benito-Calvo A, Pérez-González A, Magri O, Meza P. Assessing regional geodiversity: The Iberian Península. Earth Surface Processes and Landforms. 2009;**34**:1433-1445. DOI: 10.1002/esp.1840

[50] Forte JP, Brilha J, Pereira DI, Nolasco M. Kernel density applied to the quatitative assessment of geodiversity. Geoheritage. 2018;**10**:205-2017. DOI: 10.1007/s12371-018-0282-3

[51] Fernández A, Fernández T, Pereira DI, Nieto LM. Assessment of geodiversity in the Southern part of the Central Iberian Zone (Jaén Province): Usefulness for delimiting and managing Natural Protected Areas. Geoheritage. 2020;**12**:20. DOI: 10.1007/s12371-020-00447-6

[52] Nobre da Silva ML, Leite do Nascimento MA, Mansur KL. Quantitative assessments of geodiversity in the area of the Seridó Geopark Project, Norteast Brazil: Grid and Centroid analysis. Geoheritage. 2019;**11**:1177-1186. DOI: 10.1007/s12371-019-00368-z

[53] Ruban DA. Quantification of geodiversity and its loss. Proceedings of the Geologists' Association. 2010;**121**:326-333. DOI: 10.1016/j.pgeola.2010.07.002

[54] Hjort J, Luoto M. Geodiversity of high-latitude landscape in northern Finland. Geomorphology. 2010;**115**:109-116. DOI: 10.1016/j.geomorph.2009.09.039

[55] Bétard F, Peulvast JP. Geodiversity Hotspots: Concept, method and cartographic application for geoconservation purposes at a regional scale. Environmental Management. 2019;**63**:822-834. DOI: 10.1007/s00267-019-01168-5

[56] Silva JP, Rodrigues C, Pereira DI. Mapping and analysis of geodiversity indices in the Xingu River Basin, Amazonia Brazil. Geoheritage. 2015;**7**:337-350. DOI: 10.1007/s12371-014-0134-8

[57] Silva JP, Pereira DI, Aguiar AM, Rodrigues C. Geodiversity assessment of the Xingu drainage basin. Maps. 2013;**9**:1-9. DOI: 10.1080/17445647.2013.775085

[58] Araujo AM, Pereira DI. A new methodological contribution for the geodiversity assessment: Applicability to Ceará State (Brazil). Geoheritage. 2018;**10**:591-605. DOI: 10.1007/S12371-017-0250-3

[59] Hengl T. Finding the right pixel size. Computer & Geosciences. 2006;**32**(9):1283-1298. DOI: 10.1016/j.cageo.2005.11.008

[60] Zwoliński Z, Najwer A, Giardino M. Methods for assessing geodiversity. In: Reynard E, Brilha J, editors. Geoheritage. Assessment, Protection and Management. Amsterdam: Elsevier; 2018. pp. 27-51. DOI: 10.1016/B978-0-12-809531-7.00002-2

[61] Henriques MH, Pena Do Reis R, Brilha J, Mota T. Geoconservation as an emerging geoscience. Geoheritage. 2011;**3**:117-128. DOI: 10.1007/s12371-011-0039-8

[62] Gordon JE, Crofts R, Díaz-Martínez E, Woo KS. Enhancing the role of geoconservation in protected area management and nature conservation. Geoheritage. 2018a;**10**:191-203. DOI: 10.1007/s12371-017-0240-5

[63] Gordon JE, Crofts R, Díaz-Martínez E. Geoheritage conservation and environmental policies: Retrospect and prospect. In: Reynard E, Brilha J, editors. Geoheritage. Assessment, Protection and Management. Amsterdam: Elsevier; 2018b. pp. 213-229. DOI: 10.1016/B978-0-12-809531-7.00012-5

[64] Nieto LM, Pérez-Lorente F, Guillén-Mondéjar F, Díaz-Martínez E. Estado actual de la legislación para la Geoconservación en España. Trabajos de Geología. 2006;**26**:187-201

[65] Carcavilla L, Durán JJ, García-Cortés A, López-Martínez J. Geological heritage and geoconservation in Spain: Past, present, and future. Geoheritage. 2009;**1**:75-91

[66] Brilha J. Geoheritage and geoparks. In: Reynard E, Brilha J, editors. Geoheritage. Assessment, Protection and Management. Amsterdam: Elsevier; 2018. pp. 323-335. DOI: 10.1016/B978-0-12-809531-7.00018-6

[67] Gordon JE. Geoconservation principles and protected area management. International Journal of Geoheritage and Parks. 2019;**7**:199-210. DOI: 10.1016/j.ijgeop.2019.12.005

[68] Woo KS, Worboys G. Geological monitoring in protected areas. International Journal of Geoheritage and Parks. 2019;**7**:218-225. DOI: 10.1016/j.ijgeop.2019.12.004

[69] Gray M. Geodiversity: Developing the paradigm. Proceedings of the Geologists' Association. 2008;**119**:287-298. DOI: 10.1016/S0016-7878(08)80307-0

[70] García-Cortés A, Rábano I, Locutura J, Bellido F, Fernández-Gianotti J, Martín-Serrano A, et al. First Spanish contribution to the Geosites Proyect: List of the geological frameworks established by consensus. Episodes. 2001;**24**(2):79-92

Chapter 2

Genetic Algorithm Based Software for Optimization and Design of Piles on Slopes

Bhargav Jyoti Borah and Sasanka Borah

Abstract

Landslides in layered soil in slopes is a common phenomenon that leads to major damages to infrastructures. Piles are deep foundations which are useful structural elements to support heavy loads in difficult slopes, and to retain creeping or sliding slopes. Controlling the stability of structures made on slopes is still one of the major problems in engineering. Piles are being used successfully to support structures on slopes and have become an efficient solution for such situations which demands construction on sloping grounds, since piles can often be easily installed without disturbing the equilibrium of the layers of soil in the slope. In this paper, an optimized design approach have been adopted for design of single piles for supporting infrastructure on layered soil slopes. A standalone software has been developed as a result of this study which produces the optimum pile dimension, reinforcement details and an estimate of the design as software output. The code is written in MATLAB that incorporates Genetic Algorithm (GA) optimization technique to obtain optimum pile dimensions and the pile is designed satisfying all the structural requirements as recommended by IS:2911: Indian Standards Code for cast-in-situ Reinforced Concrete pile.

Keywords: piles on slopes, computer aided design of pile foundations, deep foundation, GA, MATLAB software, optimization algorithm

1. Introduction

Piles are deep foundations which are introduced into the soil by suitable means to support the load coming on it from the superstructure when a good bearing stratum is not available at shallow depths from the ground surface [1]. In such situations load have to be transmitted to a firm strata which is capable of supporting such tremendous loads at an appreciable deeper depth below the ground surface. Piled structures are often subjected to significant lateral loads in addition to the vertical load coming from the superstructure which are installed in soil layers present in sloping grounds. The varying properties of multi-layer soil in the slopes may further complicate the stability issue of the structure.

In this research, the model superstructure considered on multi-layer soil slope is as per Indian standards recommendation [2]. Indian standards guidelines have been followed for the design of pile foundation in the soil slope. Indian Standards [3–6] classifies Concrete Piles as Driven Cast-In situ piles, Bored Cast In-situ piles, Driven Precast piles and Precast piles in Pre-bored Holes. The Load Bearing capacity of the pile is dependent on the material used and the dimensions of the pile foundation, the spacing of individual piles in the pile group, the load bearing capacity and nature of the supporting soil. The pile installation method, and the direction of incoming loading [7] also plays a significant role in determining the load bearing capacity of the pile foundation. The load bearing capacity of the soil slope is affected by many factors such as type of the soil in each layer of the slope and strength of soil in these soil layers, foundation dimensions, unit weight of the soil, surcharge acting on the soil, the type of loading etc. [1]. The variability of the properties of the supporting soil, soil profiles and properties of the soil in these multi-layered soil profiles, which generally exists in nature, affects the load bearing capacity of the pile drastically. The choice of a pile to be used is governed by the condition of the site, economy, time available etc. The problem of landslides is also a major consideration for stability of a structure on sloping grounds. Hence, in order to counter these problems which have a large number of variability associated with them, the aid of modern high-speed computers and software has become popular.

Conventional design method for pile foundations involves determining the load carrying capacity of pile foundations from Static method, Dynamic method, Pile load test method or Penetration Test method depending upon the situation giving due consideration to data obtained from soil exploration reports. The pile foundation or group of piles are designed in such a way so as to transfer the load to the supporting soil safely giving due consideration to the load coming from the superstructure. For the design consideration of geotechnical design of the pile, the Ultimate Load Carrying Capacity and the Allowable Load Carrying Capacity is taken into consideration whereas for the structural design of the foundation, the bearing capacity, driving and handling stresses of the pile foundation is taken into consideration. Design of Pile Foundation is generally a trial-and-error process. Here an initial trial design (foundation dimensions and reinforcements) is taken and is checked against the geotechnical and structural requirements. This is done iteratively to revise the trial designs till a practical design of pile foundation is obtained. The drawback of this general method is that with these methods, the design of the pile foundation often comes out to be a conservative one. Generally such a conservative design may lead to an uneconomical and an impractical design. In a general optimization approach for design of a pile foundation, an optimization algorithm is used. A well calibrated optimization method may confirm an economic and a practical pile foundation design. In optimized design method of design for single piles the Ultimate Bearing Capacity of the pile is evaluated within stipulated limits by changing the pile dimensions iteratively until an optimized pile dimension is found to support the total incoming load. The pile is then designed structurally for bearing the loads acting on the pile satisfying all the structural requirements, may it be for vertical loading or lateral loading.

Complex studies have been carried out based on experimental and numerical investigations of piles installed in sloping grounds. But the research done in foundation engineering for the application of optimization methods using Computer Aided Design methods for structures on sloping grounds is scarce. The available research that deals with pile design optimization, assume different methodology with a number of assumptions which cannot involve all the practical parameters and thus have limited practical applications for supporting structures on sloping grounds.

Borah and Borah [1] has adopted a GA based optimization algorithm for optimization and design of Vertical piles on horizontal grounds with the Ultimate bearing capacity being the objective function and the pile dimensions as the design variables. Hoback and Truman [8] have introduced a weightless optimality rule into the original optimality criteria approach to address the design variables- the spacing and battering of the piles that has no measurable effect on the objective function. Huang and Hinduja [9] adopted a quasi-Newton method for optimizing the shape of piles. Their algorithm includes a linear force–deflection relationship for the pile-soil system while optimizing the pile design. Nikolaou and Pitilakis [10] developed a stand-alone program based on MATLAB. The have included algorithm for the calculation of bearing capacity and settlements of shallow foundations using several well-known formulas. They have utilized various literature and codes of practice that are preferred in engineering.

In this paper, the research done in Borah and Borah [1] has been taken as the base for the development of a Genetic Algorithm based software code for optimization and design of concrete cast in situ pile in a multi-layer soil slope. The Genetic Algorithm (GA) is used to optimize the pile dimensions based on Indian Standards [4–7] methodology within recommended limits and user defined practical specifications. The piles designed by the software takes into account the lateral load and the lateral moment, along with the vertical loading and moment coming from the superstructure, which will be unique for piles on sloping grounds with multiple layers of soil. A software has been developed using MATLAB coding for automating the entire process of design and optimization. An estimate [11] for construction is also presented which may further ease the choice of selection of a particular design.

2. Methodology

2.1 General

In this study a genetic algorithm (GA) has been developed for optimization and design of a pile foundation on sloping ground. The Optimization method used for optimization in the said software is genetic algorithm (GA). Genetic algorithm (GA) is a search-based optimization technique that works on the principles of Genetics and Natural Selection which is used to find optimal solutions to difficult problems which otherwise would take a considerable amount of time to solve [1]. It is generally used for solving optimization problems in research. The Pile Design, both geotechnical and structural, is as per Indian standards code [4–7, 12, 13] based design method. A preliminary estimate of conceptual design is also presented which is as per Assam Public Works Department Schedule of Rates [11]. MATLAB which is a programming software has been used to develop the interface of the stand-alone software and codes in this study.

2.2 Genetic algorithm

The Genetic Algorithm (GA) is a stochastic search-based optimization algorithm which mimics the process of evolution that includes natural selection. It is commonly used for nonlinear optimization problems. On the other hand, gradient based methods can be applied to linear optimizations due to certain defects in accuracy of the objective function [1]. The Genetic algorithm involves processes of selection, crossover, and mutation of the trial solutions so as to improve the set of solutions and converge towards an optimal solution. Each solution in every generation consists of a set of parameters, and by manipulating these parameters the Genetic Algorithm (GA) converges towards the best possible solution. In Genetic Algorithm (GA), a population of solutions, also referred to as individuals are generated. For a given optimization problem, a set of potential solutions are initially generated, also known as the first generation. Within each population, every solution or individual is assigned a corresponding fitness value which is obtained by calculating a fitness function. The fitness value ranks the fitness or appropriateness of a solution. Within each population, some solutions based on their fitness are chosen to carry forward to the next generation of solutions as clones of the original solution. These solutions thus guarantee with the best fitness value of each generation will be maintained or manipulated to be improved upon from one generation to another, while providing better quality of said parameters within a population.

Crossover represents a reproduction function. It means that for each generation, a smaller group of solutions is selected to combine the parameters associated with them and create new solutions, and these new solutions are the new generation of solutions. The group that crosses over are called parents, and the "genes" of two (or more) such parent solutions are combined to generate one (or more) new solution, as their child. It is these children that make up a new generation of solutions. These new generation of solution is expected to be better in terms of fitness as they are made from parents having best fitness in their respective generation [1].

Each solution are then subjected to mutations. It is a random change in one or more parameters (genes) of a solution based on some probability. This probability is known as the mutation rate [1]. Mutations is a must to maintain and introduce diversity into a population of solution. With more diversity in the population, the genetic algorithm lowers the risk of ending up with a solution in the sub-optimal local minima. A flowchart of the simple version of Genetic Algorithm (GA), explaining its process is shown in **Figure 1**.

2.3 Design considerations

IS 2911(Part 1/Sec 2): 2010 [5] recommends that the design of a pile foundation should be in such a way that the incoming load from the super structure can be transmitted to the sub-surface safely with appropriate factor of safety. This Factor of safety is against shear failure of sub-surface and without causing excessive settlement (differential or total). The shaft of the pile should have adequate structural capacity to withstand all types of incoming loads, may it be vertical, axial or otherwise and incoming moments which is to be transmitted to the supporting subsoil. The Pile should be structurally complying with the design recommendations given in IS 456: 2000 [13].

2.4 Pile capacity

In this study the ultimate load capacity of a pile foundation is obtained by using a static analysis methodology recommended by IS 2911(Part 1/Sec 2): 2010 [5]. The Load Carrying Capacity of the pile depends on the of the supporting soil properties of various layers of the supporting soil in which the pile is installed. The minimum factor of safety on static formula is taken to be 2.5 as is recommended by the code, IS 2911 (Part 1/Sec 2): 2010 [5].

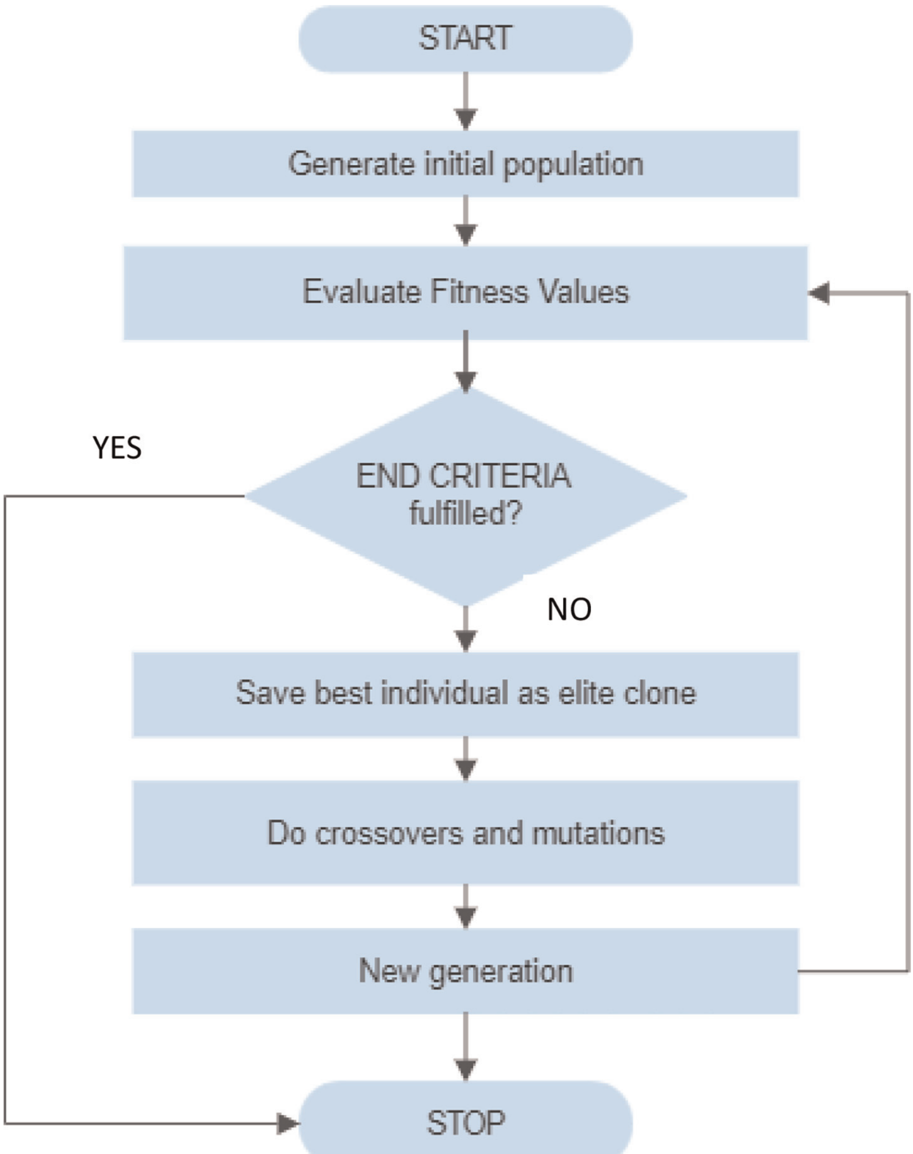

Figure 1.
Basic genetic algorithm (GA) flow chart.

2.5 Analysis of laterally loaded piles

A pile foundation which is subjected to lateral forces from a number of sources, such as, wind, earthquake, water current, earth pressure, effect of moving vehicles or ships, plant and equipment, etc. [5]. The lateral load carrying capacity of a pile foundation depends on the horizontal sub-grade modulus of the supporting soil and on the structural capacity of the shaft of the pile against bending. While considering lateral load on pile foundations, the effect of other loads acting on the pile foundation, like the axial load coming from the super structure, is to be taken into consideration.

The IS code [5] suggests that a group of three or more pile connected by a rigid pile cap is considered to have a fixed head condition. In all other cases the pile foundation is taken to be free headed.

2.6 Structural capacity

The IS code [5] suggests that the pile foundation should have necessary structural strength to transmit the imposed loads safely and ultimately to the supporting soil.

2.7 Estimation

An estimate of the pile foundation designed by the algorithm is generated by the software. In this study the software generates the design of the pile foundation as the output which includes the structural details of the pile foundation and various specifications that will be required in its construction. The structural design generated by the software serves as the drawing for estimation, the other concrete and steel parameters along with workmanship requirements specified by Indian Standards [5] are considered and the Schedule of Rates [11] provided by the Assam Public Works Department, provides the Rate of Items associated with the design.

3. Results and discussions

3.1 Software

The software which is developed in this research has been designed to optimize pile dimensions based on the incoming load (axial, eccentric and lateral) from the super structure and the supporting soil parameters of sloping ground. The software developed allows user to use optimized results generated by the software to design the pile foundation structurally or alternatively allow user input data for design of the pile foundation. All pile foundation design procedure has been adopted as per guidelines provided by Indian Standards code [4–7, 12, 13] on sloping grounds. A detailed step by step procedure for using this software for optimization and design of pile foundation based on the parameters of soil layers on sloping ground is given below:

1. Under the section named 'OPTIMIZATION' the user has to select the optimization technique, here, 'GA' is selected from the drop down list provided.

2. Under the section of 'OPTIMIZATION PARAMETERS FOR PILE' the user provides the Minimum diameter of the pile in mm, Maximum diameter of the pile in mm, Minimum Length of the pile in m, Maximum Length of the pile in m for the pile on the sloping ground. The Bi-axial Moment acting in x- direction and y- direction respectively in kNm and the incoming Column Load in kN are entered by the user.

3. Next, the number of soil layers of stratified soil are selected by selecting the radio buttons (viz. 1, 2, 3) provided in the 'SOIL PARAMETERS' section representing the soil layers on the sloping ground.

4. Based on the number of soil layers on the sloping ground the software highlights the particular layers for which soil parameter inputs are required. Here three numbers of soil layer on the sloping ground has been selected. Hence the software opts for soil parameters of these three soil layers only.

5. Under the section named 'Layer', the user needs to select the Soil type for each soil layer on the sloping ground. The software highlights the soil parameters required for that particular soil layer selected. Here Cohesive soil type has been selected for Layers 1, 2 and 3.

6. The 'Layer length' in m is entered by the user. The user enters the effective unit weight of the soil at pile tip (y), in kN/m^3; the coefficient of earth pressure applicable for the ith layer (Ki); the angle of wall friction between pile and soil for the ith layer (phi) in degrees for Granular soil layer. The user also enters the average cohesion at pile tip (cp), in kN/m^2; the adhesion factor for the ith layer depending on the consistency of soil (alpha), the average cohesion for the ith layer (ci), in kN/m^2 for cohesive soils. Here, for layer 3, which is a cohesive soil layer, the software opts the user to enter cp = average cohesion at pile tip, in kN/m^2; alpha = adhesion factor for the 1st, 2nd and 3rd layers of the soil respectively, ci = average cohesion for the 1st, 2nd and 3rd layers, in kN/m^2 for cohesive soil respectively.

7. The software takes up all the input parameters and uses the Genetic Algorithm (GA) for performing a number of iterations to obtain the optimized pile dimensions within the limits specified by the user. The Optimized results are displayed under the section 'OPTIMIZED RESULTS OF PILE' as Length of pile in m and Diameter of pile in mm.

8. User may then opt to use the optimized pile dimension by checking the check box 'Use Optimized Parameters for Design' under 'STRUCTURAL DESIGN PARAMETERS FOR REINFORCED CONCRETE PILE' section or enter the Length and diameter of the pile under the same section. Here the optimized parameters has been used for design.

9. If the user decides not to use the optimized parameters, user may enter the Vertical Load in kN, Effective eccentricity of vertical load in mm, Lateral Load in kN, Point of Lateral Load application from Ground Level in m and Modulus of sub-grade reaction in MN/m^3 for the pile foundation. The user has to select the Grade of Steel in N/mm^2, Grade of concrete in N/mm^2, Clear Cover in mm, Cover to reinforcement in mm, Diameter of Longitudinal bars in mm and Diameter of tie bars in mm from the respective drop down lists provided under the section 'STRUCTURAL DESIGN PARAMETERS FOR REINFORCED CONCRETE PILE'. The parameters used in this example are represented in **Figure 2**.

10. The software developed in this study then generates the Design results under 'PILE DESIGN RESULT' section with a Detailed Drawing of the pile.

11. Under the section of 'ESTIMATED COST ', the Schedule of Rates is to be selected by the user from the drop down list provided. The software generates an estimated cost of the pile in Rupees based on the results generated.

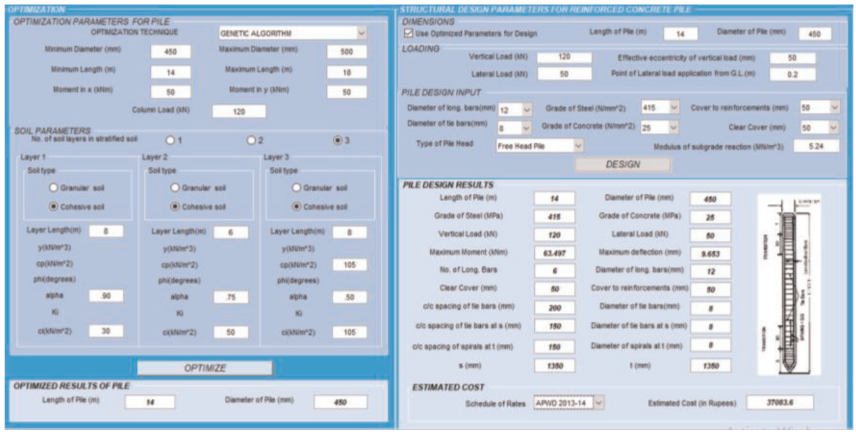

Figure 2.
Software interface.

A stand-alone software is coded with the use of MATLAB Compiler to allow users without a MATLAB license to install and run the software on different operating platforms.

The entire process is summarized in the flow diagram (see **Figure 3**).

3.2 Calibration of software

A few numerical examples [14–16] were taken from for calibrating the software developed in this study. Methodology discussed in the previous section has been adopted for optimization and design of the pile foundation on sloping ground. The results obtained by the software, by using the parameters given in these numerical problems, are then verified manually.

The basic form of the Genetic Algorithm (GA) used while developing the software is as follows:

Optimize:

$$Q_u = A_p\left(\frac{1}{2}\, D_\gamma\, N_\gamma + P_D N_q\right) + \sum_{i=0}^{n} K_i P_{Di} \tan \delta_i A_{si} \tag{1}$$

$$\text{or } Q_u = A_p N_C\, c_p + \sum_{i=0}^{n} \alpha_i\, c_i\, A_{si} \tag{2}$$

Based on the nature of the soil layers on sloping ground. The first term is the end-bearing resistance (Qp) and the second term is the skin friction resistance (Qs).

Subject to the constraints:

1. The Ultimate Load Bearing Capacity of the pile on sloping ground (Qu) ≥ 2.5 x Incoming Column Load (Q).

2. The Optimized Length of pile (L) on the sloping ground in m ≥ Minimum Length of pile (Lmin) in m and Optimized Length of pile (L) in m ≤ Maximum Length of pile (Lmax) in m.

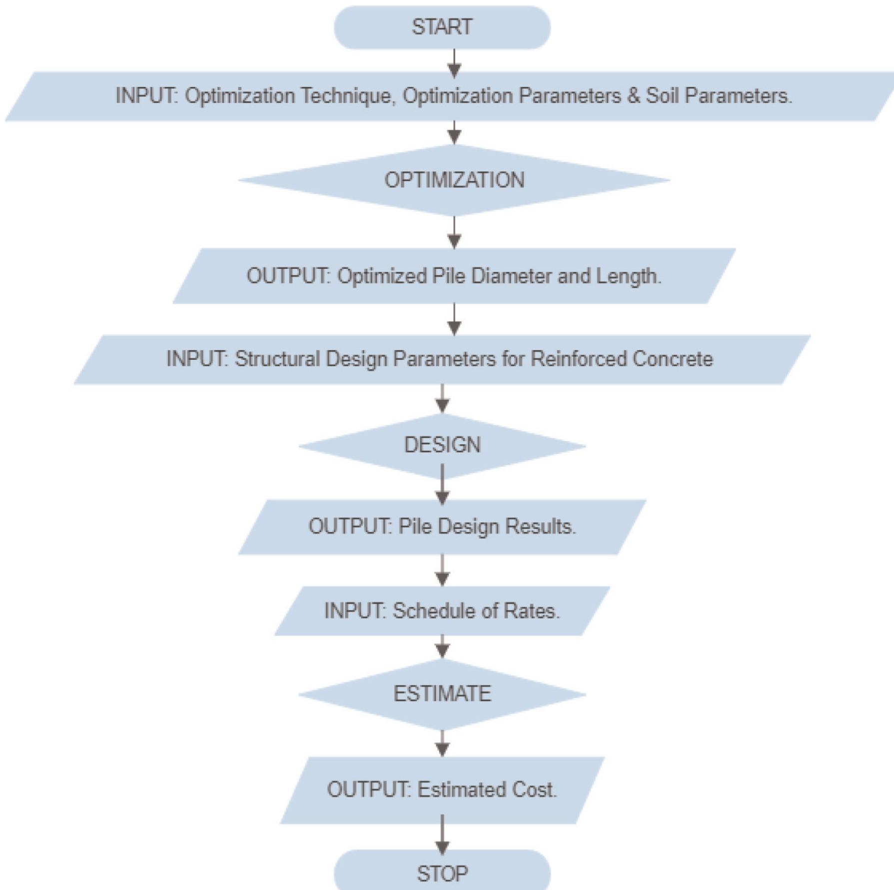

Figure 3.
Flow diagram depicting pile foundation optimization and design process.

3. The Optimized Diameter of pile (D) on the sloping ground in mm ≥ Minimum Diameter of pile (Dmin) in mm and Optimized Diameter of pile (D) in mm ≤ Maximum Diameter of pile (Dmax) in mm.

4. Optimized Length of pile (L) on sloping ground in m > 0.

5. Optimized Diameter of pile (D) on sloping ground in mm > 0.

The results of software developed in this study are verified manually and the results tallies. Hence the working process of the software has been calibrated with those of a standard.

3.3 Findings and interpretations

Based on the Results obtained from the software in this study and subsequent manual verification of the results, it can be inferred that (**Figures 4–6**):

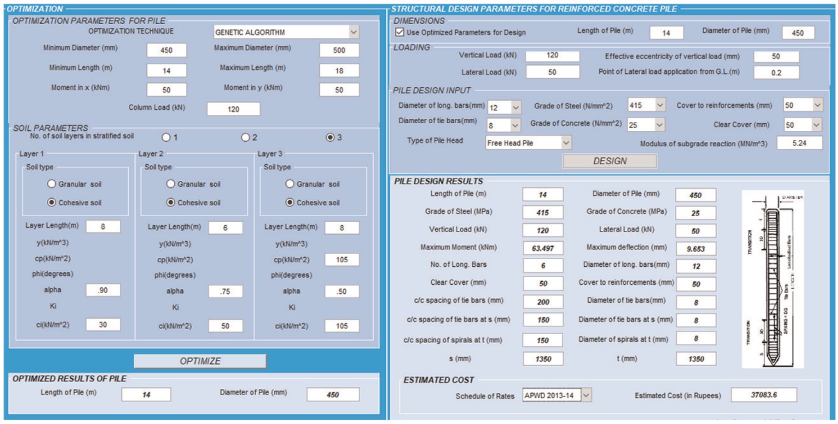

Figure 4.
Optimization and design results for three layers of soil.

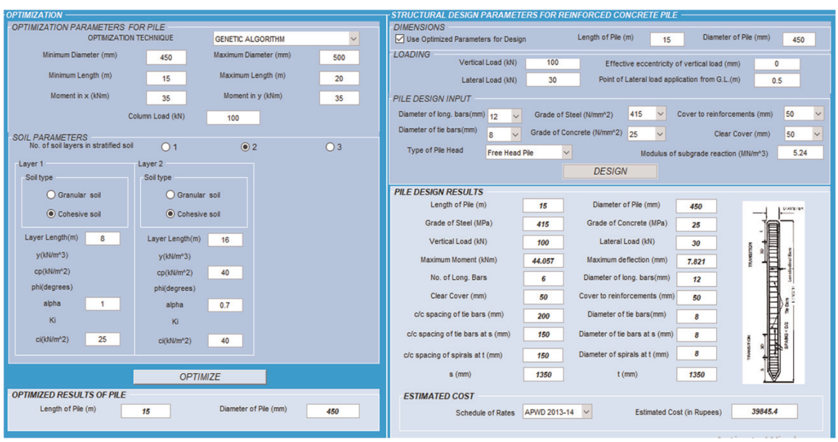

Figure 5.
Optimization and design results for two layers of soil.

1. The software developed in this study is capable of using a Genetic Algorithm for optimization of Geotechnical Design parameters of a pile foundation on sloping grounds based on the input set of variables representing the supporting soil parameters on sloping grounds.

2. The software developed in this study is capable of automating Optimization process by using code replicating the actual optimization process of piles on sloping grounds.

3. The software developed in this study generates the Structural design of pile foundation on sloping grounds by using optimized design results and/or user defined parameters for design of piles.

4. The software developed in this study is capable of generating Structural details of piles based on the recommendations of all Indian Standards [5, 12, 13, 17, 18] specifications.

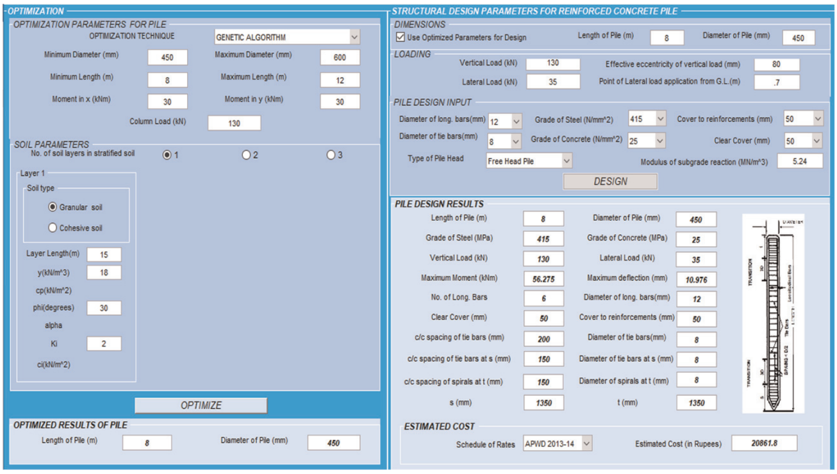

Figure 6.
Optimization and design results for single layer of soil.

5. The software developed in this study provides a user friendly interface for providing a real time optimization and design environment for Engineers.

6. The software developed in this study provides users partial or full control over the entire Optimization and Design process of the pile foundation on sloping grounds.

7. The software developed in this study is also capable of generating preliminary estimates of pile foundation design that is obtained from the software itself, thus providing better options while selecting a particular design for implementation.

4. Conclusion

The software developed through this study has adopted the design methodology and constraints considering all the variables involved in pile foundation design and construction recommended by Indian Standards code [4, 5, 6, 7, 12], which is widely used in practice in India. The software developed in this study lets user generate designs for an optimized pile foundation on sloping grounds. The software can also be used for generating structural design of a pile foundation subjected to lateral loading in addition to vertical loading. The said software takes into account the variability of soil layer parameters on sloping grounds thus enhancing the scope for further research into the code for countering complex practical problems. Due to its simplicity and user friendly interface it may cater to shorten the gap between conceptual optimization and design outputs and the actual field applicability of piles on slopes. The software also provides an estimate of the design produced so as to allow the designer to better judge the practical applicability of a particular design. Through this study an attempt has been made to bridge the gap between research and field application of an optimized foundation design on sloping grounds and incorporating computer coding to develop an application to simplify user experience.

References

[1] Borah BJ, Borah S. Genetic algorithm based optimization and Design of Pile Foundation. In: Satyanarayana Reddy CNV, Muthukkumaran K, Satyam N, Vaidya R, editors. Ground Characterization and Foundations. Lecture Notes in Civil Engineering. Vol. 167. Singapore: Springer; 2022

[2] IS 14343 (Part 2): Seclection and Development of Site for Building in Hill Areas — Guidelines —Selection and Development. New Delhi: Bureau of Indian Standards; 1995

[3] IS 2911 (Part 1/Sec 1): Design and Construction of Pile Foundations — Code of Practice Part 1 Concrete Piles Section 1 Driven Cast In-Situ Concrete Piles. New Delhi: Bureau of Indian Standards; 2010

[4] IS 2911 (Part 1/Sec 2): Design and Construction of Pile Foundations — Code of Practice Part 1 Concrete Piles Section 2 Bored Cast In-Situ Concrete Piles. New Delhi: Bureau of Indian Standards; 2010

[5] IS 2911 (Part 1/Sec 3): Design and Construction of Pile Foundations — Code of Practice Part 1 Concrete Piles Section 3 Driven Precast Concrete Piles. New Delhi: Bureau of Indian Standards; 2010

[6] IS 2911 (Part 1/Sec 4): Design and Construction of Pile Foundations — Code of Practice Part 1 Concrete Piles Section 4 Precast Concrete Piles in Pre-Bored Holes. New Delhi: Bureau of Indian Standards; 2010

[7] Abdurrahman S. Mathematical models and solution algorithms for computational design of RC piles under structural effects. Applied Mathematical Modelling. 2011;**35**(1):3611-3638

[8] Hoback AS, Truman KZ. Least weight design of steel pile foundations. Engineering Structures. 1993;**15**(5): 379-385

[9] Huang Z, Hinduja S. Shape optimization of a foundation for a large machine tool. International Journal of Machine Tool Design and Research. 1986;**26**(2):85-97

[10] Nikolaou K, Pitilakis D. SoFA: A matlab-based educational software for the shallow foundation analysis and design. Computer Applications in Engineering Education. 2017;**25**(2): 214-221

[11] Assam Public Works Department Schedule of Rates 2013–14 (Building). Assam: Commissioner & Special Secretary, Public Works Department; 2013

[12] IS 6403: Indian Standard Code of Practice for Determination of Breaking Capacity of Shallow Foundations. New Delhi: Bureau of Indian Standards; 1981

[13] IS 456: Plain and Reinforced Concrete Code of Practice. New Delhi: Bureau of Indian Standards; 2000

[14] Murthy VNS. Textbook of Soil Mechanics and Foundation Engineering. 2nd ed. New Delhi: CBS Publishers & Distributors; 2009

[15] Punmia BC, Jain AK, Jain AK. Soil Mechanics and Foundations. 16th ed. Guwahati: Laxmi Publications (P) Ltd.; 2014

[16] Ranjan G, Rao ASR. Basic and Applied Soil Mechanics. 2nd ed. Guwahati: New Age International Publishers (P) Ltd.; 2014

[17] SP:16: Design Aids for Reinforced Concrete to IS: 456-l978. New Delhi: Bureau of Indian Standards; 1987

[18] SP:34 (S&T): Handbook on Concrete Reinforcement and Detailing. New Delhi: Bureau of Indian Standards; 1987

Chapter 3

Slope Stability Analyses Subjected to Slide Head Toppling Failure Mechanisms

Victor Mwango Bowa and Abdul Samson

Abstract

It is faulty to analyze the jointed rock slopes' stability susceptible to a combination of modes of failure composed of sliding around the toe region and toppling of the rock blocks on the upper part of the slope based on the current analytical methods, which are based on assumption that the distribution of the potential failure surface bounding the potential mixed failure runs predictably from crest to toe of the slope. An Analytical model that takes into consideration the kinematic mechanism of the discontinuous rock slope with counter-tilted weak plane subjected to a combination of failure mechanisms involving sliding and toppling has hence been presented in this chapter. This involves an iterative process which involves the calculations of the dimensions of all the individual blocks as well as the forces acting on them, and then stability of every block is examined, starting at the uppermost block. The stability analysis of each block is determined. The blocks may either be stable, topple or slide. The proposed analytical methods could curtail errors incurred due to the acceptance of the single weak plane for quantifying the failure mechanisms composed of slide head toppling rock slopes in physical situations with two planar weak planes.

Keywords: failure mechanisms, jointed rock slopes, stabilizing techniques, analytical solution, slide head toppling

1. Introduction

A lot of research has been done in the current analytical models for predicting rock slope stability subjected to failure by block toppling. However, their contributions have focused always on the predictive and idealized geometry comprising blocks with joints dipping into the slope face. In addition, the jointing bounding the latent toppling blocks is predicted to be systematic running from the uppermost surface of the slope, and day-lighting near the toe. It is however possible that in some notable situations, the jointing (discontinuity) bounding the potential toppling rock blocks may not be predictive due to geological variations. Hence, the joints that bound the potential sliding and toppling blocks may be counter-tilted in the rock mass due to geological variations and may daylight on an unpredicted point on the slope face. This would lead to a combination of failure mechanisms composed of toppling and other secondary failure mechanisms such as toppling-circular, slide-head-toppling and block-flexure toppling. Not much research has been done on a combination of failure modes which involve sliding and block toppling on the discontinuous rock slope.

Regardless of this, a combination of failure mechanisms involving sliding and block toppling of the upper section of the slope respectively, continue to be a common phenomenon in sedimentary rock formation in numerous constructed and natural slopes all over the world as illustrated in **Figure 1a,** and **b**.

Furthermore, another typical example of slide-head-toppling failure is an open pit mine slope in Valencia in Spain shown in **Figure 2**. **Figure 2** shows a series of stable rock blocks in the soil mass on the upper surface of the slope, another set of toppling columnar blocks in the limestone formation midway section and finally a series of sliding blocks in the variation of the weak rock formation on the slope's lower part.

It is not entirely correct to analyze the stability of discontinuous rock slopes with a high potential to mixed toppling failure modes of toppling on the upper section of the slope and sliding on the slope's lower section using the existing limit equilibrium method, which is based on the initial assumptions of distribution of the potential failure surface bounding the blocks susceptible mixed failure mode. The theoretical/analytical model is therefore necessary that it takes into consideration the kinematic mechanisms of the discontinuous rock slopes composed of the counter-tilted jointing susceptible/subjected to a combination of failure mechanisms (sliding and toppling).

This chapter presents a two-dimensional (2D) model which incorporates the counter-tilted oriented jointing bounding the potential for both sliding and toppling. From the 2D model, a theoretical (analytical) model that is based on the trigonometry basic principles to determine the geometry of the jointed rock slope composed of the

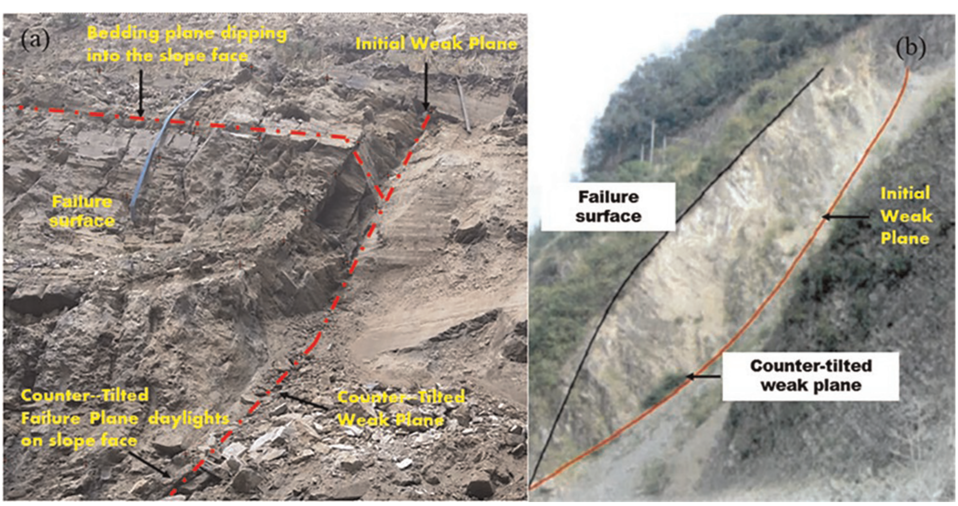

Figure 1.
Mixed toppling failure modes involving toppling and sliding failures observed in practice (a) post-failure photograph of sliding and toppling of north wall slope of Nchanga open pits, Zambia [1] (b) post-failure photograph of sliding and toppling failure in Zhongliang reservoir bank, China [2].

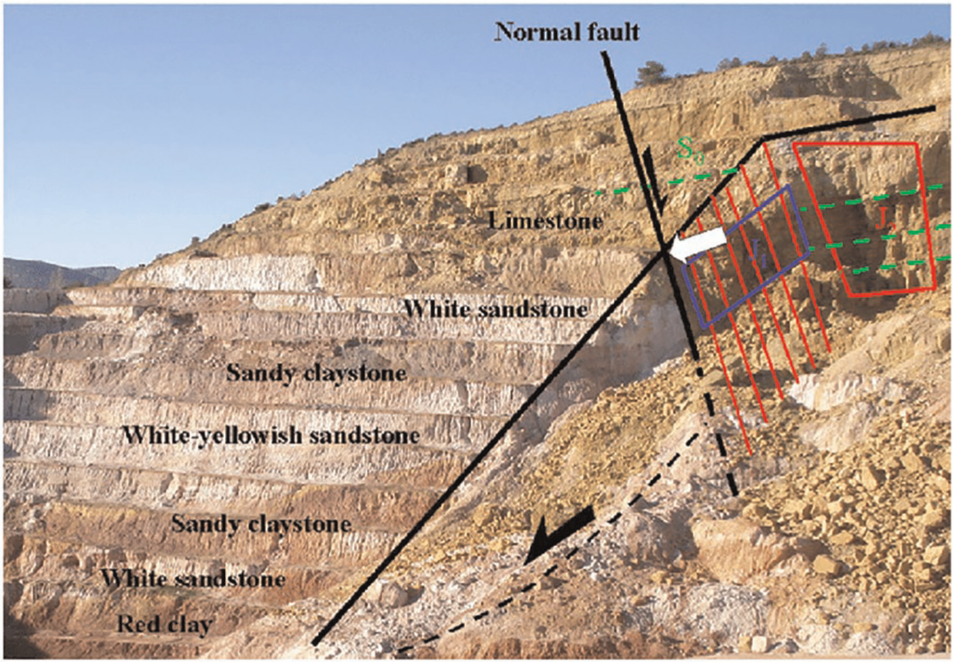

Figure 2.
Valencia open pit mine with the potential of mixed failure modes composed of toppling and sliding failures in Spain [3].

counter-tilted jointing subjected to slide-head toppling failure mechanisms have been put forward. Next, a process of iteration is followed with forces acting on each block determined. A comparative analysis between the stability against sliding and toppling of individual blocks is determined, with the highest forces between these two deciding the failure mechanism of the succeeding block. In summary, the overall slope stability is considered based on whether the lowermost block either slides or topples.

2. Rock slope geometry

For stability analyses of the slope to be achieved, detailed slope geometries must be determined at the initial stage. Let us examine a rock slope in **Figure 3**, which is composed of rectangular rock columns with width, Δx and height, yn in an orderly manner. The original failure plane dipping at ψp is counter-tilted from the preliminary weak plane approximately on the mid-way part of the slope at angle, θr. The counter-tilted failure plane then dips at ψc. Other slope parameters include the slope height indicated as H, the face angle denoted as ψf and the dip/angle of the uppermost slope face referred to as ψs. The rock block column count started from the lower most of the slope (toe) increasing cumulatively upwards. It has been observed and noted from centrifugal and numerical test models that the base plane tends to be stepped during toppling failure mechanisms [4–8]. This greatly influences the determination of the overall angle of the plane base denoted as ψb.

In rock slopes where the failure plane is counter-tilted around the midway section of the rock slope, it is important to approximate the base plane angle (ψb) considering

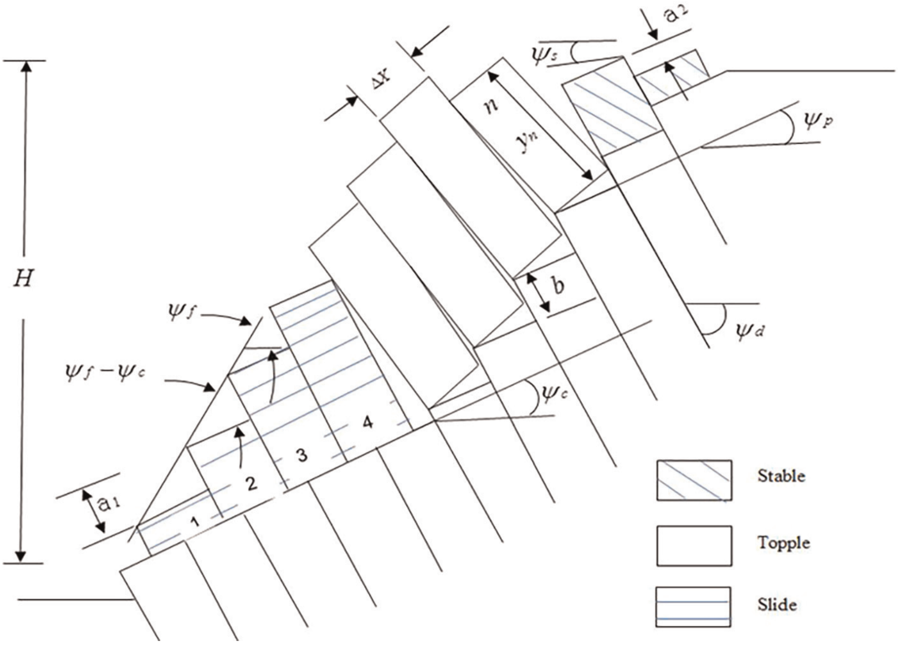

Figure 3.
Rock slope composed of counter-tilted weak surface subjected to toppling failure mechanism [1, 4].

the dipping of the failure plane bases for the rock block columns at ψp and ψc using Eq. (1)

$$\psi b \approx \left(\frac{\psi c + \psi p}{2} + 10°\right) \text{Or} \psi b \approx \left(\frac{\psi c + \psi p}{2} + 30°\right) \tag{1}$$

Based on the slope geometry in **Figure 3**. Eq. (2) is formulated to determine the number of rock columns, n, forming the regular system of the slope.

$$n = \frac{H}{\Delta x}\left[\cos ec(\psi b) + \left(\frac{\cot(\psi b) - \cot(\psi f)}{\sin(\psi b - \psi f)}\right)\sin \psi s\right] \tag{2}$$

Considering the slope model presented in **Figure 3**, the height, yn for the n$^{\text{th}}$ rock column below the slope's crest dipping/orientated into the slope face is determined by Eq. (3).

$$yn = n(\text{a}1 - b) \tag{3}$$

The height, yn for the rock column denoted as n$^{\text{th}}$ above the slope's crest dipping into the slope face is resolved by Eq. (4).

$$yn = yn - 1 - \text{a}2 - b \tag{4}$$

The constants a1, a2 and b shown in **Figure 3** are found based on the rock columns and the related slope geometry. These constants are calculated by Eqs. (5)–(7) respectively;

$$a1 = \Delta x \tan(\psi f - \psi c) \quad (5)$$

$$a2 = \Delta x \tan(\psi p - \psi s) \quad (6)$$

$$b = \Delta x \tan(\psi b - \psi p) \quad (7)$$

Other distinctive dimensions of the blocks required to be determined includes; the points of application denoted Mn and Ln for the shear and normal forces (Rn,Sn) that acts on the bases of weak planes and (Pn,Qn,Pn − 1,Qn − 1) forces applied on interfaces next to the rock columns during toppling and sliding failure mechanisms as illustrated in **Figure 3**. The application points of all forces needs to be determined every time toppling failure mechanisms takes place. Considering the case where the n^{th} block is below the slope's crest, the application points Mn and Ln are determined by Eqs. (8) and (9) respectively, at the crest block, then the application points Mn and Ln are determined by Eqs. (10) and (11) and finally when the n^{th} block is over the slope's crest, then the application points Mn and Ln are calculated by Eqs. (12) and (13).

$$Mn = yn \quad (8)$$

$$Ln = yn - a1 \quad (9)$$

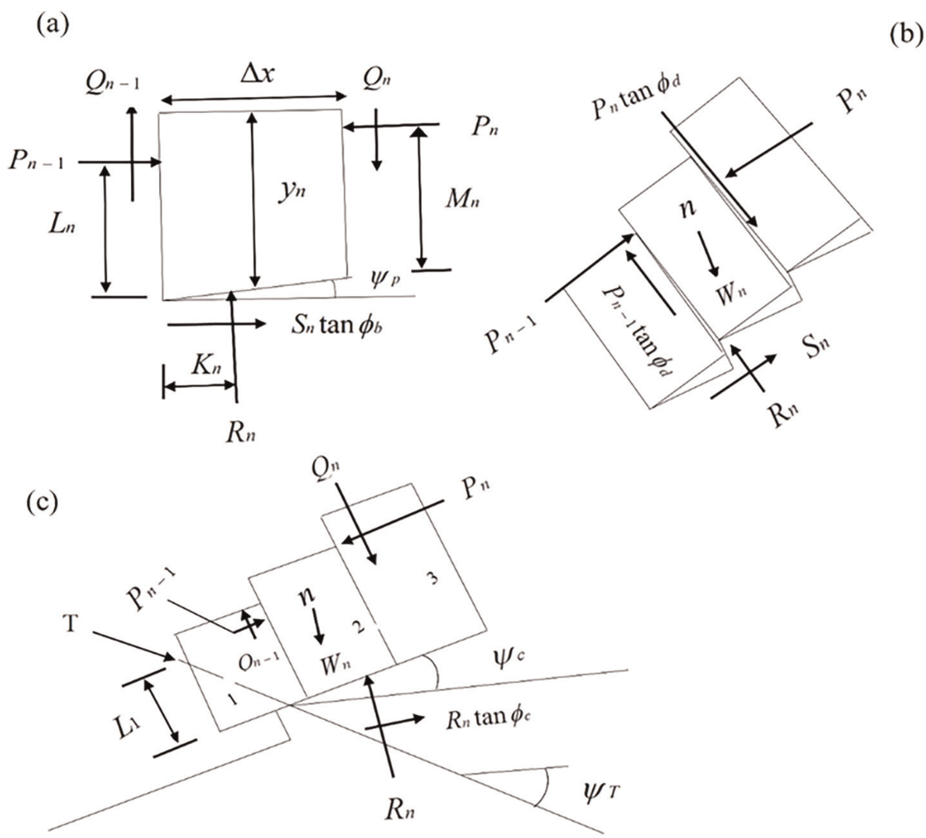

Figure 4.
Limit equilibrium conditions required for modes of failure of the nth rock columns: (a) forces applied on the nth rock columns; (b) toppling mode of failure of the nth rock columns; (c) sliding modes of failure of the nth rock columns considering the counter-tilted failure plane.

$$Mn = yn - \mathrm{a}2 \tag{10}$$

$$Ln = yn - \mathrm{a}1 \tag{11}$$

$$Mn = yn - \mathrm{a}2 \tag{12}$$

$$Ln = yn \tag{13}$$

2.1 Block stability

Figure 4 illustrates a rock slope composed of the counter-tilted weak (failure) surface composed of three sets of rock blocks that have been categorized based on their failure behavior. The rock columns for the upper most section of the slope are regarded as stable based on the fact that the rock columns' base friction angle is more than the original failure plane angle. For the rock block columns in the midway section of the slope, toppling failure is observed based on the consideration that the base plane lies outside the Centre of gravity for the rock block columns. For the blocks located around the lowermost section of the slope, there is a high possibility of rock blocks undergoing failure as the initial failure plane is counter-tilted. The modes of failure for the block columns are influenced by the geometry of the slope, the slope angle and the failure/weak plane angle. The friction angles of these failure surfaces differ with respect to characteristics of the lithology.

Generally, for such conditions, the friction angle of the block interfaces' of the rock block columns denoted (ϕd) are presumed to be equal to the angle of friction on the base plane (ϕp,ϕc). The two sides' shearing forces of the rock column are then resolved using Eqs. (14) and (15), considering the limiting equilibrium analysis. On the other hand, the forces applied on the rock column considering the orthogonal and sides' friction angles to the two base planes (ψp, ψc) of the rock column having weight, Wn, are resolved using Eqs. (16) and (17).

$$Qn = Pn \tan \phi d \tag{14}$$

$$Qn - 1 = Pn - 1 \tan \phi d \tag{15}$$

$$\begin{gathered} Rn = Wn \cos \psi p + (Pn - Pn - 1) \tan \phi d \\ Rn = Wn \cos \psi c + (Pn - Pn - 1) \tan \phi d \end{gathered} \tag{16}$$

$$\begin{gathered} Sn = Wn \sin \psi p + (Pn - Pn - 1) \\ Sn = Wn \sin \psi c + (Pn - Pn - 1) \end{gathered} \tag{17}$$

To define the magnitude of Pn, the moment force about the pivot point O is set to zero (refer **Figure 4**). We then, as discussed above, assume that the angle of friction of the interfaces of the rock block columns denoted (ϕd) is equal in magnitude to the angle of friction on the base planes (ϕp, ϕc), thus $\phi d = \phi p = \phi c = \phi$.

Considering the possibilities of rotational equilibrium, the forces Pn,t necessary to avoid toppling of the *nth* block considering the presumed angle of the failure plane is resolved based on Eq. (18) considering the derivations as follows:

The moment about the pivot point 0 is set to zero. Then we have:

$$\sum M0\oplus = 0$$

$$= \frac{yn}{2} Wn \sin\psi p - \frac{\Delta x}{2} Wn \cos\psi p + MnPn + 1 - \Delta x(Pn + 1 \tan\phi) - LnPn$$

$$= \frac{Wn}{2}(yn \sin\psi p - \Delta x \cos\psi p) + Pn + 1(Mn - \Delta x \tan\phi) - LnPn$$

We can rewrite this as follows:

$$LnPn = \frac{Wn}{2}(yn \sin\psi p - \Delta x \cos\psi p) + Pn + 1(Mn - \Delta x \tan\phi)$$

Hence this gives the following equation for Pn

$$Pn,t = \frac{\frac{Wn}{2}(yn \sin\psi p - \Delta x \cos\psi p) + Pn + 1(Mn - \Delta x \tan\phi)}{Ln} \tag{18}$$

Considering the possibilities of rotational equilibrium, the forces Pn,t necessary to avoid toppling for the *nth* block taking into consideration the counter-tilted angle of the failure plane is determined using Eq. (19) considering the derivations as follows;

Again, the moment about the pivot point O is set to zero. Then we have:

$$\sum M0\oplus = 0$$

$$= \frac{yn}{2} Wn \sin\psi c - \frac{\Delta x}{2} Wn \cos\psi c + MnPn + 1 - \Delta x(Pn + 1 \tan\phi) - LnPn$$

$$= \frac{Wn}{2}(yn \sin\psi c - \Delta x \cos\psi c) + Pn + 1(Mn - \Delta x \tan\phi) - LnPn$$

We can rewritten this as follows;

$$LnPn = \frac{Wn}{2}(yn \sin\psi c - \Delta x \cos\psi c) + Pn + 1(Mn - \Delta x \tan\phi)$$

Therefore, we obtain the following equation for Pn,t with respect to counter-tilting of the failure plane:

$$Pn,t = \frac{\frac{Wn}{2}(yn \sin\psi c - \Delta x \cos\psi c) + Pn + 1(Mn - \Delta x \tan\phi)}{Ln} \tag{19}$$

If the rock columns' failure mode on the slope's lower section shown in **Figure 4c** is noted to be sliding, then to calculate the magnitude of $P_{n,s}$, the total (sum) of the forces in the horizontal directions and vertical directions is set to zero (assuming the horizontal axis to lie along the base plane, at angles ψp or ψc considering the horizontal as the datum refer **Figure 4**. In general, it is presumed that the interfaces' angle of friction for the rock columns denoted (ϕd) is equal to the friction angle on the base plane (ϕp, ϕc), thus $\phi d = \phi p = \phi c = \phi$.

Considering the possibilities of rotational equilibrium, the forces Pn,s required to prevent sliding of block n considering the initial angle of the weak plane is resolved using Eq. (20) considering the derivations as follows;

Before counter-tilting of the failure plane along base plane angle ψp taking the horizontal as the datum, we have

$$\sum Fx = 0 = Pn - Pn + 1 - Wn \sin \psi p + Sn$$
$$\sum Fy = 0 = Rn + Pn \tan \phi - Wn \cos \psi p - Pn + 1 \tan \phi$$

Where Sn is shear force acting along the base of the column contacts, from the Mohr-Coulomb criterion, we have:

$$\tau n = c + \sigma n \tan \phi$$

Where τn shear stress acting along the base of the column contact and σn Normal stress at the base column contact.

We further assumed the cohesion (c) being negligible and divide both sides of the equation by the column-base plane contact area denoted by A. Thus, we get

$$Sn = Rn \tan \phi$$

Where; Rn is normal force acting across the base plane of the column contacts $(Wn \cos \psi p)$.

By resolving the F_y equation for Rn making substitutions into the F_x equation prior to counter-tilting of the failure plane along base plane angle ψp with regards to the horizontal, we have,

$$Pn - Pn + 1 - Wn \sin \psi p + Wn \cos \psi p \tan \phi - (Pn - Pn + 1) \tan^2 \phi = 0$$
$$(Pn - Pn + 1)\left(1 - \tan^2 \phi\right) - Wn \sin \psi p + Wn \cos \psi p \tan \phi = 0$$

This leads to:

$$(Pn - Pn + 1)\left(1 - \tan^2 \phi\right) = Wn \cos \psi p (\tan \psi p - \tan \phi)$$
$$(Pn - Pn + 1) = \frac{Wn \cos \psi p (\tan \psi p - \tan \phi)}{1 - \tan^2 \phi}$$

Hence, we obtain the following equation for $Pn{,}s$

$$Pn{,}s = Pn + 1 + \frac{Wn \cos \psi p (\tan \psi p - \tan \phi)}{1 - \tan^2 \phi} \tag{20}$$

Considering the possibilities of rotational equilibrium, the forces Pn,s necessary to avoid sliding of *nth* block taking into consideration the counter-tilted angle of the weak plane is resolved using Eq. (21) considering the derivations as follows;

Once counter-tilting of the failure plane takes place along base plane ψc taking into consideration the horizontal line, we have

$$\sum Fx = 0 = Pn - Pn + 1 - Wn \sin \psi c + Sn$$
$$\sum Fy = 0 = Rn + Pn \tan \phi - Wn \cos \psi c - Pn + 1 \tan \phi$$

By solving the F_y equation for Rn and making substitutions into the F_x equation once counter-tilting of the failure plane takes place along base plane ψc taking the horizontal as the datum, we have,

$$Pn - Pn + 1 - Wn \sin \psi c + Wn \cos \psi c \tan \phi - (Pn - Pn + 1) \tan^2 \phi = 0$$
$$(Pn - Pn + 1)\left(1 - \tan^2 \phi\right) - Wn \sin \psi c + Wn \cos \psi c \tan \phi = 0$$

This leads:

$$(Pn - Pn + 1)\left(1 - \tan^2 \phi\right) = Wn \cos \psi c(\tan \psi c - \tan \phi)$$
$$(Pn - Pn + 1) = \frac{Wn \cos \psi c(\tan \psi c - \tan \phi)}{1 - \tan^2 \phi}$$

Hence, the following equation for Pns is obtained;

$$Pn,s = Pn + 1 + \frac{Wn \cos \psi c(\tan \psi c - \tan \phi)}{1 - \tan^2 \phi} \tag{21}$$

2.2 Determination of anchor tension necessary to prevent toppling of block 1

Once a determination is made that block 1 in **Figure 4c** will topple then cables under tension can be installed through block 1 to be anchored in stable rockmass underneath the toppling zone to prevent toppling of the same. Further assumptions was made that the anchor is installed at an angle plunge of ψT through block 1 located at a distance $L1$ above the base. After the application of force T to block 1, the normal force ($R1$) as well as shear force ($S1$) on the base plane of the block 1 is determined using Eqs. (22) and (23) respectively.

$$R1 = P1 \tan \phi + T \sin(\psi p + \psi T) + W1 \cos \psi p \tag{22}$$

$$S1 = P1 - T \cos(\psi p + \psi T) + W1 \sin \psi p \tag{23}$$

To solve for the magnitude of Tt, again the moment force about the pivot point 0 is set to zero as follows:

$$\sum M0 \oplus = 0$$

$$0 = \frac{W1}{2}(y1 \sin \psi p - \Delta x \cos \psi p) + P1(y1 - \Delta x \tan \phi) - TtL1 \cos(\psi p + \psi T)$$

This is resolved as follows:

$$\frac{TtL1 \cos(\psi p + \psi T)}{L1 \cos(\psi p + \psi T)} = \frac{\frac{W1}{2}(y1 \sin \psi p - \Delta x \cos \psi p) + P1(y1 - \Delta x \tan \phi)}{L1 \cos(\psi p + \psi T)}$$

The magnitude of Tt, is deduced as shown in Eq. (24)

$$Tt = \frac{\frac{W1}{2}(y1 \sin \psi p - \Delta x \cos \psi p) + P1(y1 - \Delta x \tan \phi)}{L1 \cos(\psi p + \psi T)} \tag{24}$$

However, if there is existence of the counter-tilted failure plane at angle ψc to the horizontal plane, the normal force ($R1$) and shear force ($S1$) on the base plane of the block 1 are resolved using Eqs. (25) and (26) respectively.

$$R1 = P1 \tan\phi + T\sin(\psi c + \psi T) + W1\cos\psi p \tag{25}$$

$$S1 = P1 - T\cos(\psi c + \psi T) + W1\sin\psi c \tag{26}$$

To solve for the magnitude of Tt, again the moment about the pivot point 0 is set to zero;

$$0 = \frac{W1}{2}(y1\sin\psi c - \Delta x\cos\psi c) + P1(y1 - \Delta x\tan\phi) - TtL1\cos(\psi c + \psi T)$$

This is resolved this as follows:

$$\frac{TtL1\cos(\psi c + \psi T)}{L1\cos(\psi c + \psi T)} = \frac{\frac{W1}{2}(y1\sin\psi c - \Delta x\cos\psi c) + P1(y1 - \Delta x\tan\phi)}{L1\cos(\psi c + \psi T)}$$

The magnitude of Tt, is reduced to Eq. (27).

$$Tt = \frac{\frac{W1}{2}(y1\sin\psi c - \Delta x\cos\psi c) + P1(y1 - \Delta x\tan\phi)}{L1\cos(\psi c + \psi T)} \tag{27}$$

2.3 Anchor tension necessary to prevent sliding of block 1

After a determination is made of the sliding block 1in **Figure 4c** the cables under tension can therefore be fixed through block 1 and anchored in the stable rock mass underneath the zone of sliding to avoid movements of block 1. It is also assumed that the installed anchor at a plunge angle of ψT through block 1 at a distance $L1$ above the base plane. Therefore, with the failure plane along base angle ψp taking the horizontal as the datum, $\sum Fx$ and $\sum Fy$ are resolved using Eqs. (28) and (29) respectively.

$$\sum Fx = 0 = Pn - Pn + 1 - Wn\sin\psi p + Sn \tag{28}$$

$$\sum Fy = 0 = Rn + Pn\tan\phi - Wn\cos\psi p - Pn + 1\tan\phi \tag{29}$$

Once the force T is applied to block 1, the normal force ($R1$) and shear force ($S1$) on the base planer of the block 1 are determined using Eqs. (30) and (31) respectively.

$$R1 = P1\tan\phi + T\sin(\psi p + \psi T) + W1\cos\psi p \tag{30}$$

$$S1 = P1 - T\cos(\psi p + \psi T) + W1\sin\psi p \tag{31}$$

By solving for the Fy equation for Rn and making substitution into the Fx equation prior to counter-tilting of the failure plane along the base plane ψp taking the horizontal line as the reference point, hence, the moments about the pivot point 0 was set to zero as given below;

$$0 = P1(1 - \tan\phi p\tan\phi - W1(\tan\phi p\cos\psi p - \sin\psi p) - Ts(\tan\phi\sin(\psi p + \psi T)$$
$$- \cos(\psi p + \psi T)$$

This was resolved as follows:

$$Ts(\tan\phi\sin(\psi p + \psi T) - \cos(\psi p + \psi T) = P1(1 - \tan\phi p\tan\phi - W1(\tan\phi p\cos\psi p - \sin\psi p)$$

$$\frac{Ts(\tan\phi\sin(\psi p+\psi T)+\cos(\psi p+\psi T)}{(\tan\phi\sin(\psi p+\psi T)+\cos(\psi p+\psi T)}=\frac{P1(1-\tan\phi p\tan\phi-W1(\tan\phi p\cos\psi p-\sin\psi p)}{(\tan\phi\sin(\psi p+\psi T)+\cos(\psi p+\psi T)}$$

The magnitude of Ts, is deduced as follows:

$$Ts=\frac{P1(1-\tan\phi p\tan\phi-W1(\tan\phi p\cos\psi p-\sin\psi p)}{(\tan\phi\sin(\psi p+\psi T)+\cos(\psi p+\psi T)}$$

In general, as assumed before that the angle friction for the interfaces of the rock block columns denoted (ϕd) is the same as the friction angle on the bases plane (ϕp, ϕc), hence $\phi d=\phi p=\phi c=\phi$.

Therefore Ts is resolved using Eq. (33).

$$Ts=\frac{P1(1-\tan^2\phi)-W1(\tan\phi\cos\psi p-\sin\psi p)}{(\tan\phi\sin(\psi p+\psi T)+\cos(\psi p+\psi T)} \tag{32}$$

However, if the counter-tilted failure plane dipping at angle ψc exists considering the horizontal line, $\sum Fx$ and $\sum Fy$ are solved using Eqs. (33) and (34) respectively.

$$\sum Fx=0=Pn-Pn+1-Wn\sin\psi p+Sn \tag{33}$$

$$\sum Fy=0=Rn+Pn\tan\phi-Wn\cos\psi p-Pn+1\tan\phi \tag{34}$$

If the counter-tilted failure plane at angle ψc exists considering the horizontal line, then, when the force T is applied to block 1, the normal force ($R1$) and shear force ($S1$) on the base plane of the block 1 are reduced as follows;

$$R1=P1\tan\phi+T\sin(\psi c+\psi T)+W1\cos\psi p$$

$$S1=P1-T\cos(\psi c+\psi T)+W1\sin\psi c$$

By resolving the Fy equation for Rn and making substitutions into the Fx equation after counter-tilting of the failure plane along the counter-tilted weak plane ψc with consideration of the horizontal line, hence, we set the moments about the pivot point 0 to zero as given below;

$$\begin{aligned}0&=P1(1-\tan\phi c\tan\phi-W1(\tan\phi c\cos\psi c-\sin\psi c)-Ts(\tan\phi\sin(\psi c+\psi T)\\&+\cos(\psi c+\psi T)Ts(\tan\phi\sin(\psi c+\psi T)+\cos(\psi c+\psi T)=P1(1-\tan\phi c\tan\phi\\&-W1(\tan\phi c\cos\psi c-\sin\psi c)\end{aligned}$$

We resolved Ts as follows:

$$\frac{Ts(\tan\phi\sin(\psi c+\psi T)-\cos(\psi c+\psi T)}{(\tan\phi\sin(\psi c+\psi T)+\cos(\psi c+\psi T)}=\frac{P1(1-\tan\phi c\tan\phi-W1(\tan\phi c\cos\psi c-\sin\psi c)}{(\tan\phi\sin(\psi c+\psi T)+\cos(\psi c+\psi T)}$$

Ts, is deduced as follows:

$$Ts=\frac{P1(1-\tan\phi c\tan\phi-W1(\tan\phi c\cos\psi c-\sin\psi c)}{(\tan\phi\sin(\psi c+\psi T)+\cos(\psi c+\psi T)}$$

Based on the earlier assumptions of the angle of friction of the interfaces of the rock columns denoted (ϕd) being equal to the angle of friction on the base plane (ϕp, ϕc), thus $\phi d = \phi p = \phi c = \phi$.then Ts is resolved based on the Eq. (35)

$$Ts = \frac{P1(1 - \tan^2\phi) - W1(\tan\phi\cos\psi c - \sin\psi c)}{(\tan\phi\sin(\psi c + \psi T) + \cos(\psi c + \psi T)} \qquad (35)$$

Stabilization of rock slope by cable forces using limit equilibrium principles demonstrates that support of the “Keystone” is remarkably effective in increasing the scores of stability of the rock slopes prone to toppling. Supporting the rock block around the slope’s toe under the influence of toppling failure just at limit equilibrium is simply metastable and its metastability depends on the details of the geometric arrangement of the toppling blocks. On the other hand, reducing the strength of the “keystone” of a slope under toppling that is near failure leads to severe problems.

3. A practical application: Toppling failure

Failure by toppling of rock columns (**Figure 5**) occurred in shale rock fomations (Shale with grit, Shale with grit type 1 and Shale with grit type 2 & 3) on the northwall of the Nchanga Copper and Cobalt Open Pit situated in the mining city of Chingola in Zambia in June, 2016 [1, 4, 9, 10]. In terms of geology, the Nchanga geology is majorly controlled by Nchanga syncline regional structure with an east–west trend and at 5°-7° plunge to the north. The south limb of the Nchanga Open Pit is noted to be shallow and

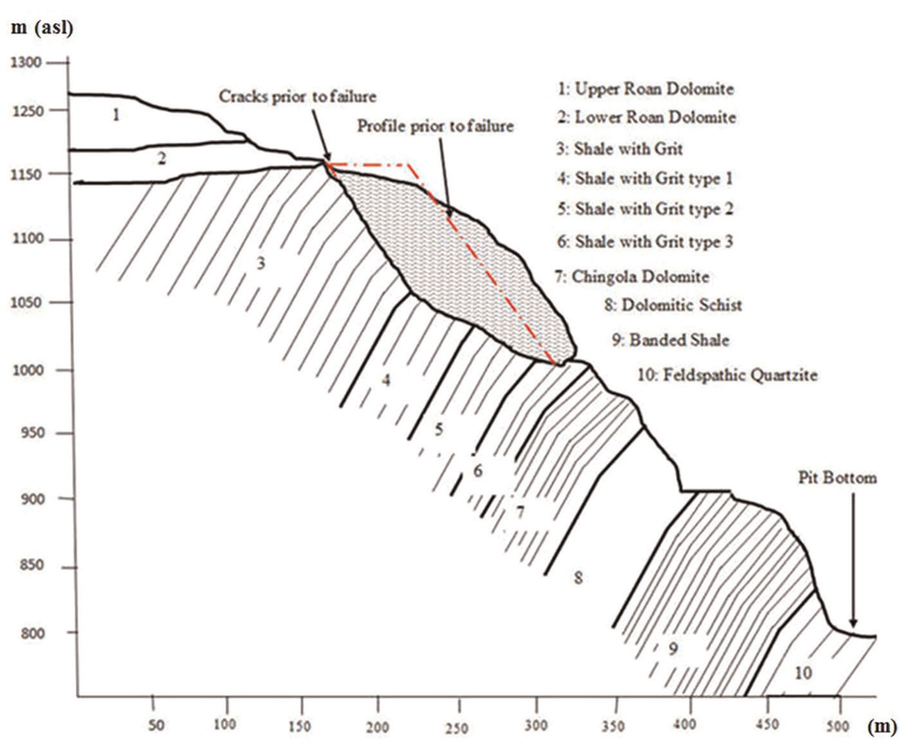

Figure 5.
Toppling failure of the slope composed of a counter-tilted failure plane.

dips to the north at 25°-35° in general together with local changes of shallow to steep dips unlike the north limb which dips at 60°. The Nchanga open pit sub-surface geology is composed of the upper and lower roan dolomites which are usually dipping neaerly horizontal and a series of sedimentary rocks formations overlays them through to basal conglomerates that dips at an angle of 60° towards the north. The slope of the north wall is cut in the ore-body northwall lithology namely; Dolomitic Schist Shale with Grit, Banded Shale, Shale with Pink Quartzite, Grit (type 1,2 & 3), upper and lower roan dolomite Chingola Dolomite, Arkose, Feldspathic Quartzite, Banded Sandstone, Basal Conglomerates partly illustrated in **Figure 5** for the geological engineering profile. Feldspathic Quartzite formation hosts the copper and cobalt that are being mined at Nchanga Open Pits. A summary of the general geological stratigraphy of the mine is shown in **Table 1**. The general slope is elevated at 1330 m – 880 m above mean sea level (asl) from the top and bottom of the elevataions respectively. The overall slope angle is 40° with an overall height of 450 m. An asymmetrical syncline limb on the north wall, the rock columns of the three rock formations (shale with grit type 1, shale with grit type 2, shale with grit) of the rock slope with counter-tilted weak surface overturned. The slope with counter-tilted weak surface under study is sited on the elevations ranging between 1170 m- 970 m above mean sea level (ASL).

Rock Unit	Rock layer (m)	Density Kg/m^3	Internal friction angle(°)	Cohesion (MPa)	RMR	Hydro-Geological unit	Description
Shale with Grit	50	2500	35	400	68	Acquiclude	Fair to good quality, bedded rockmass
Shale with Grit type 1	40	2300	30	360	49	Acquiclude	Weak rockmass, bedded
Shale with Grit type 2&3	20	2200	30	360	49	Acquiclude	Weak rockmass, bedded
Chingola Dolomite	15	2400	33	380	64	Acquifer	Fait to good quality, bedded rockmass
Dolomitic Schists	20	2800	42	540	75	Mnor Acquifer	Good quality rockmass, bedded
Banded Shale	18	2600	37	490	68	Acquiclude	Fair to good quality rockmass seam at the base,bedded
Feldspathic Quartzite	18	2900	45	800	82	Acquiclude	Very good rockmass, massive
Banded Sandstone	15	1900	28	150		Acquifer	Weak rockmass with, calcite infill material, bedded
Pink Quartzite	5	3200	59	1300	84	Acquiclude	Very good quality with random joints
Arkose	15	3300	67	4000	96	Minor Acquifer	Very strong and competent rockmass
Basement (Gneiss and red granite)	>400	3000	39	1150	90	Impearmeable	Strong and competent with some schistocity

Table 1.
The general geological layout and rock characteristics.

Before slope failure, the zone under study being mined at, 155 m high (H), and at a slope angle of 65° (ψf) in a layered shale rock mass (shale with grit type 1, shale with grit type 2shale with grit) dipping at 60° into the face (ψd = 60°); with the width (Δx) of individual rock column at 10 m. The angle above the surface of the pit slope was determined to be 5° (ψs), and the base of the rock block columns were stepped at b = 1.0 m. Cracks of less than 1 cm on the weak surface started to develop and were noticed when the pit was excavated to a depth of 145 m. The observed weak plane surface on the upper part of the slope (crest) was predicted to daylight on the slope's

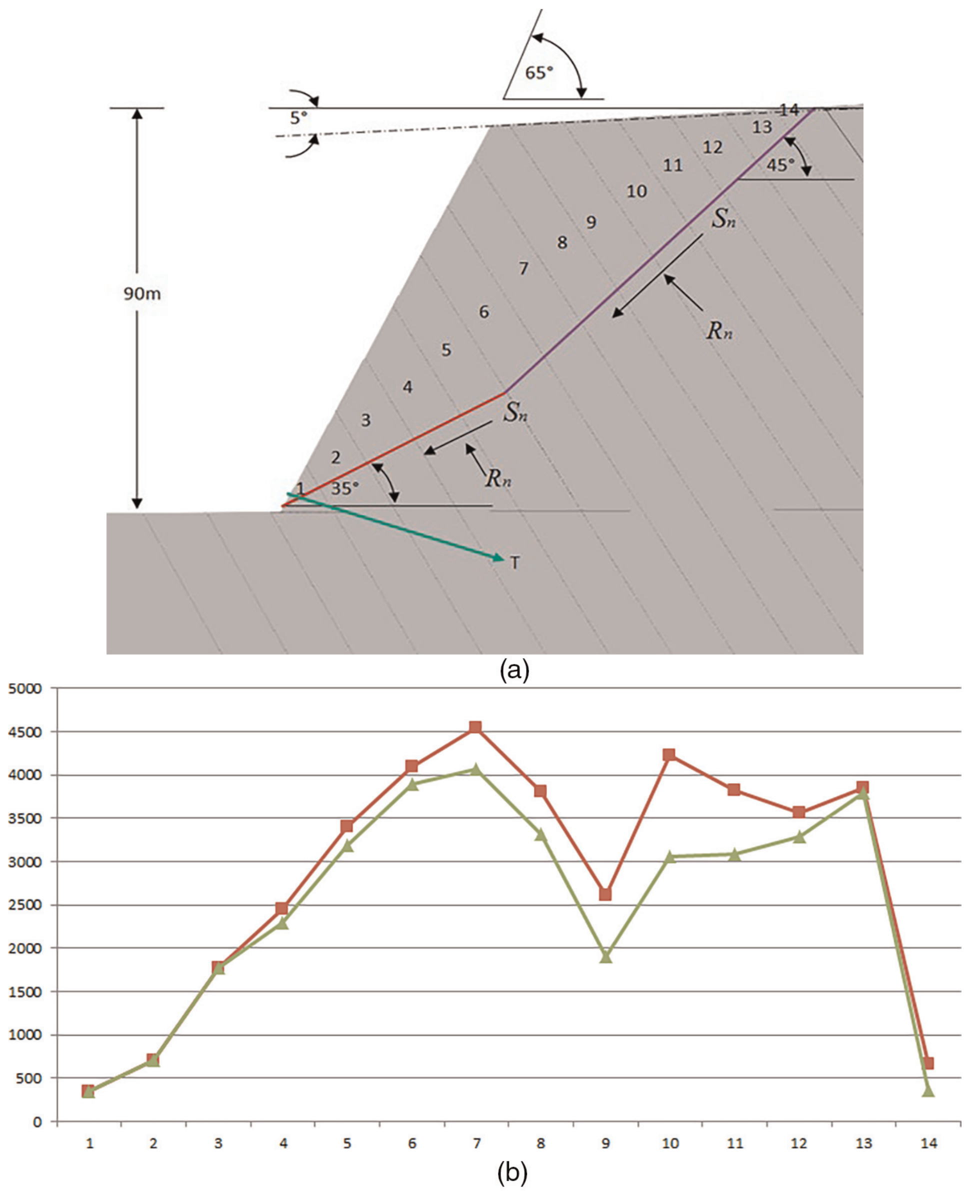

Figure 6.
(a) Limiting equilibrium analysis of a block toppling on a rock slope- conceptual slope set up and its geometry. (b) Limiting equilibrium analysis of a block toppling on a slope: Variation/distribution of normal forces (R) and shear (S) forces on the bases of the blocks.

face when the pit was to be mined at 250 m deep since the planned pit depth was at 450 m. No essential remedial measures were therefore undertaken against slope failure and no disruption of the mining operations in the pit was noted. However, based on the geological variations of the Shale rock formations at Nchanga Open Pit, failure surface inclined at 45° on the slope's upper most section day-lighted on the slope's face when the pit was at 144 m deep. It is well appreciated that the plane of weak surface dipping at an angle of 45° in shale with grit rock formation underwent counter-tilting to an angle of 35° in Shale with grit types 1 and 2 formations based on the variations in geological characteristics.

3.1 Calculational procedure

With regard to the geometry of the slope as given in **Figure 5**, it was presumed that, therefore ψb =55°. Using Eqs. (4), n = 14 see **Figure 6a** and rock block column 8 is at the slope's top most part (crest). Using Eqs. (5)–(7), the constants calculated are a1 = 5.0 m,a2 = 5.0 m and b = 1.0 m. These constants are then applied to determine the height yn of individual blocks, as well as the height to width ratio. The shale with grit type 1 and shale with grit rock formations' unit weights at Nchanga were noted to be 23kN/m^3 ^{3} and 25kN/m respectively. It is assumed that there are no noticeable external forces and that the friction angles are $\phi p = \phi d$ =30° and ϕc =30°. The base plane dips at angles of ψp =45° and ψc =35°. Therefore, cot ψp = 1.0, hence, block columns 14, 13 and 12 are noted to be stable, because for each block indicated, the height to width ratio is noted to be less or equal to1.0. In general, these three blocks are short and their center of gravity was observed to lie inside the base of the block. Block 11 topples because the height-width ratio has a value 1.6, which is greater than 1.0. Therefore, $P11$ is equal to 0 and $P10$ is determined as the greater of $P10$,t and $P10$,s given by Eqs. (20)–(23) respectively.

n	Yn	Yn/Δx	Mn	Ln	Pn-t	Pn-s	Pn	Rn	Sn	Sn/Rn	Failure Mode
14	−2	−0.2			0	0	0	353.6	353.6	1.00	Stable
13	4	0.4			0	0	0	707.1	707.1	1.00	
12	10	1	2	10	0	0	0	1767.8	1767.8	1.00	
11	16	1.6	8	16	0	0	0	2456.9	2298.1	0.94	Toppling
10	22	2.2	14	22	530.5	−1664.7	530.5	3399.6	3190	0.94	
9	26	2.6	18	26	1229.4	−1758.7	1229.4	4102.6	3891.3	0.95	
8	32	3.2	24	27	1934.3	−1475.8	1934.3	4544.8	4068.6	0.90	
7	28	2.8	28	23	3522.6	−1393.1	3522.6	3808	3319.2	0.87	
6	24	2.4	24	19	5153.1	609.3	5153.1	2605.8	1904.9	0.73	
5	20	2	20	15	5490.8	6534.3	6534.3	4225.6	3053.3	0.72	Sliding
4	16	1.6	16	11	5305.4	6140.2	6140.2	3826.5	3079.7	0.80	
3	12	1.2	12	7	4520	5146.1	5146.1	3558.1	3292.6	0.93	
2	8	0.8	8	3	2948.2	3365.6	3365.6	3855	4313.6	1.12	
1	4	0.4	4		−218.3	−9.6	−9.6	666.3	355.3	0.53	

Table 2.
Limiting equilibrium analysis of a columnar block toppling slope- listing block calculated forces, stability modes and dimensions.

This analytical procedure is key for stability determination of individual blocks, based on the failure surface angle of ψp moving downwards up to n = 6. At block denoted as n = 5 the original failure plane is counter tilted at angle θr, then ψc is substituted for ψp to determine the stability of individual blocks in turn moving down until n = 1 see Eqs. (20)–(23). The obtained block dimensions, the calculated forces and the stability modes are listed in **Table 2** which indicates that Pn − 1,t is the larger of the two forces up until a value of n = 5, where upon Pn − 1,s is larger. Hence, blocks 6 to 11 was noted to be the potential toppling zone, and blocks 1 to 5 denoted a sliding zone. The factor of safety for this slope is determined by varying (increasing) the friction angles until the base plane blocks are stable. It is noted that the required friction angle for limit equilibrium conditions to be satisfied is 36°, or 0.96 (tan 35/tan 36). If $\tan\phi$ is reduced to 0.577, blocks 1 to 5 in the region around the toe will slide while blocks denoted as 6 to 11 will topple. The anchor tension installed at an angle of 25° through block 1, required to maintain equilibrium, is resolved to be 100kN/m of slope toe based on the Eqs. (24)–(27). This is not a big number, which demonstrates that support of the "Keystone" produces very effective results in increasing stability. On the other hand, reducing the strength of the "keystone" of a slope under toppling, nearing failure, leads to serious consequences. With the definition of the distribution of P forces in the sliding region, the forces R_n and S_n on the base plane of the base blocks is calculated using Eqs. (18) and (19). With the following assumption $[Qn - 1 = Pn - 1\tan\phi s]$, the forces R_n and S_n are determined the region of sliding. **Figure 6b** illustrates the variation of the forces throughout the whole slope. The conditions defined by $R_n > 0$ and $S_n| < Rn\tan\phi p$ are satisfied everywhere.

4. Summary of the chapter

A presentation of the mathematical (analytical) method for determination of the counter-tilted failure plane angle for the discontinuous rock slope subjected to block toppling failure mechanism based on the searching technique has been presented. Geometry parameters forming the systematic arrangement of the jointed rock slope that maybe influenced by the presence of the failure planes such as; the application points for the shear and normal forces that acts on the bases of the weak planes and the number of rock columns, the overall base angles of the weak plane angles, forming the regular system have been developed. The modified limit equilibrium method for quantifying the failure mechanisms in the jointed rock slopes having a counter-tilted failure plane prone to block toppling has been proposed. This involves an iterative process in which the dimensions of all the individual blocks and the existing forces acting on them are calculated, and then each block's stability is examined, starting at the uppermost block. Each block will be stable, topple or slide, with the overall stability of the slope being rendered unstable if the lower most block either slides or topples. The iterative process involves determinations of sliding and toppling of the n^{th} block with and without consideration of counter-tilted weak plane respectively. The proposed method of analysis has the potential to curtail errors incurred due to the previous assumptions of the single weak plane for quantifying the failure mechanisms of toppling rock slopes in physical situations with two planar weak planes. It is further noticed that the existence of counter-tilted failure plane in the discontinuous rock slope influence the geometry parameters such as; overall base angles, number of blocks that forms the regular systematic arrangement of the jointed rock slope and application positions M_n and L_n and the sliding and toppling forces.

References

[1] Bowa VM, Xia YY. Influence of counter-tilted failure surface angle on the stability of rock slopes subjected to block toppling failure mechanisms. Bulletin of Engineering Geology and the Environment. 2018a;**77**(4):120-140

[2] Cai JS. Mechanism Research of Toppling Deformation for Homogeneous Equal Thickness Anti-Dip Layered Rock Slopes [Thesis]. Beijing: China University of Geosciences; 2013

[3] Alejano LR. Complex rock slope failure mechanisms involving toppling. In: XIV International Conference about Slope Stability (2018) April, 10–13. Seville, Spain; 2018

[4] Bowa VM, Xia YY. Modified analytical technique for block toppling failure of rock slopes with counter tilted failure surface. Indian Geotechnical Journal. 2018b;**48**(4):713-772

[5] Adhikary DP, Dyskin AV, Jewell RJ, Stewart DP. A study of the mechanism of flexural-toppling failure of rock slopes. Rock Mechanics and Rock Engineering. 1997;**30**:75-93

[6] Pritchard MA, Savigny KW. Numerical modeling of toppling. Canadian Geotechnical Journal. 1990;**27**: 823-834

[7] Pritchard MA, Savigny KW. The Heather Hill landslide: An example of a large scale toppling failure in a natural slope. Canadian Geotechnical Journal. 1991;**28**:410-422

[8] Bowa VM, Wenping Gong WP. Analytical technique for stability analyses of the rock slope subjected to slide head toppling failure mechanisms considering groundwater and stabilization effects. International Journal of Geo-Engineering. 2021;**2021** (12):4

[9] Bowa VM, Xia Y. Stability analyses of jointed rock slopes with counter-titled failure surface subjected to block toppling failure mechanisms. Arabian Journal for Science, Research Article: Civil Engineering. 2018;**43**(10):5315-5331

[10] Bowa VM, Xia Y, Kabwe E. Analytical technique for stability analyses of rock slopes subjected to block toppling failure. Mining Technology. 2019;**127**(4):219-229

Chapter 4

Numerical Investigation of Rainfall Infiltration-Induced Slope Stability Considering Water-Air Two-Phase Flow

Wenjing Tian, Herman Peiffer, Benny Malengier, Gang Liu and Qingchao Cheng

Abstract

For insights into rainfall infiltration on soil slopes and coupled transmission mechanisms, two-phase flow and finite element analysis were employed to examine water and air movement during the Shuping landslide. The results indicated a division of the landslide surface into two zones: an upper inflow area and a lower overflow area, driven by contrasting inflow and outflow directions. The total water and air flux remained stable, minimally affected by external factors such as rainfall attributes, surface runoff, and air temperature variations. In the inflow area of the slope surface, when rainfall intensity was greater than the total rate of the infiltration of water and air, the magnitude of infiltration equalled to the total rate infiltration of water and air, and runoff generation occurred in this area. Conversely, when infiltration matched rainfall intensity, runoff was absent in this area. In addition, water pressure in the saturated area of the slope surface can be transferred to the groundwater of the slope by pore air pressure, which could also increase the pressure head of the groundwater, and this was also detrimental to slope stability. Regarding uniform rainfall, it significantly reduces the safety factor, potentially making it the most hazardous pattern for slope failure.

Keywords: water-air two-phase flow, rainfall infiltration, finite element method, unsaturated seepage, slope stability

1. Introduction

Rainfall infiltration of a slope is a complex unsaturated seepage process, which is primarily driven by the coupling effect of water and air fluid in the soil [1–3]. The infiltration intensity is influenced by various factors, such as soil permeability, water-air viscosity, and slope boundary conditions [4, 5]. Understanding these factors is essential to predict the rainfall infiltration process and its impact on slope stability [6–8].

Most previous studies [9–12] have used the Richard's rainfall infiltration equation to describe the infiltration process. However, this equation assumes that the pore air pressure is constant and equal everywhere (usually set to atmospheric pressure), which essentially ignores the coupling and cooperation between water and air in the soil. This simplification may be valid under certain circumstances, but it may not fully capture the complex interactions between water and air in real-world engineering scenarios. Numerous research findings [13–17] indicated that, in the case of a closed boundary condition, the effect of pore air on the flow of the liquid phase (water) cannot be neglected. During the rainfall infiltration process, the liquid phase (water) exerts pressure on the air in the soil, resulting in a jacking force that opposes the direction of water movement. This phenomenon can cause a decrease in the rainfall infiltration rate because of the reduction of the water pressure gradient. This effect of air on the infiltration process has been observed and reported in numerous studies [18, 19]. Therefore, the consideration of water-air coupling effect is important for accurate modelling and prediction of rainfall infiltration in soil.

Some researchers have demonstrated that the water and air infiltration process of slope rainfall can be accurately captured by considering the influence of the air phase. Based on their findings, it is recommended to adopt the two-phase flow theory of water and air for a more practical exploration of the problem of slope rainfall infiltration. This chapter employs the basic theory and methodology of water- air two-phase flow to simulate and analyse the rainfall infiltration process of Shuping landslide in the Three Gorges Reservoir area, with the aim of investigating the general law of slope rainfall infiltration. While most studies on two-phase flow primarily focus on exploring changes in pressure and other parameters during infiltration and verifying the impact of the air phase, there is a lack of research on the overall induction of rainfall infiltration laws. By studying the general law of slope rainfall infiltration, this research serves as a complement to existing laws of rainfall infiltration and provides a more comprehensive basis for engineering applications. In addition, the effect of rainfall pattern on slope failure is also analysed in this research.

2. Governing differential equation for water-air two-phase flow

Liquid phase (water) flow equation and air phase flow equation are included in the governing differential equations for water-air two-phase flow. These two equations can realize the coupling process by correlation of some variables including saturation, pore air pressure, matric suction as well as porosity. The flow of water and air not only conforms with mass conservation equation driven by pressure but also considers some variation factors including soil deformation, compressibility, viscosity as well as saturation. The governing differential equations for water-air two-phase flow can be described as follows [20]:

$$\mathrm{nS}\frac{\partial \ln \rho_l}{\partial t} + S\frac{\partial n}{\partial t} + n\frac{\partial S}{\partial t} + \nabla \cdot \left[-\frac{k_r^l k}{\mu_l} \cdot \left(\nabla p_l + \rho_l g\right)\right] - \frac{1}{\rho_l} Q_l = 0 \tag{1}$$

$$\mathrm{n}(1-\mathrm{S})\frac{\partial \ln \rho_g}{\partial t} + (1-S)\frac{\partial n}{\partial t} - n\frac{\partial S}{\partial t} + \nabla \cdot \left[-\frac{k_r^g k}{\mu_g} \cdot \left(\nabla p_g + \rho_g g\right)\right] - \frac{1}{\rho_g} Q_g = 0 \tag{2}$$

Where n represents the porosity; S_r represents the degree of saturation; ρ_β represents the density of the phase (β = 1 represents the water phase, β = grepresents the air phase); Q_β represents the source of phase (kg/m); k represents the intrinsic permeability of soil determined by pore characteristics (m^2); k_r^β represents the relative permeability coefficient of the phase; μ_β represents the viscosity coefficient of the phase ($\mathrm{N \cdot s/m^2}$); p_β is the pore pressure of the β phase ($\mathrm{N/m^2}$); g is the gravitational acceleration (N/kg).

The dynamics of water-air two-phase flow are described by a complex system of partial differential equations that are nonlinear and depend on both space and time variables. To tackle the spatial domain, the Galerkin finite element method is utilized, while the time domain is discretized using a difference method. This approach enables a robust and accurate calculation of the flow dynamics by considering two unknowns, namely the pore pressure (ρ_g) and the saturation (S_r), which are solved iteratively through a cyclic calculation of Eq. (1) and Eq. (2). This iterative process ensures that the solution converges to the correct values. Overall, this methodology provides an efficient and reliable approach for investigating water-air two-phase flow dynamics, which can help to understand the behaviour of fluid flow in porous media, and provide insights into the optimization of industrial processes.

3. Computational model

In pursuit of a more profound understanding of the underlying principles governing rainfall infiltration, this section employs the illustrative framework of the Shuping landslide case study. Through the application of advanced simulation techniques, the dynamic interplay between water and air within the slope during the process of rainfall infiltration is meticulously recreated. This simulation endeavour is strategically designed to shed light on the fundamental tenets that dictate the behaviour of rainfall infiltration on slopes. It takes into account the distinctive attributes of this process, the variations in its intensity, and its propensity for generating runoff.

Subsequent to this, the discussion takes a comprehensive turn by delving into the intricate mechanisms that underpin the intermingling of water and air within the environmental context of the slope. By deciphering these mechanisms, the study aims to offer deeper insights into the multifaceted factors influencing the behaviour of water and air during rainfall infiltration. The discourse seeks to unravel the dynamics that govern their coexistence within the slope's environment, ultimately contributing to a more holistic and accurate comprehension of this intricate natural process.

3.1 Study area and geometric model

This study presents a case study of the Shuping landslide, which is located on the north bank of the Yangtze River, 61 km away from the dam site of the Three Gorges Project. The landslide body comprises a loose rock clastic layer and a loess soil layer, which have good permeability and are conducive to groundwater infiltration. The bottom of the landslide body is composed of phyllite, which has relatively weak permeability and can form a relative waterproof layer.

The Shuping landslide is characterized as a relict landslide, characterized by a historical chronicle of recurring sliding occurrences. Since the initiation of the Three Gorges Reservoir impoundment in June 2003, a persistent sequence of deformations

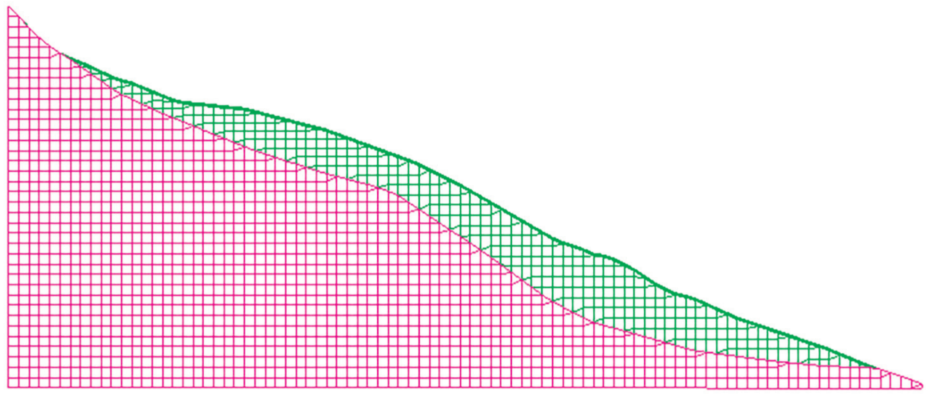

Figure 1.
Finite element grid diagram of the slope cross-section.

has been discerned. Consequently, there has been a progressively escalating manifestation of surface deformations within the sliding mass. Particularly notable is the observable trend of continuous propagation observed in the emergence of cracks within the slope. Furthermore, instances of localized significant collapses have been identified. Presently, the landslide remains subjected to an ongoing process of deformation.

The Shuping landslide boasts a historical record marked by recurrent events of collapse and sliding. Its stability is relatively compromised, thereby rendering it susceptible to deformations and failures instigated by external variables such as precipitation and fluctuations in reservoir water levels. If a substantial decrease in the Three Gorges Reservoir water level, reducing it from 175 meters to 145 meters, coincides with intense rainfall, the sliding mass would be susceptible to incurring substantial deformations, thereby possibly precipitating a precarious state of instability.

The thickness of the sliding body provides the material foundation for the landslide. The front edge of the Shuping landslide is 1100 m wide, the back edge is 800 m wide, and the longitudinal length is 550 m. The back edge is distributed in the line of the elevation of 280–338 m. For numerical modelling, the main sliding section is considered, with a horizontal length of 600 m and a vertical height of 350 m. To accurately simulate rainfall infiltration, the surface layer of the landslide body is discretized into elements with varying thicknesses, ranging from 0.25 to 0.75 m along the slope depth direction. The finite element calculation grid obtained by subdivision consists of 3499 elements and 3427 nodes, as shown in **Figure 1** (geometric model for numerical simulation). This approach provides a comprehensive understanding of the landslide characteristics and the factors that influence its behaviour, which can contribute to the development of effective mitigation strategies for similar geological hazards.

3.2 Initial and boundary conditions

To reduce the uncertainty impact of initial state on this research, this study incorporates measured rainfall data from the Three Gorges Reservoir area spanning several years (provided by the Headquarters of Geological Disaster Prevention in the Three Gorges Reservoir Area of the Ministry of Land and Resources). The seepage field of the slope is calculated and simulated in the fully saturated state until it reaches to a relatively stable state, which is used as the initial condition for subsequent calculations. By adopting this approach, the study aims to minimize potential errors or biases that may arise from using arbitrary initial conditions. The use of measured data and stable conditions provides a more accurate and realistic representation of the initial state of the system, which is critical for achieving meaningful and reliable results. This study conducts a thorough examination of the real-world system under investigation. It investigates various aspects, including the behaviour of materials, the system's boundaries, its geometries, and significant variables such as the impact of rainfall. The interplay of these diverse elements collectively influences the system's behaviour. Through a detailed analysis of these factors, the study aims to unravel the intricate dynamics that govern the system's behaviour within its environmental context.

In this research, the side and bottom of the rear edge of the model are treated as impervious boundaries, and the water level and its variation at the boundary are calculated. The slope surface and leading edge below the reservoir water level are considered as known water pressure boundaries, and their values are dependent on the reservoir water level elevation (145 m). On the other hand, the slope surface above the reservoir water level is treated as the known air pressure boundary. As the runoff water head on the slope is relatively small compared with the atmospheric pressure, it is assumed to be negligible. In the present analysis, the air pressure on the air pressure boundary is set to atmospheric pressure. The proposed approach enables the determination of infiltration rates of both water and air from calculation results, without the need for their *a priori* specification as flow boundaries. Compared to the traditional single-phase flow calculations, this approach provides a more comprehensive understanding of the dynamics of the water-air two-phase flow, which is important for achieving more accurate predictions and more effective risk assessments in geotechnical engineering applications.

3.3 Constitutive relations and parameters

For the given slope, the mathematical description of the rainfall infiltration process is determined by the governing differential equation, initial and boundary conditions, constitutive relation, and corresponding parameters of water and air two-phase flow. Eq. (1) and Eq. (2) involve five unknowns: S, k_r^l, k_r^g, p_l and p_g, which are solved concurrently by incorporating the relationship between soil-water characteristics determined by soil properties and the relative permeability function of water and air.

In this research, the commonly used Van Genuchten model is adopted to represent the soil-water characteristic curve. The mathematical relationship between matric suction $\left(p_c \equiv p_g - p_l\right)$ and saturation is expressed as follows [21]:

$$p_c = -p_0\left(S_e^{-1/\lambda} - 1\right)^{1-\lambda} \tag{3}$$

Where S_e represents the effective water saturation $\left(S_e = \frac{S-S_{rl}}{1-S_{rl}}\right)$; S_{rl} represents the residual water saturation; p_0 and λ are parameters of this model. According to some literature data [22], this calculation adopts the value of $p_0 = 1.33$, $\lambda = 0.41$, $S_{rl} = 0.15$ as three parameters.

The relative permeability coefficients of water (k_r^l) and air (k_r^g) are using the Van Genuchten-Mualem [22] model and Corey model, respectively. In this study, the relative permeability coefficients that contain effective saturation variable can be expressed as follows [23, 24]:

$$k_r^l = \sqrt{S_e}\left\{1 - \left[1 - (S_e)^{1/\lambda}\right]^{\lambda}\right\}^2 \tag{4}$$

$$k_r^g = (1 - S_e)^2\left[1 - S_e^2\right] \tag{5}$$

The values of some other parameters are as follows [22]: n = 0.15, k = $4.0 * 10^{-12} m^2$, g = 9.8N/kg, $\rho_g = 1.29 kg/m^3$, $\rho_l = 1 * 10^3 kg/m^3$, $\mu_l = 1 * 10^3 N \cdot s/m^2$, $\mu_g = 1 * 10^{-5} N \cdot s/m^2$.

3.4 Slope stability analysis method considering pore air pressure

In this study, the slope stability analysis is conducted to use the residual thrust method, which incorporates the consideration of matric suction and pore air pressure. The calculation procedure involves several steps: an initial assumption of the safety factor, subsequent calculation of the thrust starting from the first slide at the top of the slope and progressing towards the last slide, and finally determining the safety factor value at which the thrust reached zero. This zero-thrust condition represents the equilibrium state, thus yielding the final safety factor value [25–28].

$$\begin{aligned} P_i &= W_i \sin\alpha_i - \frac{c_i' l_i + \left(W_i \cos\alpha_i - p_\alpha^i l_i\right)\tan\varphi_i' + l_i\left(p_a^i - p_w^i\right)\tan\varphi^b}{F_s} + P_{i-1}\psi_i \\ \psi_i &= \left[\cos(\alpha_{i-1} - \alpha_i) - \frac{\tan\varphi_i'}{F_s}\sin(\alpha_{i-1} - \alpha_i)\right. \end{aligned} \tag{6}$$

Where F_s is the safety factor of the slope, P_i is the sliding force of soil slice, c_i' is the effective cohesive force of slice, φ_i' is the effective internal friction angle of slice, l_i is the width of soil slice, W_i is the weight of soil slice, α_i is the angle of bottom soil slice, p_a^i and p_w^i are pore air pressure and pore water pressure of slice, $\tan\varphi^b$ is the rate of shear strength that increases with an increase in matric suction, and ψ_i is the transfer coefficient of slice i. The model recommended by Vanapalli [29] in this research can be expressed as a function of effective saturation. The equation is as follows:

$$\tan\varphi^b = S^* \cdot \tan\varphi' \tag{7}$$

Where the effective saturation is expressed as follows:

$$S^* = (S_r - S_{rw})/(1 - S_{rw}) \tag{8}$$

4. Rainfall infiltration analysis of slope

In this research, we present the results of finite element calculations of two-phase flow (water and air) in Shuping landslide. Our findings reveal the general rule of rainfall infiltration in slopes, examining characteristics such as infiltration intensity, flow-producing strips, and infiltration patterns. Additionally, we elucidate the coupling force transfer mechanism between water and air in slopes. Through our analysis, we aim to contribute to a deeper understanding of the complex processes that govern the behaviour of landslides under the influence of rainfall infiltration.

4.1 Rainfall infiltration characteristics of slope surfaces

According to the calculation results of Shuping landslide, the direction and total velocity of material (water, air) entering and leaving the slope surface show a certain regularity. According to different directions of material (water and air) inflow and outflow, the slope surface can be divided into inflow area and overflow area. If the fluid tends to flow in the direction of the slope, exhibiting an upward or uphill movement, this area is commonly known as the inflow area. Conversely, the overflow area represents the zone where the flow rate of water or air predominantly moves away from the slope (**Figure 2**). The distribution of inflow area and overflow area of slope surface has strong regularity. The water and air inflow area is usually located in the middle and upper part of the slope, while the overflow area is generally located in the lower part. The boundary line between the suction zone and the overflow zone is usually not fixed. It is not only related to the geometric characteristics and permeability characteristics of slope, but also affected by rainfall characteristics such as rainfall duration, rainfall interval, and rainfall intensity. With the extension of rainfall duration, the boundary line between inflow area and overflow area will move upward, the inflow area of slope surface will shrink, and the overflow area will increase. With the increase of rainfall interval, the boundary line will gradually move down, and the inflow area of slope surface will increase, while the overflow area will decrease.

Based on numerical analysis, the total flow rate of water and air through the slope surface exhibits phase-pair stability, and its magnitude is primarily influenced by slope geometry and the transmission characteristics of geotechnical materials, while external factors such as rainfall characteristics, slope flow production, and air temperature variation have relatively little effect. The flow rate of water and air into and out of the slope surface provides a measure of the intensity of rainfall inflow and overflow. **Figure 3** depicts the relationship between the intensity of water and air inflow (overflow) and time. The curve indicates that, as the rainfall duration increases, the maximum inflow and overflow intensities of the Shuping landslide slope attain a certain stability, with the

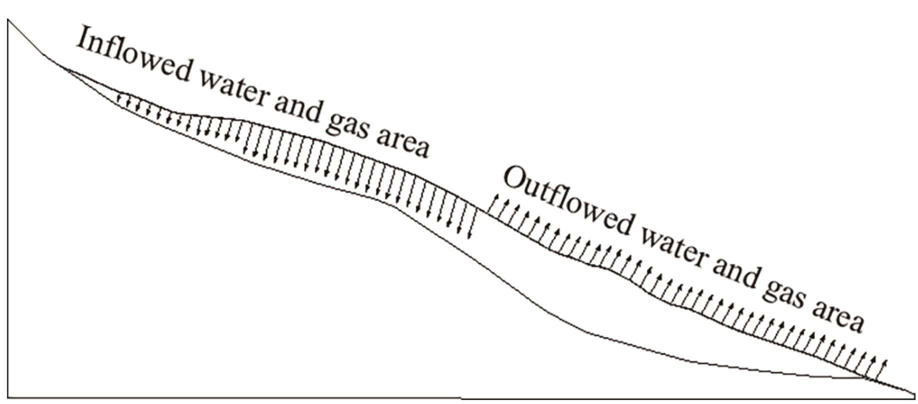

Figure 2.
Slope surface (water, air): Inflow and overflow area.

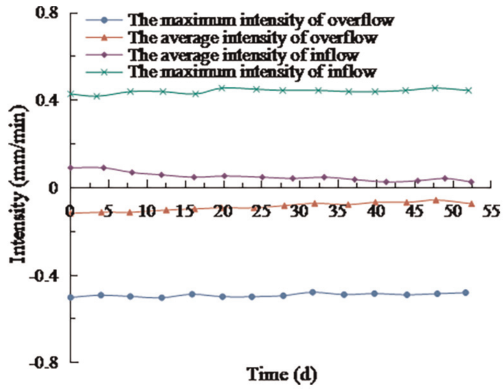

Figure 3.
Variation of inflow and overflow intensity over time.

former being around 0.4 mm/min and the latter around 0.5 mm/min. The average inflow and overflow intensity values of water and air on the slope exhibit a slight downward trend, with both values being quite similar at approximately 0.1 mm/min.

4.2 Rainfall infiltration intensity and flow-producing conditions on slope surface

The assessment of rainfall infiltration intensity and runoff production on slope surfaces is closely linked to the relative magnitude of infiltration and the total inflow rate of the slope surface, comprising both water and air. In the inflow area of the slope surface, infiltration of water and air relies primarily on the composition of water and air at the slope's boundary. In the absence of rainfall on the surface, air is drawn into the inflow area through its boundary. Conversely, when rainfall occurs on the surface, if the rainfall intensity is lower than the total inflow rate of the slope (consisting of water and air), the slope's inflow area will not produce flow, and the infiltration intensity of rainwater will match the rainfall intensity. The slope's boundary will absorb a mixture of water and air with varying compositions. However, if the rainfall intensity exceeds the total inflow rate of the slope (comprising both water and air), runoff will occur on the slope, and the infiltration intensity will equal the total inflow intensity of water and air. In such cases, the surface of the slope is covered by air, while water is drawn at the inflow area's boundary.

Regarding the Shuping landslide, rainfall intensity is much greater than the total inflow intensity of the slope, approximately 0.1 mm/min, which is a prerequisite for runoff to be generated on the slope. The maximum inflow area is located at the top of the slope, when the rainfall intensity exceeds the maximum inflow intensity of the slope surface, which is approximately 0.4 mm/min, and the slope may experience full flow generation. These observations suggest that rainfall intensity and the total inflow rate of the slope surface are essential factors to consider when analysing the potential for runoff generation and slope stability during rainfall events.

In the overflow area of the slope surface, the overflow of water and air is closely linked to the water and air content at the slope's boundary and the slope saturation. According to a report by the Yangtze River Scientific Research Institute in 2017, when rainfall infiltration intensity was 0, the slope surface produced runoff, and the outflow at the boundary of the overflow area was water. In an unsaturated state, the infiltration intensity of rainfall is equivalent to the intensity of the rainfall itself, resulting in a lack of flow on the slope surface. The outflow from the boundary of the overflow zone consists of a combination of water and air. In scenarios where the entire overflow area is dry, the outflow at the boundary of the overflow area exclusively consists of pore air.

These observations yield insights into the pivotal roles played by several key factors in the process of water and air overflow on the slope surface. Among these factors, the water and air content existing at the boundary of the overflow region, as well as the saturation state of the slope, emerges as critical determinants. Moreover, these findings indicate that a confluence of variables, namely rainfall intensity, slope saturation, and the water and air content at the slope's boundary, collectively governs the production of runoff and the characteristics of overflow events.

In essence, these insights underscore the intricate interplay of factors that orchestrate the dynamics of water and air behaviour within the context of slope surface overflow. The water and air content at the boundary of the overflow zone, alongside the slope's saturation state, serves as foundational considerations that shape the overflow process. Furthermore, the interrelation between these variables and external factors such as rainfall intensity adds layers of complexity to the observed behaviours. These findings contribute to an enhanced understanding of the multifaceted mechanisms governing the overflow dynamics, thereby facilitating more accurate assessments and predictions in geotechnical and hydrological investigations.

4.3 Water-air coupling force transfer mechanism

Rainfall infiltration is a process where water and air interact within soil pores, influencing each other's movement. Water moves downward due to gravity, causing air to move within the pores. The compression of air generates a counteracting force against the water's movement. However, due to its low viscosity (about 1% that of

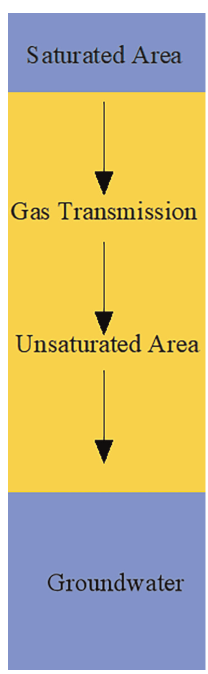

Figure 4.
Mechanism of water-air coupling in force transfer.

water), air's effect on slope stability is unfavourable. **Figure 4** depicts the force transfer mechanism resulting from water-air coupling. This coupling leads to pressure on the subsurface water, highlighting the detrimental influence of air on slope stability.

Figures 5–7 show the saturation, pore air pressure, and pore water pressure distribution cloudy map of Shuping landslide at a specific time. It reveals that the saturated water pressure at the top of the slope is transmitted to the saturated area at the slope's front through closed pore air in the unsaturated area. This phenomenon leads to a partial elevation of groundwater level in the anti-sliding area at the slope's front, resulting in the formation of external normal thrust that adversely affects slope stability.

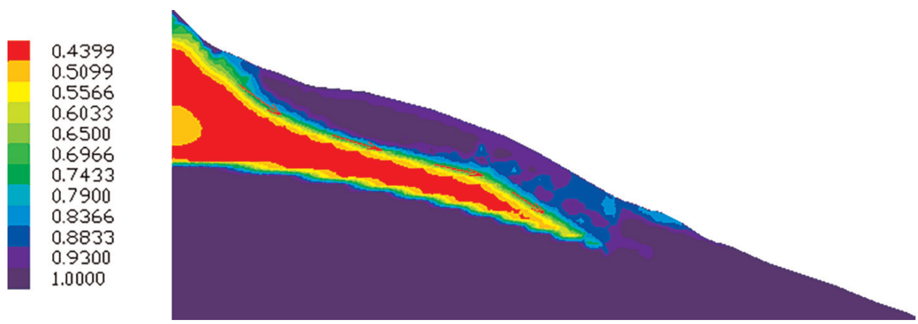

Figure 5.
Distribution of water saturation for Shuping landslide at one time.

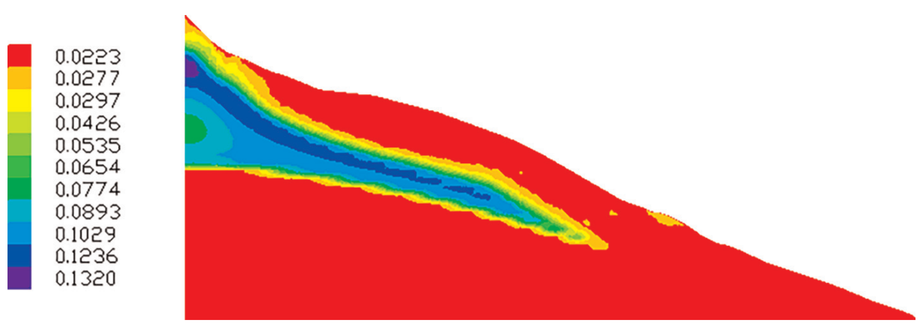

Figure 6.
Distribution of pore air pressure for Shuping landslide at one time.

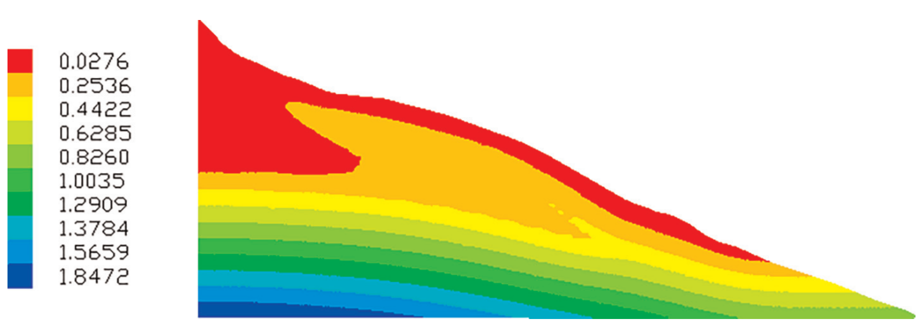

Figure 7.
Distribution of pore water pressure for Shuping landslide at one time.

4.4 Effect of rainfall type on infiltration

By analysing pertinent data, the rainfall pattern can be categorized into four distinct conditions, as depicted in **Figure 8**. These conditions are characterized as four rainfall patterns. Uniform rainfall pattern: during this condition, the rainfall intensity remains relatively constant over the specified time period. Pre-peak rainfall pattern: this condition exhibits a linear decrease in rainfall intensity over time, leading up to a peak point. Post-peak rainfall pattern: in this condition, the rainfall intensity demonstrates a linear increase over time, following a peak point. Mid-peak rainfall pattern: this condition displays a rainfall intensity that initially increases and then subsequently decreases, forming a peak point.

Figures 9 and **10** illustrate the variations in pore air pressure and safety factor under four different rainfall patterns. In the case of uniform rainfall pattern, when the rainfall intensity remains constant, the saturation of the soil on the slope surface becomes saturated. Consequently, the slope surface forms a relatively impermeable state, which limits the outflow of air from the slope surface. As a result, the pore air pressure continues to rise. With increasing saturation, the matric suction decreases, leading to an increase in pore water pressure. During this period, the rainfall not only increases the load on the slope but also weakens the strength parameters, causing a decrease in the safety factor of the reservoir bank slope. As the rainfall duration increases, the infiltration intensity on the slope surface gradually decreases, resulting in a reduction in the amount of infiltrated water. Consequently, the pore air pressure, pore water pressure, and safety factor eventually reach a stable state. In the case of pre-peak rainfall, the initial stage shows a similar pattern to uniform rainfall, where the

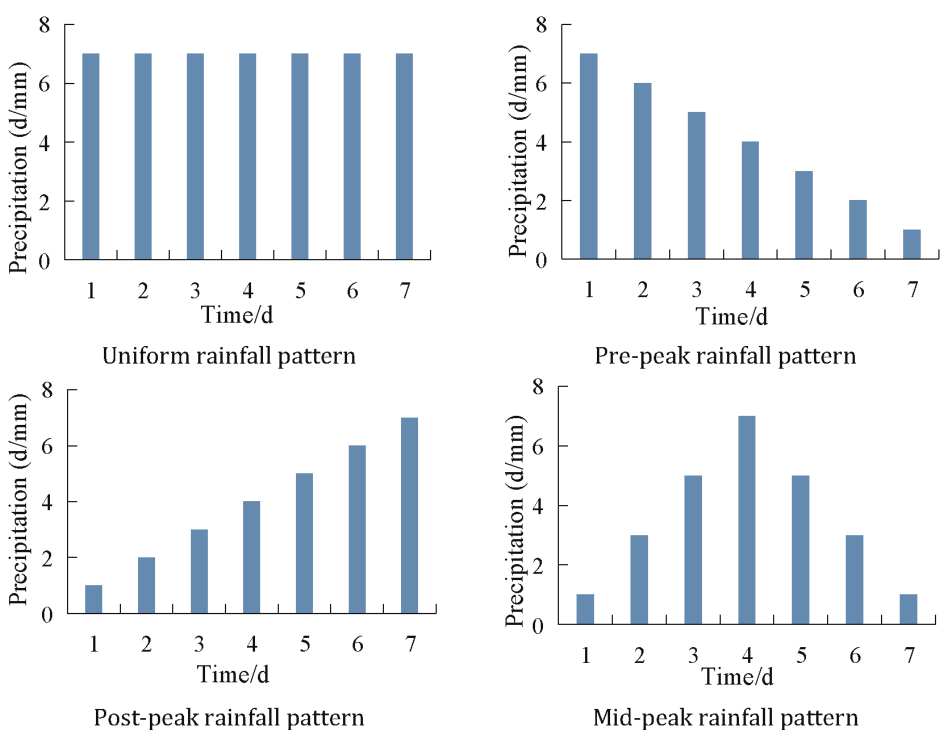

Figure 8.
Four types of rainfall patterns.

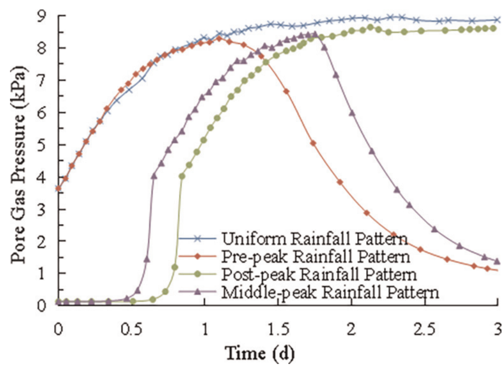

Figure 9.
Temporal variation in pore air pressure associated with four rainfall patterns.

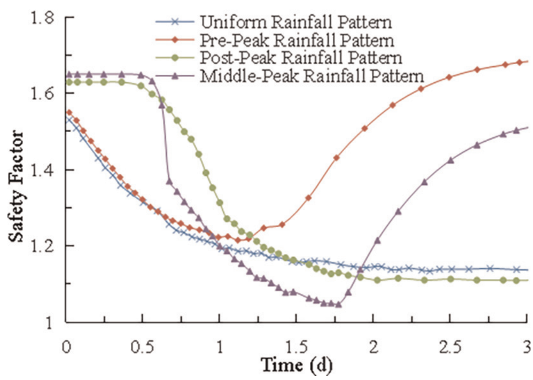

Figure 10.
Temporal variation in safety associated with four rainfall patterns.

pore air pressure and pore water pressure increase non-linearly, leading to a decrease in the safety factor. During linearly decreasing rainfall, the slope surface gradually transitions from a saturated state to an unsaturated state. Pores in unsaturated soil provide a pathway for the overflow of pore air pressure from the slope body. In comparison with the early stages of rainfall, the pore air pressure decreases rapidly, while the pore water pressure increases in the latter half of the pre-peak rainfall. Consequently, the slope safety factor is gradually recovered. As the rainfall intensity is relatively low in the early period, the pore air pressure begins to increase from 0. As the rainfall continues, the intensity gradually increases. As a result, the surface soil becomes saturated rapidly during the later stage of rainfall, leading to a rapid increase in pore air pressure and pore water pressure, while the safety factor of the slope decreases. In the case of mid- peak rainfall, the rainfall intensity gradually increases during the early stages, and the pore air pressure increases gradually from 0. As a result, the safety factor experiences a slow decrease in the initial stage. With the continuous increase in rainfall intensity, the pore air pressure decreases rapidly, while the pore water pressure increases, leading to a rapid decrease in the safety factor. At the point when the rainfall intensity reaches its maximum, both the pore air pressure and pore water pressure reach their maximum values, resulting in the minimum safety factor. Subsequently, as the rainfall intensity starts to decrease, the pore air pressure and pore water pressure also decrease, causing a slow increase in the safety factor.

5. Conclusions

This study initially presents the fundamental patterns governing rainfall infiltration on slopes. This presentation encompasses various aspects, including slope surface characteristics related to rainfall infiltration, the intensity of rainfall infiltration, and the prevailing runoff conditions. Subsequently, a comprehensive explanation is provided regarding the intricate mechanism underlying the coupled transmission forces of water and air within the slope's environment, which also constitutes the novelty of this work. Furthermore, this research also encompasses an analysis of the impact of rainfall patterns on slope failure.

Based on the principles of water-air two-phase flow, the rainfall infiltration process of Shuping landslide is analysed through finite element method. The following conclusions could be drawn from the analysis:

1. The direction of water and air entering and leaving the slope differs, resulting in the formation of an inflow zone and an overflow zone on the slope surface, with the former typically located at the upper part and the latter at the lower part of the slope.

2. The total flow rate of water and air in and out of the slope surface depends mainly on the material transmission characteristics and geometric characteristics of the slope and is relatively stable, with less influence from the flow production condition and runoff depth.

3. The relative relationship between rainfall intensity and the total inflow rate of water and air can serve as a judgement criterion for rainfall infiltration intensity and runoff production condition on the slope surface. In the inflow area, when the rainfall intensity is less than the total inflow rate of water and air, no flow is produced, and the infiltration intensity is equal to the rainfall intensity. Conversely, the slope produces flow, and the infiltration intensity is equal to the total inflow intensity of water and air.

4. The water pressure in the saturated area of the slope surface can be transferred to the underground saturated area through the pore air in the unsaturated area, which increases the underground water pressure and the normal thrust outside the slope foot, and adversely affects the slope stability. The analysis provides a theoretical basis for engineering examples by simulating and generalizing the law of rainfall infiltration.

5. During period of uniform rainfall, there is a noticeable decline in the safety factor. When the rainfall type transitioned to post-peak rainfall, the safety factor exhibits an overall downward trend. Notably, during the initial stage of rainfall, the reduction rate of the safety factor was significantly lower compared to the subsequent stages of rainfall. In contrast, both mid-peak rainfall and pre-peak rainfall experienced minimal precipitation in the later period, resulting in an increase in the safety factor. However, due to the numerous factors affecting the process, quantitative analysis of the infiltration rule is still limited. Therefore, further studies will focus on analysing and controlling the influencing factors and quantifying the general rule of the infiltration process.

Acknowledgements

The work was supported by the Geotechnical Laboratory at Ghent University and Geosound.be. The first author would like to acknowledge the financial support received from the China Scholarship Council (No.201908420298).

References

[1] Li B, Tian B, Tong FG, Liu C, Xu XL. Effect of the water-air coupling on the stability of rainfall-induced landslides using a coupled infiltration and hydromechanical model. Geofluids. 2022;**8**:1-16. DOI: 10.1155/2022/3036905

[2] Liu G, Tong FG, Zhao YT. A force transfer mechanism for triggering landslides during rainfall infiltration. Journal of Mountain Science. 2018;**15**: 2480-2491. DOI: 10.1007/s11629-018-5043-x

[3] Liu G, Tong FG, Tian B. A finite element model for simulating surface run-off and unsaturated seepage flow in the shallow subsurface. Hydrological Processes. 2019;**33**(26):3378-3390. DOI: 10.1002/hyp.13564

[4] Hou XK, Vanapalli SK, Li TL. Water infiltration characteristics in loess associated with irrigation activities and its influence on the slope stability in Heifangtai loess highland, China. Engineering Geology. 2018;**234**:27-37. DOI: 10.1016/j.enggeo.2017.12.020

[5] Airmo JM, Rahardjo H, Leong EC. Infiltration effects on stability of a residual soil slope. Computers and Geotechnics. 2000;**26**(2):145-165. DOI: 10.1016/S0266352X (99)00035-X

[6] Liu G, Tong FG, Tian B, Tian WJ. Influence of atmospheric temperature on shallow slope stability. Environmental Earth Sciences. 2019;**78**(22):632. DOI: 10.1007/s12665-019-8649-6

[7] Tong FG, Jing L, Zimmerman RW. A fully coupled thermo-hydro-mechanical model for simulating multiphase flow, deformation and heat transfer in buffer material and rock masses. International Journal of Rock Mechanics and Mining Sciences. 2010;**47**(2):205-217. DOI: 10.1016/j.ijrmms.2009.11.002

[8] Zhou YF, Tham LG, Yan WM, Dai FC, Xu L. Laboratory study on soil behavior in loess slope subjected to infiltration. Engineering Geology. 2014; **183**:31-38. DOI: 10.1016/j.enggeo.2014.09.010

[9] Koyama A, Fujimoto T, Suetsugu T, Fukubayashi Y. Analysis of embankment failure mechanism in reservoirs due to rainfall infiltration during heavy rainfall. Natural Hazards and Risk. 2022;**13**(1): 1849-1866. DOI: 10.1080/19475705.2022.2102440

[10] Komori D, Rangsiwanichpong P, Inoue N, Ono K, Watanabe S, Kazama S. Distributed probability of slope failure in Thailand under climate change. Climate Risk Management. 2018;**20**:126-137. DOI: 10.1016/j.crm.2018.03.002

[11] Sharma RH, Nakagawa H. Numerical model and flume experiments of single and two-layered hillslope flow related to slope failure. Landslides. 2010;**7**:425-432. DOI: 10.1007/s10346-010-0205-0

[12] Liu C, Tong F, Li B, et al. A water retention curve model describing the effect of temperature. European Journal of Soil Science. 2020;**71**(1):44-54. DOI: 10.1111/ejss.12825

[13] Sun DM, Zang YG, Semprich S. Effects of airflow induced by rainfall infiltration on unsaturated soil slope stability. Transport in Porous Media. 2015;**107**:821-841. DOI: 10.1007/s11242-015-0469-x

[14] Sung EC. Stability analysis of unsaturated soil slopes considering water-air flow caused by rainfall

infiltration. Engineering Geology. 2016; **211**:184-197. DOI: 10.101 6/j. enggeo.2016.07.008

[15] Sun DM, Li XM, Feng P, Zang YG. Stability analysis of unsaturated soil slope during rainfall infiltration using coupled liquid-air-solid three-phase model. Water Science and Engineering. 2016;**9**(3):183-194. DOI: 10.1016/j.wse. 2016.06.008

[16] Hu R, Chen YF, Zhou CB. Modelling of coupled deformation, water flow and air transport in soil slopes subjected to rain infiltration. Science China Technological Sciences. 2011;**54**: 2561-2575. DOI: 10.1007/s11431-011-4504-z

[17] Touma J, Vauclin M. Experimental and numerical analysis of two-phase infiltration in a partially saturated soil. Transport Porous Media. 1986;**1**:27-55. DOI: 10.1007/BF01036524

[18] Xue S, Yang Z, Hu R, et al. Splitting dynamics of liquid slugs at a T-junction. Water Resources Research. 2020;**56**(8): e2020WR027730. DOI: 10.1002/ essoar.10503637.1

[19] Chen P, Wei CF. Numerical procedure for simulating the two-phase flow in unsaturated soils with hydraulic hysteresis. International Journal of Geomechanics. 2016;**16**(1):1532-3641. DOI: 10.1061/(ASCE)GM.1943-5622.0000505

[20] Tong FG. Numerical Modelling of Coupled Thermo-Hydro-Mechanical Processes in Geological Porous Media. Stockholm, Sweden: KTH; 2010

[21] Van Genuchten MT. A closed-form equation for predicting the hydraulic conductivity of unsaturated soils. Soil Science Society of America Journal. 1980;**44**:892-898. DOI: 10.2136/ sssaj1980.03615995004400050002x

[22] Mualem Y. A new model for predicting the hydraulic conductivity of unsaturated porous media. Water Resources Research. 1976;**12**:513-522. DOI: 10.1029/WR0 12i003p00513

[23] Corey AT. The interrelation between air and oil relative permeabilities. Producers Monthly. 1954;**19**:38-41

[24] Tian W, Peiffer H, Malengier B, Xue S, Chen Z. Slope stability analysis method of unsaturated soil slopes considering pore air pressure caused by rainfall infiltration. Applied Science. 2022;**12**:11060. DOI: 10.3390/ app122111060

[25] Wei WB, Cheng YM, Li L. Three-dimensional slope failure analysis by the strength reduction and limit equilibrium methods. Computers and Geotechnics. 2009;**36**(1-2):70-80. DOI: 10.1016/ j.compgeo.2008.03.003

[26] Fang N, Ji CS, Crusoe GE. Stability analysis of the sliding process of the west slope in Buzhaoba open-pit mine. International Journal of Mining Science and Technology. 2016;**26**(5):869-875. DOI: 10.1016/j.ijmst.2016.05.033

[27] Su AJ, Zou ZX, Lu ZC, Wang JG. The inclination of the interslice resultant force in the limit equilibrium slope stability analysis. Engineering Geology. 2018;**240**:140-148. DOI: 10.1016/ j.enggeo.2018.04.016

[28] Yao W, Li C, Zhan H. Time-dependent slope stability during intense rainfall with stratified soil water content. Bulletin of Engineering Geology and the Environment. 2019;**78**: 4805-4819. DOI: 10.1007/s10064-018-01437-3

[29] Vanapalli SK, Sillers WS, Fredlund MD. The meaning and relevance of residual state to unsaturated soils. In: 51st Canadian Geotechnical Conference. Vol 8. Edmonton Alberta, Canada; 1998

Chapter 5

The Impact of Earthquakes on Dropout Doline (Cover Collapse Sinkhole) Development: A Case Study from the Environs of Mečenčani and Borojevići (Croatia)

Márton Veress, Natalija Matić, Zoltán Mitre and Gábor Szunyogh

Abstract

In this study, the effect of earthquakes, beginning on 28 December 2020, on dropout doline development in the environs of Mečenčani and Borojevići was investigated. For that purpose, the shape of the doline, the inclination of the bearing surface and the rate of doline development were determined. A further analysis involved the characteristics of groundwater in the environs of the dolines and a functional relationship between the depth and the diameter of the dolines was sought. A model is proposed for the failure of the ceiling of cover cavities without support. The intensity of doline development is explained by favourable environment (dual cavity system, low inclination of the bearing surface, the presence and fluctuation of groundwater, etc.), the direct effect of earthquakes (material failure induced by earthquakes) and by their indirect effect (the partial solifluction of the ceiling material, lowered groundwater level).

Keywords: dropout doline, earthquake, groundwater, karst water, cavity

1. Introduction

In this study, the development of dropout dolines (cover collapse sinkholes) in the environs of Mečenčani and Borojevići (Croatia) to the effect of the earthquakes of Petrinja between 28 December 2020 and 03 March 2021 is interpreted. Croatian researchers compiled a comprehensive documentation on the effect of the Petrinja earthquakes and also described the dolines that were formed during this time [1, 2]. All other investigations are of geomorphological nature [3], those concerned with remediation measures and priorities for immediate action [4], ground displacement using data from orbits of the Sentinel-1 mission action [5, 6]; fault geometry and the coseismic slip distribution [7], earthquake and deformations [8, 9]. To date, not a single investigation considered the effect of earthquakes on dropout doline development in the environs of Mečenčani and Borojevići such as the shape of the doline, the inclination of the bearing surface and the rate of doline formation. It is very important to emphasize that doline development damaged houses in the villages. The novelty of this investigation includes a model for the failure of the ceiling of cover cavities without support, analysis of the characteristics of groundwater in the environs of the dolines and a functional relationship between the depth and the diameter of the dolines.

Subsidence dolines (subsidence sinkholes) develop on unconsolidated, permeable or partly permeable rock (on concealed karst). Their varieties are dropout dolines (cover collapse sinkholes), suffosion dolines and compaction dolines [10, 11]. Dropout dolines are formed by collapse, while suffosion dolines develop by suffosion [10, 12].

The development of dropout dolines is also contributed by earthquakes [13, 14]. Earthquake waves may trigger rock failure and thus, the collapse of rocks that became looser.

Irreversible and reversible (fluctuating) water level changes occur to the effect of earthquakes [15], and they also affect collapses.

2. Description of the area

The Sunja River Valley is situated between two larger geographical/landscape units of Sisak Posavina and Banovina (Banija) (**Figure 1**) and belongs to the Petrinja-Sunja hilly terrain. Permanent surface watercourses constitute a highly developed parallel drainage network with significant amounts of surface water. The Sunja River is a right-bank tributary of the Sava River and is a part of the Sava River Basin (Danube River Basin).

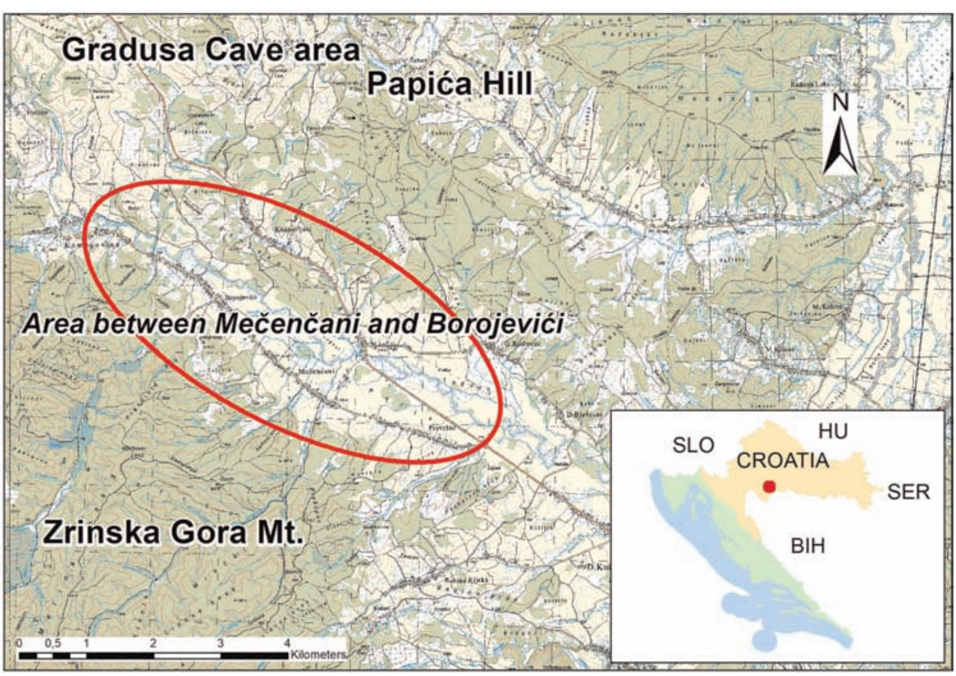

Figure 1.
Overview map of the area with geographical coordinates 45°16′59 N and 16°25′30 E.

The Sunja River Valley is a covered karst where subsidence dolines occur, but they are also widespread between Hrvatska Kostajnica and Petrinja. Following the earthquakes of 2020–2021, further subsidence (dropout) dolines developed within a relatively short time in relatively great numbers [16, 17]. The altitude of the bearing surface is 175–190 m. The established level of the groundwater is 177–183 m and

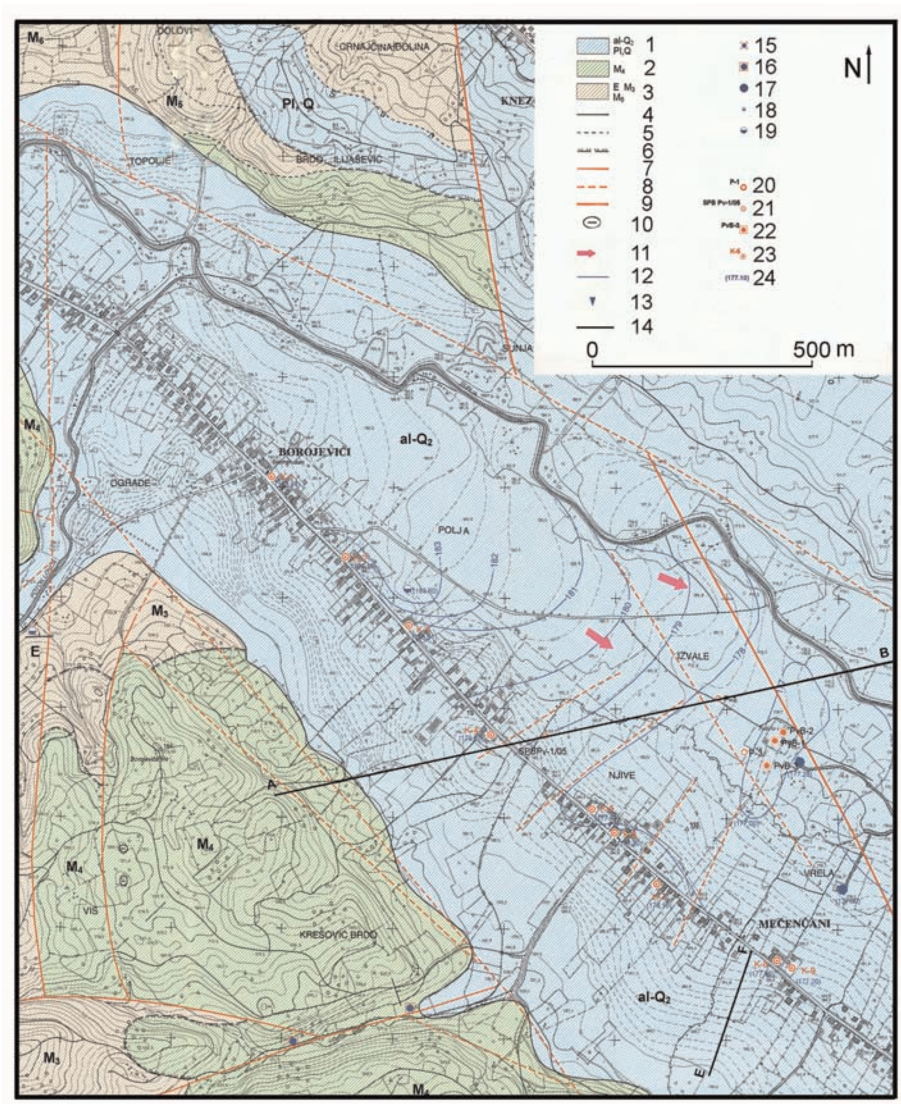

Figure 2.
Hydrological map of the environs of the dolines ([18], modified). 1. Gravel, sandy clay, clay, coarse-grained stream load and boulder, 2. Badenian limestone, 3. Sandstone, conglomerate, marl, calcareous and clayey marl, sand, clay, 4. Detected geological boundary, 5. Assumed geological boundary, 6. Erosional-discordance boundary, 7. Detected fracture, 8. Assumed fracture, 9. Fracture series, 10. Doline, 11. Direction of groundwater flow, 12. Water level according to the state of 11 November 2005, 13. Fluvial measurement site, 14. Geological cross section (A-B) and the cross section of its groundwater level (C-D), and geophysical cross section (E-F) 15. Occupied permanent spring with permanent water, 16. Occupied spring with permanent water, for local use, 17. Spring of permanent water with low discharge, 18. Intermittent spring with higher discharge, 19. Intermittent spring, 20. Drilling, 21. Planned drilling, 22. Drilled well, 23. Dug well, 24. Subsurface water level.

generally flows in S-E and N-E direction towards the springs Pašino vrelo, Bojanića vrelo and Davidovića vrelo (**Figure 2**). These springs create lakes in inactive dolines. The spring water of Pašino vrelo originates from Quaternary sediments in 70%, from Badenian limestone in 30%, while at Bojanića vrelo this proportion is 66% and 34%, at Davidovića vrelo 90% and 10% and at PBV-3 well 56% and 44% [18, 19].

The appearance of the springs is the consequence of a pronounced diagonal fault in the Sunja River Valley, which brought into direct contact permeable Upper Badenian predominantly carbonate rocks especially lithothamnium limestones (M_4) and poorly permeable to impermeable Pannonian marls (M_6) [18, 19]. Also, the area consists of Plio-Pleistocene age (Pl-Q) constituted by clay, clayey sand and pebbles and the alluvium (al- Q_2) constituted by pebbles, clay, clayey pebbles, older rocks, deluvial and proluvial sediments (**Figures 2** and **3**) [18, 20].

Geological structures in the investigated area extend mostly in NNW-SSE or NW-SE directions and follow the so-called 'Dinaric' strike (NW-SE), with predominantly dip-slip movements which are tectonically disturbed by the intersection of longitudinal NW-SE right-lateral and transverse NE-SW left-lateral faults of different size and importance along the transitional contact zone of the Dinarides and the Pannonian Basin [8]. The most important fault zone in the area is an active fault zone Pokupsko-Banja Luka in the Dinaridic ophiolite zone, Sava zone. According to [21], the strongest earthquake in the Kupa Valley M = 5.8 was recorded in the year 1909 (Mohorovičić discontinuity). The first strong earthquake in the wider Petrinja area was recorded on 28 December 2020. The day after, the second and third ones had magnitudes of M = 5 and M = 6.2 (h = 10 km). These earthquakes occurred on the Hrastovički fault, a segment of the Pokupsko Fault Zone stretching from Jastrebarsko through Pokupsko towards Banja Luka. These earthquakes caused the opening of approximately 100 new sinkholes (dolines) in the wider Mečenčani and Borojevići area.

Water inflow features are dolines, which are covered karst features and occur on the floor of the Sunja Valley. Among the dolines, there are distinguished [20] old dolines (they developed preceding the earthquake), more recent dolines (which

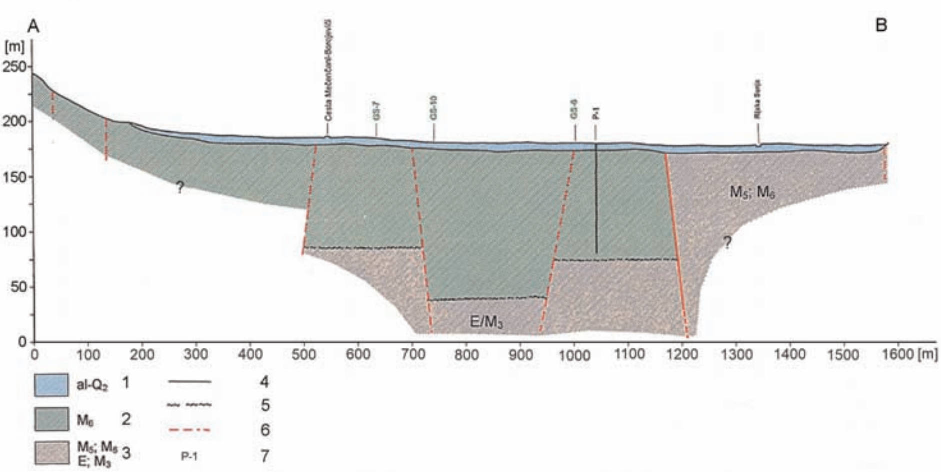

Figure 3.
Geological cross section (A-B) [18]. 1. Alluvium of the Sunja River: gravel, clay, sand, boulder, 2. Badenian limestone, 3. Eocene, Ottnangian, Sarmatian, Pannonian clastic sediments, 4. Boundary of beds, 5. Erosional discordance boundary, 6. Fracture, 7. Structural-piezometric drilling.

developed during the earthquakes) and even newer dolines (which developed after the earthquakes) and primitive dolines and buried dolines (**Figures 4** and **5**). Old features (42 dolines) have gentle slopes, are covered with vegetation and without

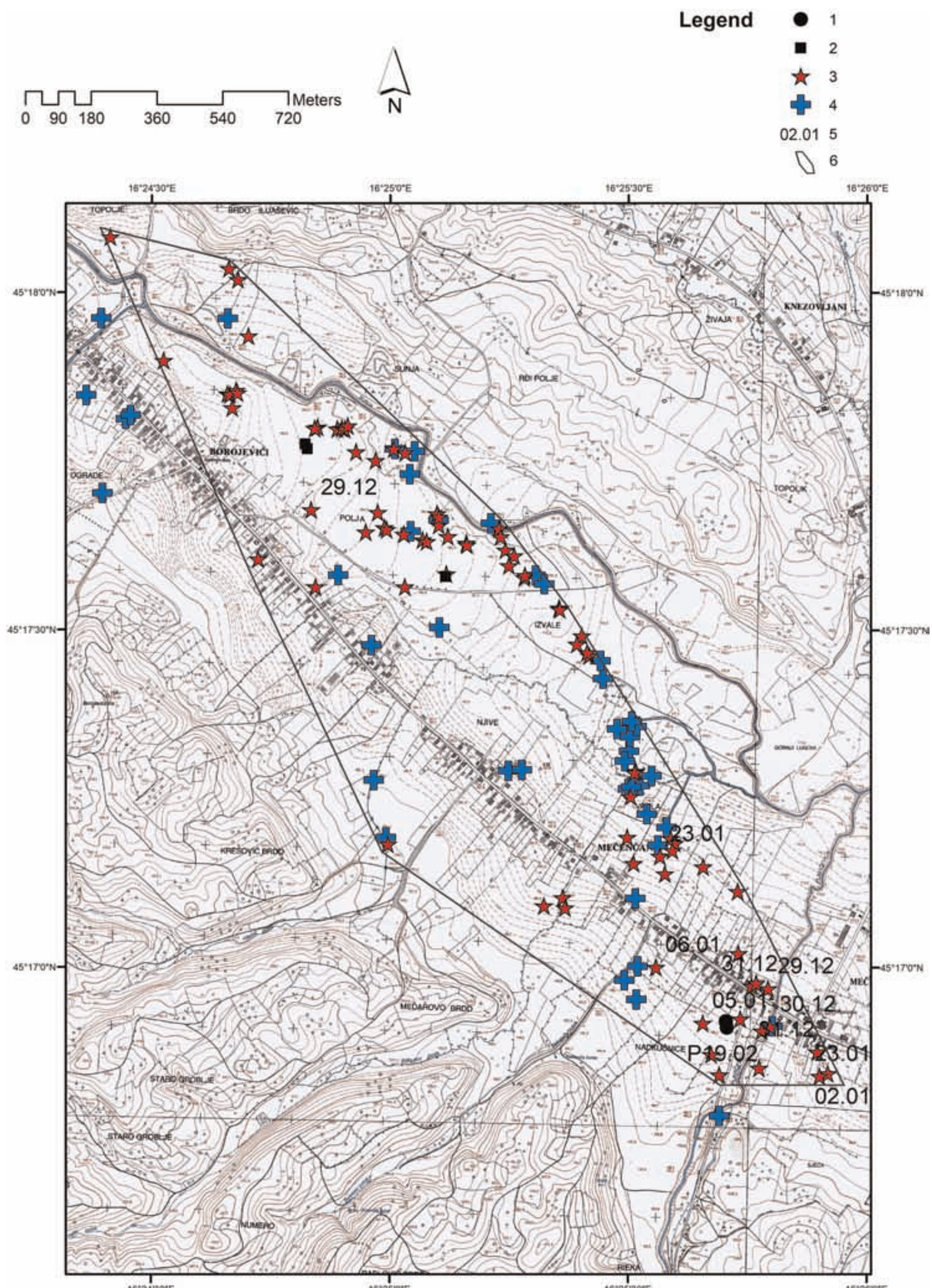

Figure 4.
Distribution of dolines (modified from [20]). 1. Buried doline, 2. Primitive doline, 3. New doline, 4. Old doline, 5. Development date (year that is missing from the map: in 2020, the month is 12 and in 2021, the months are January and February), 6. Boundary of the area marked for the calculation of the development rate.

5

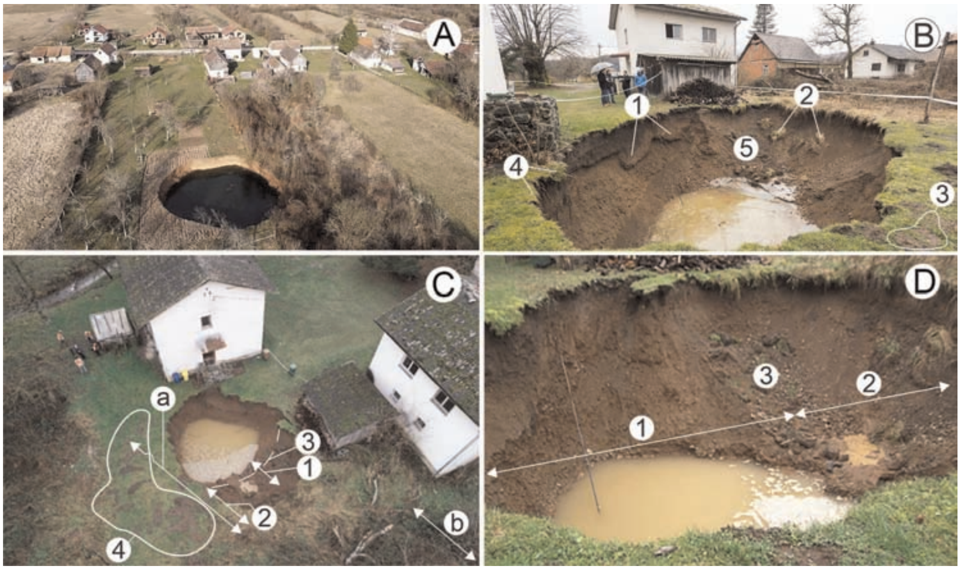

Figure 5.
New (dropout) subsidence dolines: A. non-narrowing dropout doline with lake (photo taken by Željko Grgić in February 2021), B. dropout doline with lake that is narrowing towards its floor from close-up (photo taken in February 2021 by Ronald Goršić): 1. Traces of liquefaction, 2. Limestone block, 3. Thrown out material, 4. Ragged lawn with traces of primary collapse, 5. Secondary collapse, C. narrowing dropout doline with lake from far view (a) and dropout doline without water (b) (photo taken in January 2021 by Marijan Car, Mario Bačić, Josip Terzić). D. Twin-like doline: Partial depression at the right side of the photo which developed either by the newer collapse of the cover cavity or during the secondary collapse of the side slope (photo taken by Sonja Zlatovič) 1, 2. Partial depressions, 3. Secondary collapse. All dolines were survey measured and monitored by Jeronim Moharić from January to September 2021 for the purpose of this study.

water. During the earthquakes, 82 new dolines developed in an area of 4 km^2 (but doline development also continued after the earthquake activity, and by the beginning of May, their number was 91 and by the beginning of December 2021, they numbered more than 100), which are collapse features with steep slopes (**Figure 5**). Several boreholes reached greater depths in order to get information on the composition of the cover. In case of a dropout doline, the sediments of the cover are organic soil, sandy lean clay and lean clay in 8-metre thickness [22].

Water outflow sites are springs and spring lakes and the depressions containing water (paleodolines) such as the spring Pašino vrelo.

3. Methods

- Earthquake and precipitation data and the distribution of dolines were analysed.
- The water-level elevation of a lake of a doline with permanent water was compared with the water-level elevation of one of the wells.
- A hydrological profile was made, and the characteristics of water outflow as well as its relation to flow systems was analysed.
- The morphological and hydrological characteristics of the dolines were studied.

- The inclination of the bearing slope was calculated, the average width and depth of the dolines with various ages were compared, and the doline development rate was calculated (for the calculation of rate, density was calculated and for density, the occurrence area of new dolines was confined with tangent lines).

- The shape of dolines was calculated by the quotient of depth and diameter. Shape values were described according to frequency by putting them into classes, a functional relationship was determined between the shape of old and new dolines and the number of dolines belonging to different classes. A conclusion was drawn from the shape of dolines to the shape of their former cavities.

- Putting the new dolines into two groups (at one group, the depth was greater, and at the other group, the width was larger), a function relation was looked for between the width and the depth of the dolines.

- A theoretical study of the failure of cavity ceilings was performed in the following way.

The calculation of the ceiling thickness that can collapse without earthquakes for a given cavity diameter was done and led to the formation of a dropout doline at the surface. Using this relatively simple theoretical model, it is possible to determine the critical ceiling thickness at which collapse will necessarily occur.

The model under consideration is shown in **Figure 6**. It depicts a cylindrical cavity of diameter *D* at depth *H* below the surface. The initial assumption of model is that the ceiling of the cavity is not subject to any supporting forces from below, so the

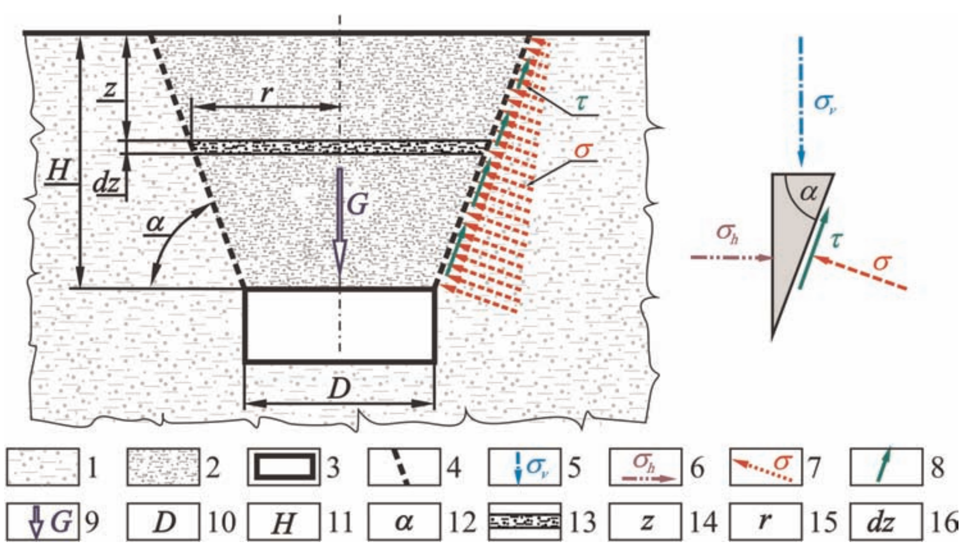

Figure 6.
Sketch of a theoretical model of dropout dolines. Explanation: 1. Uncollapsed rock mass, 2. Collapsed rock mass, 3. Cavity, 4. Interface between collapsed and intact rock masses, 5. Vertical stress in the rock, 6. Horizontal stress in the rock, 7. Compressive stress along the discontinuity surface, 8. Shear stress along the discontinuity surface, 9. The gravity of the destroyed rock aggregate, 10. The diameter of the cavity, 11. The thickness of the ceiling, 12. The slope of the discontinuity surface, 13. The infinitely thin layer of rock (imaginary) cut from the destroyed aggregate, 14. The depth below the surface of the selected layer, 15. The radius of the cut rock layer (disc), 16. The thickness of the cut rock layer.

7

equilibrium of the rock mass above the cavity is ensured by the cohesion force and internal friction between the particles of the overlying aggregate. If these forces cannot counterbalance the weight of the rock mass, collapse will occur.

Experience from mining and soil mechanics shows that in low-strength rocks such as the alluvium of the Mečenčani and Borojevići areas, collapse occurs along the upward-expanding fracture surfaces that start at the edge of the cavity and bound a conoidal frustum. The rock beds within the conoidal frustum are subjected vertically downwards to the gravitational forces of the Earth's gravity and upwards to the cohesive and frictional forces of the rock particles outside the fracture surface along the conoidal frustum mantle. These forces are defined below. The rock beds within the stump cone are vertically downwardly influenced by the gravitational forces due to the Earth's gravity and upwardly by the cohesive and frictional forces of rock particles outside the fracture surface along the conoidal frustum mantle. The formulae defining these forces are derived below.

The weight of the falling rock (G)

$$G = \rho g V, \tag{1}$$

where ρ is the density of the rock [kg/m^3], g is the acceleration due to gravity (g = 9,81 m/s^2), V is the volume of the rock mass [m^3], which in the case of a conoidal frustum is

$$V = \frac{\pi}{12} H \cdot \left(3D^2 + 3H \cdot D \operatorname{ctg} \alpha + H^2 \operatorname{ctg}^2 \alpha\right). \tag{2}$$

α is the angle of the fracture surface with respect to the horizontal, which, according to the relationship known from soil mechanics [23]

$$\alpha = 45° + \frac{\phi}{2}, \tag{3}$$

where ϕ is the angle of internal friction of the rock.

There are two types of forces acting along the conoidal frustum sheath (i.e. the discontinuity surface). One is proportional to the compressive stress (σ) perpendicular to the cone surface, the other proportional to the shear stress (τ) parallel to the cone's surface. To determine σ and τ, let us imagine a prismatic body in the rock, infinitesimally small, bounded by a horizontal surface, a vertical surface and a surface parallel to the discontinuity surface. This body is loaded from above (in the vertical direction) by the pressure (σ_v):

$$\sigma_v = \rho g z, \tag{4}$$

and sideward (on the vertical side of the imaginary prism), a horizontal stress (σ_h) is applied:

$$\sigma_h = \frac{\nu}{1-\nu} \rho g z, \tag{5}$$

where z is the depth below-ground surface [m], and ν is the Poisson's ratio of the rock. (Poisson's ratio is the relationship between the transverse and longitudinal deformation of rock under uniaxial pressure. Its value varies between 0 and 0.5.) The equilibrium of forces acting on the prism requires that stresses (σ, τ) also occur on the inclined side. These give the stresses along the discontinuity surface. The compressive stress, which is perpendicular to the surface (according to the elementary relationship known from the strength theory), is

$$\sigma = \sin^2\alpha \cdot \sigma_h + \cos^2\alpha \cdot \sigma_v. \tag{6}$$

The shear stress (τ) acting parallel to the discontinuity surface at the moment of initiation of collapse consists of the internal friction between the rock particles sliding side by side, which is directly proportional to the sum of the compressive stress on either side of the fracture surface and the specific cohesive force "pulling" the particles together:

$$\tau = \operatorname{tg}\phi \cdot \sigma + c, \tag{7}$$

where c is cohesion [N/m^2].

The stresses σ and τ are specific, that is they give the force per unit area of the envelope of cone. Let f_v denote the vertical component of the resultant of these forces, which, according to elementary calculations, is

$$f_v = \cos\alpha \cdot \sigma + \sin\alpha \cdot \tau. \tag{8}$$

According to terms (3)-(7) (after appropriate aggregations)

$$f_v = \left(\nu \frac{\cos\alpha \sin^2\alpha + \operatorname{tg}\phi \sin^3\alpha}{1-\nu} + \cos^3\alpha + \operatorname{tg}\phi \sin\alpha \cos^2\alpha\right)\rho g z + \sin\alpha \cdot c. \tag{9}$$

Imagine cutting out a 'ring' of height dz from the cone's mantle at depth z. Its radius (r), is obviously

$$r = \frac{D}{2} + (H - z)\operatorname{ctg}\alpha. \tag{10}$$

Mark the area of the cloak of this ring dA:

$$dA = \frac{2r\pi}{\sin\alpha} dz. \tag{11}$$

Since f_v is constant along this ring, the resultant of the vertical component of the compressive and frictional forces acting on the rock bed is

$$dF = f_v \cdot dA, \tag{12}$$

If we add up the forces acting on all the elementary rings covering the envelope of cone of the rock-face before the collapse, we obtain the resultant F of the forces acting upwards (opposite to gravity) on the body, which, taking into account (9), (10) and (11)

$$F = \int_0^h \pi[D + 2(H-z)\operatorname{ctg}\alpha] \cdot \left[\left(\nu \frac{\cos\alpha \sin\alpha + \operatorname{tg}\phi \sin^2\alpha}{1-\nu} + \frac{\cos^3\alpha}{\sin\alpha} + \operatorname{tg}\phi \cos^2\alpha\right)\rho g z + c\right] dz \tag{13}$$

9

For ease of writing, let us introduce the symbol

$$\kappa = \frac{1}{6}\left(\nu\frac{\cos\alpha\sin\alpha + \operatorname{tg}\phi\sin^2\alpha}{1-\nu} + \frac{\cos^3\alpha}{\sin\alpha} + \operatorname{tg}\phi\cos^2\alpha\right). \tag{14}$$

Performing the integration formulated in (13)

$$F = \pi\kappa\left(2H^3\operatorname{ctg}\alpha + 3DH^2\right)\rho g + \pi\left(H^2\operatorname{ctg}\alpha + DH\right)c. \tag{15}$$

Eq. (15) gives the force that ensures the equilibrium of the cavity ceiling. It can be seen that this has a linear (first-order) relationship with cohesion, that is the more cohesive, more frictional rocks have a greater 'holding power' at the same depth than rocks with less cohesion or less internal friction. There is also a linear relationship between the retention force and the density of the rock.

The formation of a doline starts when the balance of forces is upset for some reason, that is when

$$F \leq G, \tag{16}$$

The critical (H) cavity depth at which collapse can occur is given by $F = G$. Expressions (1) and (14) yield a second-degree equation for H:

$$\left(24\kappa\operatorname{ctg}\alpha - \operatorname{ctg}^2\alpha\right)\rho g H^2 + \left[12\sigma_c\operatorname{tg}\phi\operatorname{ctg}\alpha + (36\kappa D - 3D\operatorname{ctg}\alpha)\rho g\right]H + \left(12Dc - 3D^2\rho g\right) = 0 \tag{17}$$

A numerical analysis of (17) (with realistic data for the Mečenčani and Borojevići area) shows that the first term is several orders of magnitude smaller than the second and third terms and is therefore negligible. The numerical analysis also shows that the first member of the second bracket term is negligible next to the second and third. The solution to the simplified equation for H (taking into account the expression (14) for κ) is given by:

$$H = \frac{1-\nu}{2\nu}\,\frac{D - \frac{4c}{\rho g}}{\sin\alpha(\cos\alpha + \operatorname{tg}\phi\sin\alpha)}. \tag{18}$$

H is the critical ceiling thickness (expression 18) at which the roof covering is 'just' not yet collapsing. However, at this ceiling thickness, the cavity is already unstable, that is the slightest disturbance (earthquake, rock scour, soil moisture variation, etc.) will cause immediate collapse.

4. Results

The pattern of doline distribution shows their tectonic determination. The fault zone detected in the bedrock [3, 17, 19] directed the karst water flow, the transportation of dissolved material and thus, the direction of cavity formation there. However, the cavities that formed in this way determined the site of the material loss of the cover and the zone in which it took place. The geoelectrical resistance values of the profiles indicate the extent of fracturing and cavity formation of the bedrock below the zone of the dolines.

Based on the earthquake and precipitation data of the area, the following can be established:

- Between 28 December 2020 and 3 March 2021, two foreshocks and 14 aftershocks took place with magnitudes of 3.3–5.2. Their hypocentres were at depths of 8.7–10.9 km and their epicentre was in Strašnik 3 km away from Petrinja in WSW direction [1]. The development of dolines, some of them exactly dated, was mainly related to the earthquakes in January (**Figure 4**).

- According to the data of the Kostajnica Meteorological station, January was an especially rainy month, with a total of 106.4 mm rainfall, but February was also wet (72.7 mm). In January, there was a daily 6 mm or more rainfall eight times per month (once its value was 21 mm and on another occasion 28 mm).

Taking into consideration the observed dates of doline development (**Figure 4**, available only for some dolines), the earthquakes may have triggered immediately (on the day of the earthquake) and delayed doline development (days after the earthquakes). An example for immediate doline formation was what happened on 29 December 2020 when two dolines were formed and 30 December 2020 and 31 December 2020 when one doline developed each day. A similar situation was observable on the days of earthquakes of 2 January 2021, 4 January 2021, 5 January 2021 and on 6 January 2021 when one doline was formed each day. On the contrary, a delayed doline formation took place on 23 January 2021 when two dolines developed; however, no earthquake occurred on that day, but they happened only on the days of 7 January 2021, 9 January 2021, 10 January 2021 and 15 January 2021. No doline development coincides with the day of significant amount of rainfall. However, on 29 December 2020 when two dolines developed, the quantity of precipitation was significant. The relation between rainfall (infiltration) and doline development is less obvious. On 29 December 2020, two dolines developed at rainfall of 6 mm, while one doline was formed at precipitation of 12 mm on 30 December 2020. It is more probable that precipitation has a delayed effect. On 26 December 2020 when precipitation was 31 mm, it must have ensured favourable conditions for the development of the above-mentioned dolines on the 29th and 30th of December. The role of precipitation in doline development is indicated by the fact that dolines continued to take shape at the end of 2021. Thus, in December 2021, four new dolines developed probably to the effect of autumn rainfalls and also after a stronger M 3.2 earthquake.

The distribution of depressions is of banded (at some places, of linear) pattern. The band has a NW-SE direction and a length of 3100 m (outside that band only six dolines occur which developed during the earthquakes). Perpendicular to this direction, the width of the band is maximum 800–850 m (**Figure 4**). The band of dolines intersects the Sunja River in NW, and only some new dolines occur on its left bank. The width of the band covered by old dolines is larger; thus, the appearance of new dolines is more concentrated than that of the old dolines. The occurrence of new dolines at the north-western and south-eastern ends of the band (mainly at the latter) is slightly dispersed. However, older dolines frequently group along this arcuate band. The occurrence of dolines is combined in the band: there are sections made up of only new and only old depressions, but mixed sections are also present. Depressions outside this arcuate band are in groups of an irregular pattern. These may be constituted by homogeneous depressions (made up of only new or only old dolines), but by depressions that developed at various time. The direction of the band and the tectonic structure as well as the concordance of the directions of some fractures (faults) refers to the fact that doline development is controlled by tectonics. The area bearing the dolines (this is the floor of the Sunja River Valley) is of a very low inclination. It is 1.29° along the profile perpendicular to the Sunja River (**Figure 2**).

The development rate of new dolines is extremely high. If we consider the area with dolines and presume a period from 28 December to the end of March (doline development is probably shorter than this: in March no doline development was likely to the direct effect of the earthquakes, but the last earthquake, as we observed, took place on 3 March) calculating with 93 days, in the bearing area of 0.0113 km^2, the average rate of doline development is 27.33 dolines per month. Calculating this to 1 km^2 and 1 month, the rate is 2418.70 doline/month or calculating with the actual area to 1 year, it is 327.96 doline/1 km^2, calculating to 1 km^2 and 1 year, 201.56 doline develops, and to 1000 m^2 and 1 month the development rate is 29.02 doline/month. Calculating with the actual area, the development rate is 0.91 doline per day. Thus, comparing with the development rates of literary data, in the area of Mečenčani and Borojevići, the same number or more dolines per day were formed during a day than in other karst areas during a year. This high rate of doline development can only be explained by the impact of the series of earthquakes.

The morphological and hydrological characteristics of the dolines are the following:

- Dolines that developed preceding the earthquakes have gentle slopes with vegetation.

- Two varieties of new dolines that were formed during the earthquakes can be distinguished morphologically. Dolines belonging to one variety have gentler slopes, narrowing towards their floor, but their margins are made up of arcuate sections (**Figure 5B**). The other variety involves dolines with steep slopes (sub-vertical) and a wide, expanded floor (**Figure 5A**). The cover is exposed on the dolines of both varieties, their margin is sharp and the lawn is ragged. The morphology of new dolines refers to the collapse origin. Dolines collapse for two reasons: primarily resulting in their development and secondarily which collapse on their side slopes (**Figure 5**). The result of secondary collapses is that dolines are widening and their slopes are becoming gentle. At some sites, patchy and zone-like sediment accumulations can be seen beyond the margins (**Figure 5B** and **C**). On their side slopes, flow traces (**Figure 5B**) and the scars and slides of subsequent, secondary collapses occur (**Figure 5D**). Sometimes, the side slope is constituted by parts of various steepness (parts of low inclination replace steeper slope sections or the floor of variable elevation (**Figure 5C** and **D**). They have a circular ground plan, but elongated dolines and twin-like complex dolines also occur (**Figure 5D**). The surface is flat in the environs of the dolines, and no drainage feature is connected to it.

The depth of new depressions does not exceed 5 m predominantly; thus, they were formed in the unconsolidated superficial deposit (al-Q_2). Therefore, they are subsidence dolines. Only one doline has a depth of 12 m. However, it refers to the fact that the collapse triggering its development also spreads over the Badenian limestone. The cavity of the Badenian limestone must have been without water (or partly without water) at least during the time of the earthquake which triggered its collapse since the collapse of the cavity is only possible if the ceiling of the cavity is not supported. However, the development of some depressions (those with a depth close to 5 m) may have started at the Badenian limestone since the depth of the doline was reduced by the collapsed material.

Among the new ones, there are depressions that have been dry since their development, there may be constantly wet depressions (there is a lake with permanent water on their floor) and there are depressions that are intermittently wet (a lake appears on their floor intermittently). The altitude difference between the water level of the doline with permanent water and the groundwater table is 4.5 m, and the distance between the distance between the doline with lake and the well is 80 m. The similarity in water levels indicates that the water of dolines with lake partly originates from groundwater or the dolines developed from cavities that had at least partly been below the groundwater table. (The reason for the difference of the above water levels may be that the collapse of the cavity increased the water level in the doline and the water level of the lake follows the subsidence of the groundwater level with delay.) The water-level fluctuates in both the permanent and intermittent lakes.

If the altitude of the floor of new dolines is almost the same as the altitude of the cavities from which they developed, then the extent to which the dolines are filled with water or its lack indicates the position of former cavities as compared to the groundwater level. As compared to the groundwater level, the dolines and their cavities may be and may have been of the following types:

- Dolines which are constantly dry (a depression that has been dry since its development can be seen at the right side of **Figure 5C**), the floor of their cavity has always been above the groundwater level. These are dolines of small depth (shallower than 1–2 m).

- Dolines with intermittent lakes, and their cavity was situated at least partly between the high and low groundwater levels (according to drying traces visible on its floor, its depression lost its water by the observation date of 5 June 2021.) The water level of the lakes changes in the dolines because their floor is in the groundwater fluctuation zone. These dolines are deeper than the former. Their depth ranges from 1 to 2 to 5 m.

- Dolines with permanent lake, the floor of their cavity was below the current groundwater level. An example is the 12-m-deep doline, but probably at least three other dolines whose depth is about 5 m belong to this group. This doline still had a lake at an observation of November 2021.

- Dolines that developed after the earthquakes do not have water intermittently either; thus, they also developed from cavities above high groundwater level.

Dolines of water outflow sites have steep slopes and permanent lakes. These features are not active (paleodolines) such as the spring Pašino vrelo. They are situated at the emergence sites of groundwater and karstwater. Based on the composition of their water, they are drainage sites for them. According to [19], groundwater from limestones and water from Quaternary deposits are mixed. The groundwater is the water of the al-Q_2 beds; in the NE, it follows the Sunja River and is situated at a depth of 1–2 m. Its position as compared to the surface SW from Mečenčani is unknown. However, it can be observed that the altitude difference between the surface and the water level increases farther from the Sunja River (**Figure 7**). The different proportion of the two waters at various drainage sites refers to the existence of two kinds of flow

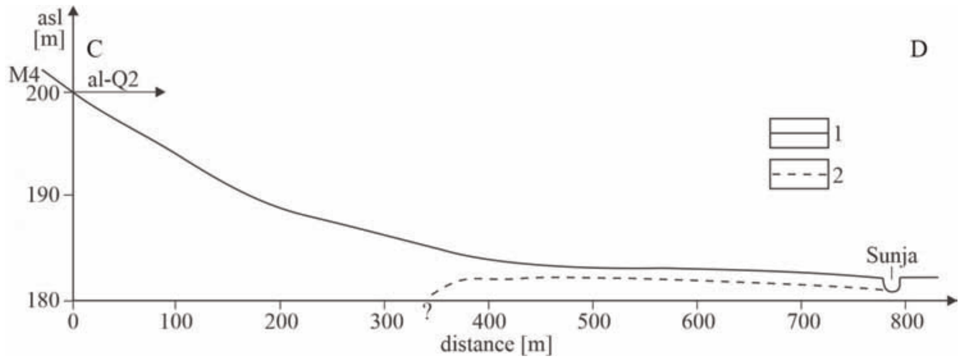

Figure 7.
Position of groundwater. Legend: 1. surface, 2. groundwater level.

systems, but also to their partial or widespread relation. Their discharge fluctuation was between 24.4 and 12.4 l/s at the spring of Pašino vrelo. The fluctuation of the groundwater discharge and also the fluctuation of its water level [18, 19] refer to the presence of high and low water levels.

The size of dolines that developed at water inflow sites at various times is different. Older dolines are of a greater diameter and a smaller depth (the average diameter is 5.1 m, the average depth is 0.47 m), newer dolines have a smaller diameter, but they are deeper (their average diameter is 3.7 m, and their average depth is 1.5 m). These values are more striking if we only consider the sizes of those with a shape index below 0.3 in case of old dolines (**Figure 8**): here, the average diameter is 5.73 m, and the average depth is 0.34 m. The latter are the smallest, with a diameter of only 1–2 m, and having steep slopes, they are passage-like and aligned with a collapse yard of small depth. The shape of 34 old dolines is in the 0.0–0.1, 0.1–0.2, 0.2–0.3 classes and only eight dolines have a shape larger than class 0.3 (**Figure 8**). The shape of 63 new dolines is in classes larger than 0.3. Thus, at old dolines, a larger diameter belongs to a given depth, while in case of young dolines, a smaller diameter belongs to a given

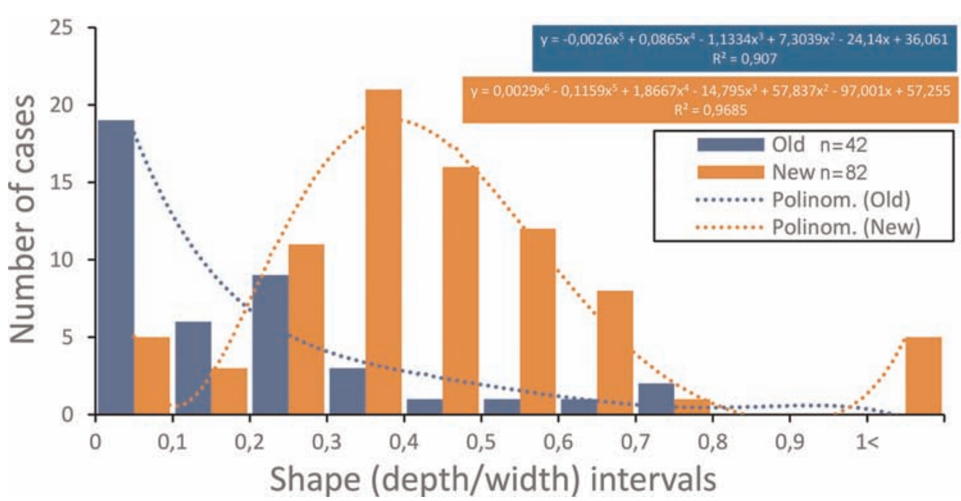

Figure 8.
Shape distribution of old and new dolines and the functions of shape distributions.

depth. The class distribution of the two doline groups is also different. The distribution of old dolines can be described with a decreasing polynomial function, while that of new dolines can be described with a polynomial function with two maximum values (**Figure 8**).

New dolines can be referred into two groups. At one of them, the depth is dominant (the depth is larger than the width), at the other, the width is dominant (the width is larger than the depth) since there is a functional relationship between the width and depth at the members (at every depression) of the group (**Figure 9**). If the depressions developed from cover cavities, the former cavities can also be put into two types: at one of them, the vertical expansion is dominant, while at the other, the horizontal expansion is dominant. Therefore, the cavities that were situated at a similar depth as compared to the surface were mainly either vertical or horizontal. During the collapse, the cavities preserved their horizontal and vertical dimensions and they were only modified to a small degree. The small number of vertical depressions (there are four) and the large number of depressions with large width prove that great width favours the denudation of the cavity ceiling.

In case of depressions whose depth exceeds their diameter, there is a strong relation between the width and the depth at the width and depth function (**Figure 9**). Depressions becoming wider and wider are more and more expanded vertically. Thus, former wider cavities were probably more and more expanded downwards. At depressions where their width exceeds their depth, in case of those with a small width, depths are less diverse. At depressions whose width is larger, the diversity of their depth increases. Therefore, in the latter case, the cavities from which the depressions

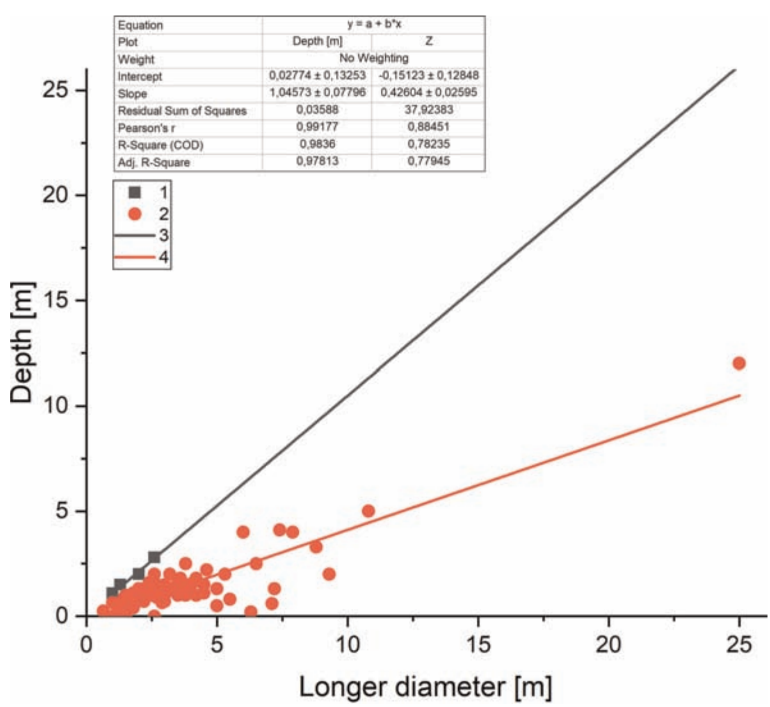

Figure 9.
Functional relationship between the width and depth of new (dropout) dolines. 1. Dolines whose depth exceeds their width, 2. Dolines whose width is larger than their depth, 3. Function fitted to deeper dolines, 4. Function fitted to wider dolines.

15

D [m]	*H* [m]											
	c = 10 [kPa]			*c* = 20 [kPa]			*c* = 30 [kPa]			*c* = 40 [kPa]		
	Φ = 20°	*Φ* = 25°	*Φ* = 30°	*Φ* = 20°	*Φ* = 25°	*Φ* = 30°	*Φ* = 20°	*Φ* = 25°	*Φ* = 30°	*Φ* = 20°	*Φ* = 25°	*Φ* = 30°
2	—	—	—	—	—	—	—	—	—	—	—	—
4	2.8	2.5	2.3	—	—	—	—	—	—	—	—	—
6	5.6	5.1	4.6	2.7	2.5	2.3	—	—	—	—	—	—
8	8.5	7.7	7.0	5.6	5.1	4.6	2.7	2.4	2.2	—	—	—
10	11.3	10.3	9.3	8.4	7.7	6.9	5.5	5.0	4.6	2.6	2.4	2.2
12	14.2	12.9	11.7	11.3	10.2	9.3	8.4	7.6	6.9	5.5	5.0	4.5
14	17.0	15.5	14.0	14.1	12.8	11.6	11.2	10.2	9.2	8.3	7.6	6.9
16	19.8	18.1	16.4	16.9	15.4	14.0	14.1	12.8	11.6	11.2	10.1	9.2
18	22.7	20.6	18.7	19.8	18.0	16.3	16.9	15.4	13.9	14.0	12.7	11.5
20	25.5	23.2	21.1	22.6	20.6	18.7	19.7	18.0	16.3	16.8	15.3	13.9

Table 1.
Critical (on a limit of stability) ceiling thickness (H) *as a function of cavity size* (D) *for different cohesion* (c) *and internal friction* (ϕ).

developed had an extremely diverse vertical cavity size during their widening. This is possible since the floors of some cavities from which the depressions developed had a deeper and deeper position in case of similar thicknesses of the cavity ceilings.

According to soil mechanics studies in the Mečenčani and Borojevići area (Tomac et al. 2021c), the alluvium has an angle of internal friction of $\phi \approx 24–28°$, a specific cohesive strength $c \approx$ 20–50 kPa, a density of $\rho \approx 1800–2000$ kg/m^3, a Poisson's ratio $\nu \approx 0.25–0.33$ and a gravity acceleration $g = 9.81$ m/s^2 (Tomac et al. 2021c). Based on the mean value of these ($\phi = 25°$, $c = 20$ kPa, $\rho = 1800$ kg/m^3, $\nu = 0.33$), the ceiling may stop above a cavity of diameter $D = 10$ m at a thickness of $H = 6.7$ m.

To illustrate the relationship (18), the evolution of the ceiling thicknesses at the stability limit as a function of the size of the cavity before collapse for different realistic values of cohesion *(c)* and internal friction angle (ϕ) is presented in **Table 1**. ($\rho = 2000$ kg/m^3, $\nu = 0.33$) It can be seen that H is very sensitive to both ϕ and c. During earthquakes, these factors can undergo significant changes, which can result in previously quiescent cavity ceilings losing their stability and collapsing.

5. Discussion

The morphology and shape of the dolines indicate that the dolines of the area between Mečenčani and Borojevići originated by suffosion, collapse and probably compaction.

Old dolines with a shape smaller than 0.3 have a small depth because of limited material transport (suffosion and/or compaction), a large diameter (widespread material transport can take place) and gentle slopes (as a result of slow subsidence and slope denudation). New dolines with a shape larger than 0.3 are deeper because of collapses. Therefore, old dolines with a shape index smaller than 0.3 are suffosion dolines, while new dolines with a shape larger than this are dropout dolines.

Among old dolines occur dolines with a shape larger than 0.3 (**Figure 8**). Therefore, old dolines may also have developed by collapse, but their side slopes became gentle subsequently (pseudo-suffosion doline). Among new dolines, there occur dolines with a shape smaller than 0.3. This may refer to the fact that in case of new dolines of this type, collapse already stopped at an early phase or was followed by subsidence.

In the case of some new (dropout) dolines, the reason for shape increase is not width decrease, but ever greater depth. Presuming a cavity ceiling of small thickness (which is a precondition of collapse), this is possible if the former cavities were increasingly expanded downwards. Thus, cavities develop in the zone of groundwater fluctuation; in addition, in case of those with a shape larger than 1, there was a cavity which was originally in the bedrock; then, its development spreads onto the cover.

The relatively large number of old (suffosion) doline refers to the fact that in this area the tendency to doline development might have been significant earlier as well. This can probably be explained by the low inclination of the bearing terrain in addition to cavity formation that is discussed below. In our case, surface inclination on the valley floor, as already mentioned, is low. This can partly be traced back to the fact that on such terrains, the infiltration proportion of precipitation is large; on the other hand, as a result of its low inclination, the groundwater level is in wide expansion close to the surface (and the karstwater level is also close to the bedrock surface). The water level being close to the surface favours widespread subsurface cavity formation, which enables widespread material transport from the cover. However, collapse tendency is high because the cover cavities are close to the surface. The cavity formation in the bedrock favours collapses and the reception of the material transported from the cover.

Regarding the water outflow sites of the area, it can be established that the water level oscillates at Pašino vrelo whose degree alternates between 0.46 and 0.52 m since the discharge of its spring fluctuates between 22.8 and 12.8 l/min [18, 19]. This indicates the fluctuation of groundwater level, that is high groundwater level and low groundwater level. Their range between dry and wet seasons is 2 m [16].

Since the groundwater of the cover and the karstwater of the Badenian limestone are present to various proportions at springs Pašino vrelo, at Davidovića vrelo [18, 19], the two kinds of water are separated from each other at least temporarily, and they are primarily mixed at the water outflow sites. The water of the Badenian limestone functions as artesian water in wet seasons [16]. Therefore, the groundwater and the karstwater flow circulate individually.

A two-storey cavity system developed as a result of the two water bodies and their circulation and the fluctuation of groundwater level. The lower level is in the Badenian limestone, while the upper is in the cover.

The shape and size of cover cavities were different. This is proved by the fact that the depth and shape of dolines differ for the dolines (it is presumed that during their development, the dolines preserve the shape and size of former cavities). The shape of the former cavity can be determined from the shape of the depression. The shape, but also the size and position of the cavity point to a collapse tendency. The wider the cavity (the smaller shape it has) and the closer to the surface, the greater its collapse tendency.

Cover cavities are of various positions as compared to the changing groundwater level, since among the developed dropout dolines there occur dry dolines, dolines with permanent lakes and dolines with intermittent lakes. (According to the observation of 05 June 2021, some dolines lost their water.) Among former cavities there were some which were situated in their whole expansion above the high groundwater level and there were others which were above the low groundwater level in their whole expansion. Cavities, whose lower part was below the groundwater table developed by the partial collapse of the bedrock and the cover above it since the permanent presence of groundwater, hindered suffosion.

The altitude of the groundwater level affects the size and development of the cavities and the way of material transport out of the cavities. The difference between the altitude of the groundwater level and the altitude of the surface increases in SW direction from the Sunja River (**Figure 7**). However, the extent of the fluctuation of high and low groundwater levels also increases in the same direction since the water supply from the Sunja River into the groundwater and thus, its affect raising the water level, diminishes moving farther from the river. In case of low water level, its water level reducing effect is limited since the water level cannot reach below the water level of the river.

Consequently, the cavities of the cover may have developed in the following manner:

- By suffosion, cavities in the environs of which the cover is at least temporarily without groundwater and it is coarse-grained. Suffosion is possible because a passage develops above the cavity of the bedrock that reaches above the karstwater level and this transports the material of the cover into the karstic cavity.

- By the further collapse of the suffosional embryonic cavities of the cover.

- By the collapse of the bedrock. The cavity of the bedrock is inherited onto the cover, and then to the surface. This rarely observed process must have taken place, for example in the case of the doline with a depth of 12 m. If inheritance happens only onto the cover, a cavity is formed in the cover by collapse and with its later collapse a doline develops. If the cover follows the bedrock collapse in its total expansion, no cavity develops in the cover, but a depression is formed immediately at the surface.

There are a large number of cavities in the upper level of the Badenian limestone according to measurements [18]. The cavities are situated both above and below the water level. Evidence for the existence of cavities above the water level is the already mentioned 12-m-deep-doline. Since it could have developed in a way that it continues in the bedrock, thus, the bedrock cavity had to collapse as well. It is only possible if the cavity reached above the water level.

The material flow of the two-level cavity system may be the following:

- Material transport solely happens by suffosion. This is possible at those cavities that are above the high groundwater level (and at cavity parts which are situated above this level). Suffosion always takes place during the rainy season. In the cover, vertical passages develop between the surface and the cavity and at the portion of the cavity above the high groundwater level. Passage development is associated with suffosion doline formation and with the partial filling up of the cavity. If suffosion material transport takes place from the cavity, the cavity increases and its sediments are transported away.

- Material transport is partly of suffosion and partly of collapse origin. The cavity is between the high and the low groundwater level in its partial or complete expansion. Suffosion only takes place and only for the period until the groundwater level is below the floor of the cavity. In this case, passages may form too. If the groundwater is above the cavity, suffosion is horizontal, which does not generate passages, but it induces material transport in the groundwater. If the amount of precipitation increases, vertical suffosion stops because of the rise of the groundwater level.

- The transport of the cover material is solely of collapse origin if the cavities of the Badenian limestone above the karstwater level collapse. Suffosion may be present accessorily, temporarily which may be expressed by the reworking of the collapse material. The cavity is either in the bedrock or both in the bedrock and in the cover. The cavity of the cover may continue its development by collapse (dropout doline) or by suffosion (suffosion doline).

There is a higher probability of old (suffosion) doline development at sites where:

- the cavity is situated above the high groundwater level in its total expansion,

- the host rock of the cover cavity is less cohesive,

- there is no earthquake.

19

New (dropout) dolines may develop in the following ways.

- By cover collapse. The cover cavity may be formed by bedrock collapse, which is inherited onto the cover or by suffosion. The cover cavity collapses if the pore water pressure increases in its environs, to the effect of earthquakes if the water level decreases in the cavity, but it may also take place without any external effect if the width of the cavity reaches a critical value and the ceiling is thin.

- By the collapse of the bedrock which is inherited onto the cover in a way that no cavity is formed there, the material of the bedrock ceiling and the cover collapse together. This may happen if the cavity is above the karstwater level, close to the bedrock surface and horizontally developed.

The collapse of cover cavities may take place only during the failure of the ceiling in case of cavities above the high groundwater level (direct earthquake effect) and when it was contributed by other factors too (indirect earthquake effect). The collapses that triggered the development of dolines in the environs of Mečenčani and Borojevići may have been affected by several factors too if the ceiling did not directly collapse because of the failure such as the partial liquefaction of the ceiling material may have happened at cover cavities situated below the high groundwater level. Traces of liquefaction can be seen in **Figure 5B**. Concomitant phenomena, material shots can be recognized in the environs of some dolines (**Figure 5B** and **C**).

In the area of Mečenčani and Borojevići, after the series of earthquakes, the groundwater level became (and stayed) somewhere 30–50 cm lower than earlier in the wells (conversations with locals in 2021). This was probably caused by the irreversible displacement of karstic blocks and the resulting karstwater subsidence spreads onto the groundwater too and/or because of the decrease of cover compaction the groundwater level sank in an irreversible way. The groundwater subsidence reduced the support of cavity ceilings (doline development is without support), which launched a process that is well known in karst literature [24]: the collapse of the ceiling weakened by liquefaction. The thinning out of the ceilings was also enabled by the fact that parts became separated from there, partly because the infiltration of precipitation increased pore water pressure and partly because of liquefaction. However, the infiltrating precipitation also caused an increase in burden, which resulted in the warping of the ceilings. Local people reported on surface subsidence preceding doline formation [16]. This may also have enhanced the separation of parts from the ceilings. To the effect of repeating shocks, the chance of the collapse of thicker ceilings may also increase. Cavities with thin ceilings probably collapsed to the immediate effect of earthquakes, while the cavities with thicker ceilings collapsed due to the delayed effect from the cumulative impact of the shocks.

Dolines, the ceilings of whose cavities had been above the high groundwater level, may have developed during the failure of the cover due to direct earthquake effect by collapse. A favourable condition for this, as already mentioned, is that the cover thickness is less than 1–2 m, and it is not greater than some tens of centimetres. Similarly, the collapse of bedrock cavities was caused by the direct effect of earthquakes.

The relationship (18) highlights several factors that are important for the formation of dropout dolines and even allows a quantitative analysis of these factors.

It can be seen that there is a linear relationship between the thickness (H) of the still stable cavity ceiling and the diameter (D) of the cavity: the main thickness of a cavity with a stable ceiling (i.e. not yet collapsing) is proportionally larger. It is noteworthy that according to this model, there is a minimum cavity diameter below which the ceiling of smaller cavities (due to their own weight) does not collapse. If

$$D < \frac{4c}{\rho g}, \tag{19}$$

then the numerator of (19) becomes negative, which means that no matter how thin the cavity ceiling is, it is held together by cohesion. (Of course, in this extreme case, other external factors neglected in the present model may still trigger collapse.)

From (18), it can be seen that if the cohesion (c) of the rock is larger, then H is smaller. This is consistent with the experience that more consolidated rocks do not collapse even with thinner ceilings. It also turns out that if the Poisson's ratio (ν) of the rock is smaller, a larger cover thickness is required to avoid collapse. The reason for this is because, with a smaller Poisson's ratio, the primary vertical rock pressure (σ_v) results in a smaller horizontal pressure (σ_h) (see relation (4)), which results in a smaller frictional force balancing the cover assembly.

The relationship (18) gives an account of all the effects of earthquakes that lead to the formation of dropout sinkholes. The most important of these (which also play a central role in building damage) are the accelerations induced by the quake waves. These can be calculated from seismology (using the distance from the epicentre or hypocentre of the quake and the magnitude of the quake) and are added to the gravity acceleration. For example, for a 5-magnitude quake, this can increase the value of g by up to 30%. Since in expression (18) g is contained in the denominator of a subtraction term, and an increase in g reduces the subtraction term and therefore increases the value of H. In practice, this means that a cavity whose ceiling thickness still ensures stability under 'normal' conditions will no longer comply and collapse due to the increased critical principal strain during an earthquake.

Similarly, the reduction in internal friction and cohesion due to the shear stress of the earthquake increases the value of H: a reduction in both c and ϕ leads to an increase in the value of H according to (18); that is, the effective cover thickness becomes less than the minimum value required to avoid collapse.

6. Conclusions

The karst features of Mečenčani area were classified, the morphology of dolines was described and dolines were put into groups based on their position as compared to the groundwater level. The coincidence of the development of dolines and the time of earthquakes was described. The shape distribution of old and new dolines was also studied.

Statements related to doline development are as follows:

- The variability of doline development was due to the diversity of hosting sediments. Therefore, dolines of various types and different formation date may occur next to each other.

- The dropout dolines may have developed by the collapse of the cover cavity of suffosion origin, by the inheritance of the bedrock cavity onto the cover by collapse, from which a dropout doline develops by collapse too. They may develop by the inheritance of the bedrock cavity onto the surface through the cover.

- Based on the model proposed, the effect of rock mechanics parameters that influence the stability of cavities can be given in numbers.

- Earthquakes may result in collapse directly on the ceiling of the cover or of the bedrock. Collapse can take place because accelerations due to earthquakes are added to acceleration of gravity increasing the weight of the rock mass and decreasing friction and cohesion. Collapse may also take place indirectly by earthquakes when the ceiling loses its support and it becomes thinner by liquefaction.

- During periods without earthquakes primarily suffosion dolines develop, while the periods of earthquakes result in dropout dolines. As a result of the presence of groundwater, suffosion dolines can only develop at cavities situated above lower groundwater level.

- The high development rate during earthquakes was accompanied by cavity formation due to dual water body and groundwater-level fluctuation and attributed to the thin ceiling of the cavities and low slope angle.

- Doline development would have taken place in any case because of the cavities of the bedrock and the cover, but not within such short time, but during several hundreds or thousands of years and probably partly by suffosion.

- Wide cavities situated in the fluctuating groundwater level have the highest probability of dropout doline formation due to earthquakes.

- In contrast to literary data, the development of suffosion dolines in the areas of Mečenčani and Borojevići did not take place by the transport of the cover material into the bedrock, but it also happened by transport into the cover cavity.

The study of the dolines of the Mečenčani area draws attention to the fact that doline development is influenced by several factors. Some factors are only specific of this area (the closeness of the karstwater level to the bedrock), while others are generally valid (groundwater, earthquake). The significance of our study is that the role of various factors in doline development was given in quantities. Thus, a better prognosis for doline development can be given on various covered karsts of the Earth and human made structures can be planned more safely.

Acknowledgements

Many thanks for overall support to Mr. Gordan Hanžek (State Secretary of the Central State Office for Reconstruction and Housing of the Republic of Croatia) and the Ministry of Physical Planning, Construction and State Property. We are very grateful for the help with collection data on the field to Mr. Jeronim Moharić with colleagues (Geo Gauss d.o.o. from Čakovec), Borna Gašpert and Mirko Stanković. The English language was edited by Tatjana Jauk (linguist at Hrvatske vode) and by Dénes Lóczy (University of Pécs), and we thank them a lot for her kind help.

References

[1] Miranda E, Brzev S, Bijelić N, Arbanas Ž, Bartolac M, Bijelić N, et al. Petrinja Croatia. December 29, 2020 Mw 6.4 Earthquake, Joint reconnaissance report, LFE Program of the Earthquake Engineering Research Institute (EERI), Structural Extreme Events Reconnaissance (StEER) Network, ETH Z¨rich, PRJ-2959, 2021. p. 206. DOI: 10.3929/ethz-b-000465058

[2] Tondi E, Blumetti AM, Čičak M, Di Manna P, Galli P, Invernizzi C, et al. Conjugate coseismic surface faulting related with the 29 December 2020. Scientific Reports. 2021;**11**:9150

[3] Bočić N. Structural-geomorphological aspects of the Petrinja earthquake M6.2 (Croatia) preliminary considerations. Hrvatski geografski glasnik. 2021;**83**(1): 5-24. DOI: 10.21861/HGG.2021.83.01.01

[4] Pollak D, Gulam V, Novosel T, Avanić R, Tomljenović B, Hećej N, et al. The preliminary inventory of coseismic ground failures related to December 2020 – January 2021 Petrinja earthquake series. Geologia Croatica. 2021;**74**(1): 189-208. DOI: 10.4154/gc.2021.08

[5] Karimzadeh S, Matsuoka M. A preliminary damage assessment using dual path synthetic aperture radar analysis for the M 6.4 Petrinja earthquake (2021). Remote Sensing. 2021;**13**(12):2267. DOI: 10.3390/rs13122267

[6] Boncio P, Amoroso S, Atanackov J, Baize S, Barbača J et al., Surface faulting during the 29 December 2020 Mw 6.4 Petrinja earthquake (Croatia), EGU General Assembly, EGU21-16575, vEGU21:Gather online. 2021. DOI: 10.5194/egusphere-egu21-16575

[7] Xiong W, Yu P, Chen W, Liu G, Zhao B, Nie Z, et al. Mw 6.4 Petrinja earthquake: a dextral event with large coseismic slip highlights a complex fault system in northwestern Croatia. Geophysical Journal International 2021. 2020;**228**(3):1935-1945. DOI: 10.1093/gji/ggab440

[8] Markušić S, Stanko D, Penava D, Ivančić I, Bjelotomić Oršulić O, Korbar T, et al. Destructive M6.2 Petrinja earthquake (Croatia) in 2020—Preliminary multidisciplinary research. Remote Sensing. 2021;**13**:1095. DOI: 10.3390/rs13061095

[9] Tomac I, Zlatović S, Athanasopoulos-Zekkos A, Bleiziffer J, Domitrović D, Frangen T, et al. Geotechnical Reconnaissance and Engineering Effects of the December 29, 2020, M6.4 Petrinja, Croatia Earthquake, and Associated S eismic Sequence, Report GEER-072. USA: GEER Association; 2021a. pp. 5-38. DOI: 10.18118/G63T0S

[10] Williams PW, Dolines. In: Gunn J, editor. Encyclopedia of Caves and Karst Science. Routledge, New York, London: Fitzroy Dearborn; 2004. pp. 304-310

[11] Veress M, Covered Karst. Book. Dordrecht: Springer, Springer Geology; 2016. p. 536. DOI: 10.1007/978-94-017-7518-2

[12] Waltham T, Bell F, Culshaw M. Sinkholes and Subsidence. Berlin, Heidelberg, New York: Springer-Verlag; 2005. p. 382

[13] Yuan D. Environmental and engineering problems of karst geology in China. In: Beck BF, Wilson WL, editors. Karst Hydrogeology, Engineering and Environmental Applications. 1987. pp. 1-11

[14] Gutierrez F, Parise M, De Waele J, Jourde H. A review on natural and

human-induced geohazards and impacts in karst. Earth Sciences Review. 2014; **138**:61-88

[15] Mádl Szőnyi J, Czaune B, Simon Sz, Erőss A, Zsemle F, Pulay E, et al. Hidrogeológia (Hydrogeology), Digitális Tankönyv, Hungary: ELTE; 2013

[16] Tomac I, Vlahović I, Parlov J, Matoš B, Matešić D, Kosović I, et al. In: Tomac I, editor. Cover-collapse sinkholes. Geotechnical Reconnaissance and Engineering Effects of the December 29, 2020, M6.4 Petrinja, Croatia Earthquake, and Associated Seismic Sequence, Geotechnical Extreme Events Reconnaissance Report GEER-072. USA: GEER Association; 2021b. pp. 52-99. DOI: 10.18118/G63T0S

[17] Tomljenović B, Cvetković M, Sečanj M, Palenik D, Vukovski M, Belić N, et al. Geological engineering, hydrogeological and geophysical investigations for the purpose of defining an effective concept of organized reconstruction in earthquake-affected areas. Study on seismically induced effects of Petrinja series of earthquakes 2020-2021 – preliminary identification of risks. Zagreb: University of Zagreb Faculty of Mining, Geology and Petroleum Engineering; 2021

[18] Mraz V, Dolić S, Kolarić J, Marković T, Dolić M, Košćal S. Water survey works "Pašino vrelo". Croatian Geological Survey. 2005;**2005**:12-49

[19] Larva O, Marković T, Mraz V. Hydrodynamic and hydrochemical conditions at the groundwater source "Pašino vrelo". Geologia Croatica. 2010; **63**(3):299-312. DOI: 104154/gc.2010.24

[20] UZFMGPE, Records of koseismic surface phenomena in the zone of the main seismogenic fault and maps of safety corridors in relation to collapsed sinkholes in the settlements of Mechenčani and Borojevići. Book 2. Zagreb: University of Zagreb , Republic of Croatia Ministry of physical planning, construction and state property. 2021. pp. 10-25

[21] Herak M, Herak D, Markušić S. Revision of the earthquake catalogue and seismicity of Croatia, Terra Nova. 1996; **8**:86-94

[22] Tomac I, Salković I, Kovačević-Zelić B, Domitrović D, Vučenović H, Hrženjak P. Complementary geotechnical and geophysical investigation works. In: Tomac I, editor. Geotechnical Reconnaissance and Engineering Effects of the December 29, 2020. Report GEER-072, USA: GEER Association; 2021c. pp. 164-196. DOI: 10.18118/G63T0S

[23] Hudson J, Harrison J, Engineering Rock Mechanics: An Introduction to the Principles, Second Impression. London: Elsevier Science Ltd; 2000. p. 114

[24] Jia L, Li L, Meng Y, Wu Y, Pan Z, Yin R, Responses of cover-collapse sinkholes to groundwater changes A case study of early warning of soil cave and sinkhole activity on Datansha Island in Guangzhou, China. Environmental Earth Sciences. 2018;**77**:488. DOI: 10.1007/s12665-018-7603-3